

**AE3610**

# Welcome

Here you will find the lab manuals for all experiments that will take place this semester. Navigate to the appropriate experiment on the left-hand menu. You can export each experiment as a PDF if you want a copy for your records, or to print as a hard copy. Also, bookmark this page on your smartphone or tablet as well as your PC/laptop as a handy guide during your lab session.

Note that this semester is the first-time we are rolling out Gitbook to deliver the manuals, so please let your TA or Instructor know if there are any typos, or suggested improvements...

Best of luck for the semester!

## Experiments

# Digital Sampling

## Objective

The primary objective of this experiment is to familiarize the student with digital data acquisition of time-varying signals. This lab covers concepts in frequency analysis of time varying signals and sampling theory. It also provides an introduction to computer-based data acquisition systems. In this experiment, you will use a computer data acquisition system to sample signals produced by waveforms stored in mp3 formats and converted to analog electrical signals by the computer's audio system. You will explore issues in sampling, including the Nyquist limit and aliasing, and the use of analog filters. This will help prepare you for future experiments in this laboratory course that employ computerized data acquisition and involve frequency based interpretation of measured data.

---

## Background

Most experimental measurements involve the dimension of **time**. Experimental data is acquired over the course of some time, and during this time the signal can change. In some cases, the actual physical parameter of interest (the *measurand*) may change with time. For example, the velocity in a wind tunnel generally varies with time due to turbulence or variations in the speed of the fan blades used to drive the tunnel. Even when the measurand is nominally constant in time, other parameters that influence the measurement may vary, for example drifts in the measurement device. Thus, the experimenter is often interested in measuring a variable that could be described by the general function (or *waveform*),

$$v = v(t)$$

(1)

## Waveforms, Frequency Content and Discrete Sampling

### Fourier Series

One of the simplest time-dependent functions we encounter is the sine (or cosine\*),

 \*Either function is acceptable, since  $\sin(wt) = \cos(wt - \pi/2)$ , i.e., the two functions are identical except for a phase difference of  $\pi/2$  or  $90^\circ$ , meaning that shifted by one-fourth of a cycle, cosine looks just like sine.

$$v(t) = A \sin(\omega t + \phi) = A \sin(2\pi n f t + \phi)$$

(2)

where  $A$  is the amplitude,  $\omega$  is the circular frequency (e.g., rad/s),  $f$  is the cyclic frequency (e.g., cycles/s, Hertz or  $s^{-1}$ ), and  $\phi$  is the phase, which represents the time-shift of the sine-wave from some reference time that defines  $t=0$ . Such a function is often denoted as a *simple harmonic* waveform.

More general periodic waveforms, which repeat themselves with a period  $T$  and thus have a frequency  $f=1/T$ , can be **written as a linear combination of simple harmonic modes**. There is the basic, **fundamental** mode (with frequency  $f$ ), and **harmonics** of the fundamental mode, with integer multiples of its frequency ( $2f, 3f, \dots$ ). For example, we could describe the vibrations of a tuning fork or the acoustic oscillations in a pipe this way. Mathematically, this linear combination of modes is expressed as a **Fourier series expansion**,

$$v(t) = a_0 + \sum_{n=1}^{\infty} [a_n \cos(2\pi n f t) + b_n \sin(2\pi n f t)]$$

(3)

where  $nf$  represents the frequency of the  $n^{th}$  mode ( $n=1$  for the fundamental,  $n=2$  for the first harmonic, etc.),  $a_0$  represents the steady component of the waveform, and the  $a_n, -b_n$  are the harmonic coefficients (or amplitudes) of each mode. The steady amplitude,  $a_0$ , is often called the DC component of the waveform, in reference to classical electrical power systems, which are either **Direct Current** (steady) or **Alternating Current** (sinusoidal with a zero average).

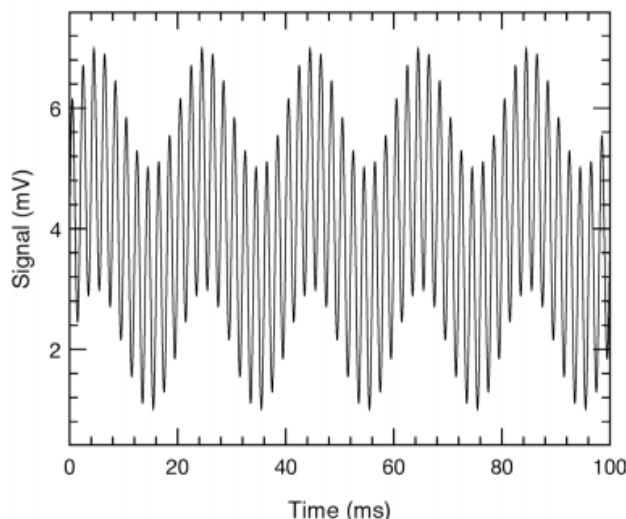


**Figure 1.** A waveform composed of a fundamental mode (at 50 Hz) and its 9th harmonic (at 10 times the fundamental frequency, or 500 Hz). The waveform also has a DC, or time-averaged, component of 4 mV.

Specifically, the signal (in millivolts) is  $4+\sin(100\pi t)+2\sin(1000\pi t)$ , or equivalently, based on cosines,  $4+\cos(100\pi t-\pi/2)+2\cos(1000\pi t-\pi/2)$ , which simply represents a phase shift of  $-\pi/2$ .

For example, Figure 1 shows a simple waveform composed of two frequencies, a fundamental mode at 50 Hz and its 9th harmonic (at 500 Hz). Thus the complete waveform is repeated every 20 ms (=1/fundamental frequency =1/50 s). The waveform shown in the figure also has a DC component. In other words, the signal has a nonzero value when averaged over its period. In general, we can write the DC amplitude as

$$a_0 = \frac{1}{T} \int_{-T/2}^{T/2} v(t) dt = f \int_{-T/2}^{T/2} v(t) dt$$

(4)

The other coefficients of the Fourier expansion are given by

$$a_n = 2f \int_{-T/2}^{T/2} v(t) \cos(2\pi n ft) dt$$

$$b_n = 2f \int_{-T/2}^{T/2} v(t) \sin(2\pi n ft) dt$$

(5)

and they can be combined into a complex number (since,  $e^{-ix} = \cos x - i \sin x$ ),

$$a_n - ib_n = 2f \int_{-T/2}^{T/2} v(t) e^{-i2\pi n ft} dt$$

(6)

The power,  $P$ , contained in single mode is given by the square of the amplitude

$$P(n) = a_n^2 + b_n^2$$

(7)

and the phase  $\phi$  (or phase angle) of a mode is given by

$$\phi(n) = \tan^{-1}(b_n/a_n)$$

(8)

A second example that shows the ability of a combination of sine waves to create an arbitrary periodic function is shown in Fig. 2. Five sine waves and a DC component (see Fig. 3) were combined to create a function approaching a square wave. While the constructed function resembles a square wave, it is clear that more sine waves would be needed to produce a sharp square wave.

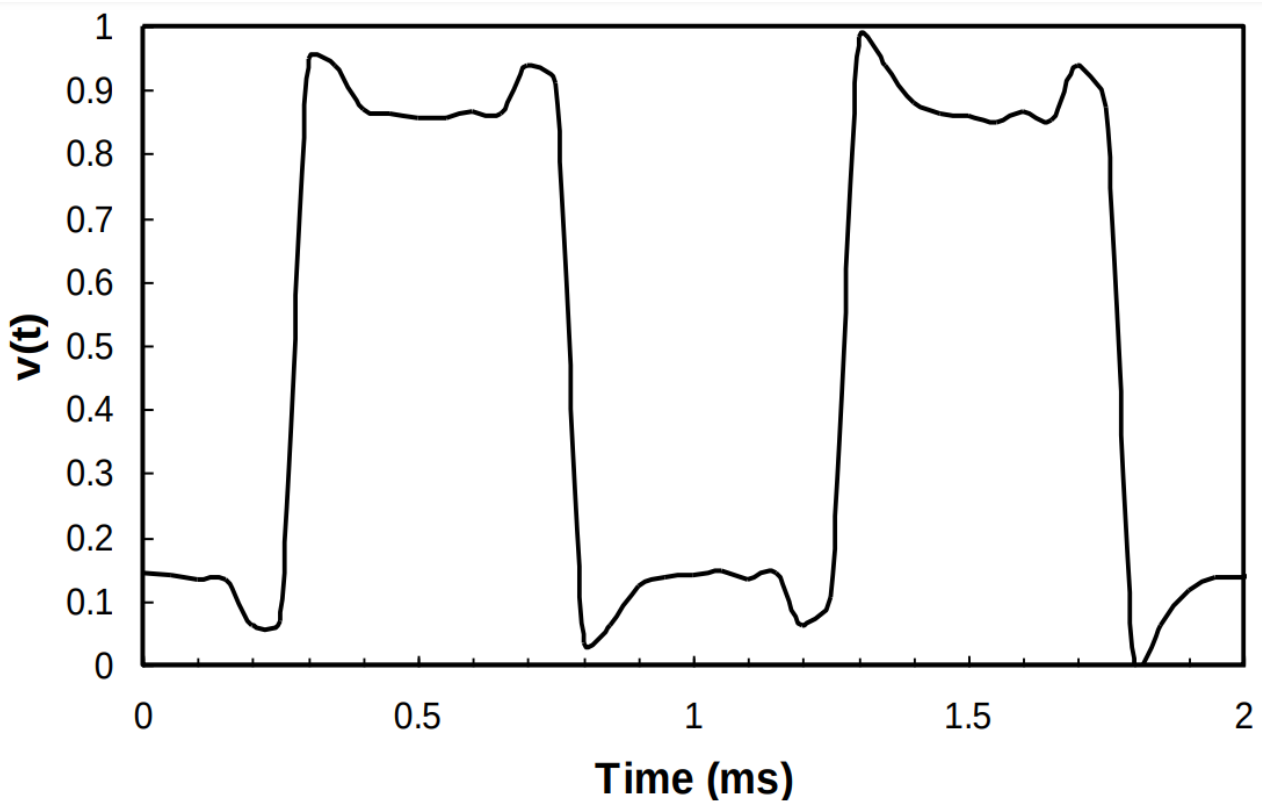


**Figure 2.** Partial reconstruction of a square wave using five sine waves, each with a different amplitude, frequency and phase, and a separate DC component. The individual waves are shown in Fig. 3.

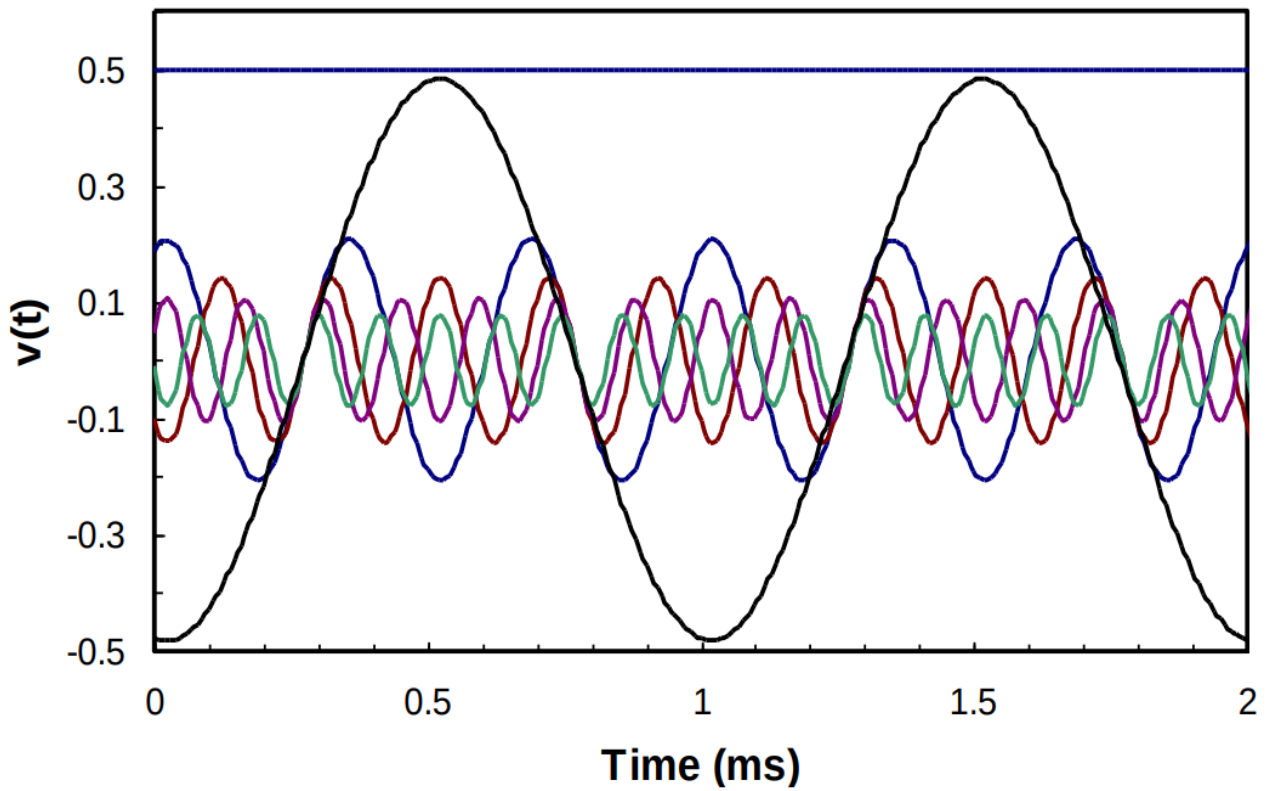


**Figure 3.** The five sine waves and constant function used to construct the square wave shown in Fig. 2.

### Fourier Transforms

The procedure outlined above for periodic functions can be extended to general functions, which are not necessarily periodic, by considering any arbitrary function to be periodic with an infinitely long period. This approach leads to the **Fourier Transform**. Given a function  $v(t)$ , its Fourier Transform  $V(f)$  is a complex function defined by

$$V(f) = \int_{-\infty}^{\infty} v(t) e^{-i2\pi ft} dt$$

(9)

in parallel to the complex Fourier function of equation (6). The function  $V(f)$  represents the **information** given by  $v(t)$  **transformed from the time domain to the frequency domain**. The transformation is nearly identical in the reverse direction, with simply a change in the phase (note the sign of the exponent), i.e.,

$$V(t) = \int_{-\infty}^{\infty} v(f) e^{+i2\pi ft} df$$

(10)

For example, Figure 4 graphically shows the Fourier transforms of various functions, including sine and cosine waves, a rectangle function ( $\Pi$ ), a triangle function ( $\Delta$ ) and a constant, or DC, function. The sine, cosine and DC waveforms result in Fourier transforms that are nonzero at a single frequency\*\*;

- ⓘ \*\*The negative frequencies relate to phase information for the sine and cosine and do not actually represent different frequencies, i.e., for real functions  $v(t)$ , it can be shown that  $|V(f)| = |V(-f)|$ . That means that if you take the absolute value of V, the part of V below 0 frequency looks like a reflection of the part for  $f > 0$ .

in other words, they contain information at only one frequency (the DC function, which does not change in time, is associated with a frequency of zero). The Fourier transforms of the rectangle and triangle functions result in *sinc* and *sinc*<sup>2</sup> functions, where  $\text{sinc}(f) = \sin(\pi f)/\pi f$ , which contains information at many frequencies, but with multiple frequency “peaks”.

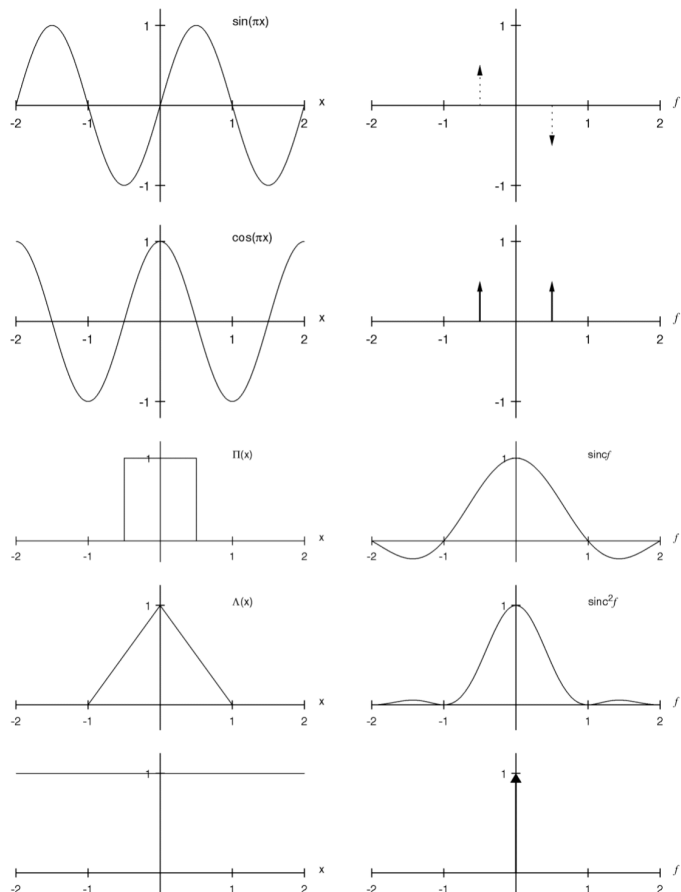


**Figure 4.** Fourier transforms of various functions (left and right pairs). The arrows represent impulse functions (i.e., delta functions), which extend infinitesimally along the x-axis, but have a integrated area corresponding to the height indicated by the arrow. The dashed regions indicate imaginary values.

Instead of looking at the Fourier transform, we often are interested in the **power spectrum** (or **power spectral density, PSD**) of a waveform. This represents the amount of power or energy in a region between  $f$  and  $f+df$ . For real (noncomplex) functions  $v(t)$ , this is given by

$$PSD(f) = |V(f)|^2$$

(11)

where it is sufficient to consider only  $0 < f < \infty$  since the PSD of a real function is symmetric about  $f=0$ .\*\*

Thus the PSD of the rectangle function,  $\Pi(x)$  as shown in Figure 4, is the square of its Fourier transform, or  $\text{sinc}^2(f)$  (also shown in Figure 4).

Extensions of the Fourier Transform method have been developed for non-continuous functions, specifically for signals that have been discretely sampled by a computer, data acquisition system, or produced by digital means. These are generally known as Discrete Fourier Transforms. In addition, methods to quickly compute the Fourier Transform have also been developed, e.g., the Fast Fourier Transform. These concepts are described in detail in references 2 and 4. The computer data acquisition system you will use employs these techniques to compute the power and phase spectra of the signals that are sampled in this lab.

### Discrete Sampling

In most situations, especially for computer-based data acquisition, the continuous function  $v(t)$  is sampled (i.e., the data is acquired) at evenly spaced, discrete intervals in time, separated by an amount  $\Delta t$ . The sampling frequency (or data acquisition rate) is thus  $f_s = 1/\Delta t$ .

For a given sampling rate, we might ask how accurately the discretely acquired data can reproduce the actual waveform being sampled. The answer depends on the frequency content of the waveform and a special frequency, called the **Nyquist frequency** ( $f_N$ ), which is half the sampling frequency, i.e.,  $f_N = f_s/2$ . If the waveform contains no components above the Nyquist frequency, then the waveform can be completely determined by the sampled data (assuming no errors in the measurement).\*\*\* This is known as the **Sampling Theorem**.

**i** \*\*\*A waveform that has information in only a limited range of frequencies is called **bandwidth limited**. Due to phase ambiguity, the sampling frequency should actually be more than twice the maximum frequency in the waveform. For example, a sine wave sampled at  $0, \pi, 2\pi$ , etc. would always have a 0 result and could be confused with a null function.

As a simple example, consider a single sine wave. If we know we are dealing with a single frequency sine wave, it takes at least two measurements per period to determine its frequency, which means we must sample at twice the sine wave's frequency. If we sample any slower, we actually infer a lower frequency than the actual frequency of

the sine wave (you will see this in the lab). This process, by which information at a higher frequency shows up at a lower frequency is known as **aliasing**.

Aliasing occurs for any sampled waveform having components with frequencies above the sampling system's Nyquist frequency, i.e., ( $f > f_N$ ). One way to remove this problem is to filter the data before it is sampled. This can be accomplished by a low pass filter, a filter that only passes frequencies below some cut-off frequency. One would set the cut-off at or below the Nyquist frequency. The high frequency information is thus removed before it can be aliased. In essence, the filter produces a bandwidth limited waveform.

## Computer Data Acquisition System

Data will be acquired with an board in a computer, utilizing a LabView™ interface. The computer data acquisition board, which measures the voltage of the input signal, essentially consists of a multiplexer, a sample-and-hold device, an analog-to-digital converter, a memory buffer, an interface to the computer's memory, a master clock, and controller (see Figure 5).

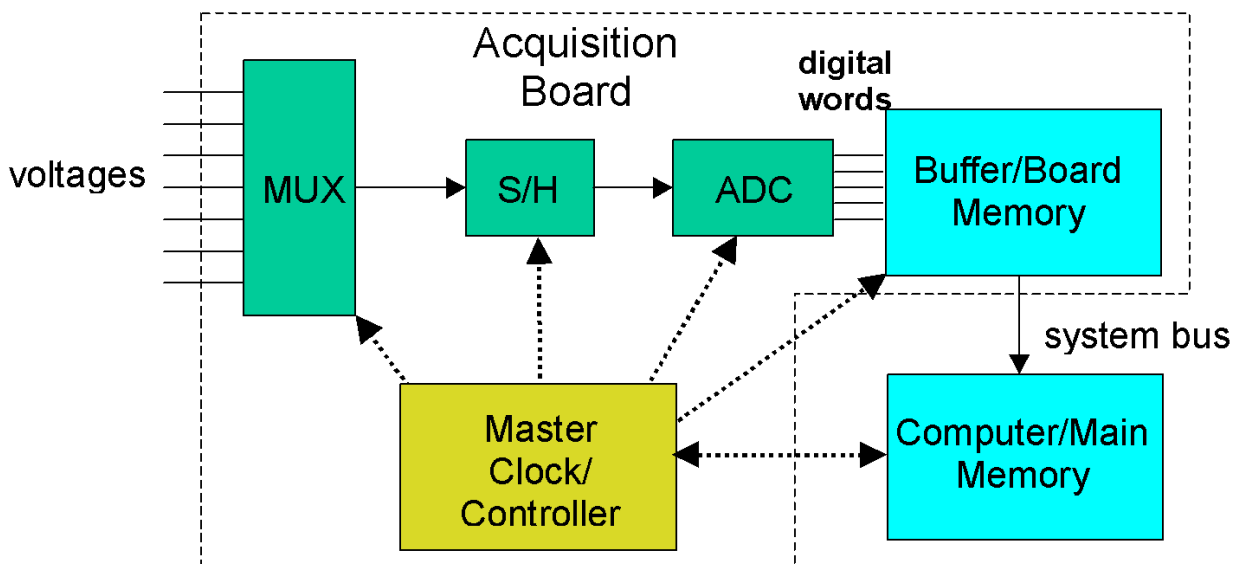


**Figure 5.** Schematic of multiplexed, sequential sampling, computer data acquisition board and its connection to the computer.

The *multiplexer* (MUX) is a switch that connects one of a number of input channels (usually numbered starting at 0) to the *sample-and-hold* (S/H). The input voltage on the channel switched by the MUX "charges up" the sample-and-hold during some time interval, which is a fraction of the sampling period (the time between samples). This circuit is then disconnected from the input voltage, and some of the stored charge is drained from it. From this charge, the original voltage value connected to the S/H is determined, and the result is converted to a digital value by the *analog-to-digital converter* (ADC). The digital value (sometimes referred to as a "word" of data depends on the input voltage, the *voltage range* of the ADC (the *minimum* and *maximum* voltages it reads, e.g., 0-5 V), and its digital dynamic range (number of "bits" =  $N$ ). The relation between the digitizer output and the voltage input is given by

$$output = \frac{input - minimum}{maximum - minimum} \times (2^N - 1)$$

(12)

where *output* has to be an **integer value**. For example, consider a 2 V input into an ADC with a 0-10 V range, and an 8-bit digitizer ( $2^8$  possible values, or digital values of 0-255). The output of the ADC would be a digital value of 51. The digital result is then moved to the buffer memory on the board, and shifted to the computer memory, usually through the computer's *direct memory access* (DMA) system.

Multiple signal inputs are recorded by using the MUX to cycle through each of the input channels at a rate that must be faster than the overall sampling rate (how often a given channel is read) times the number of input channels being read. In the sequential sampling system illustrated in Fig. 5 (and which is representative of the system you will be using), note that the channels are *not read at exactly the same time*. There is a time delay (**skew**) between when one channel and the next is read. The skew determined by the maximum switching and reading rates of the MUX, S/H and ADC. This is illustrated in Fig. 6. Simultaneous data acquisition systems, which have negligible skew, typically employ multiple, synchronized S/H systems just upstream of the MUX (see Fig. 7).

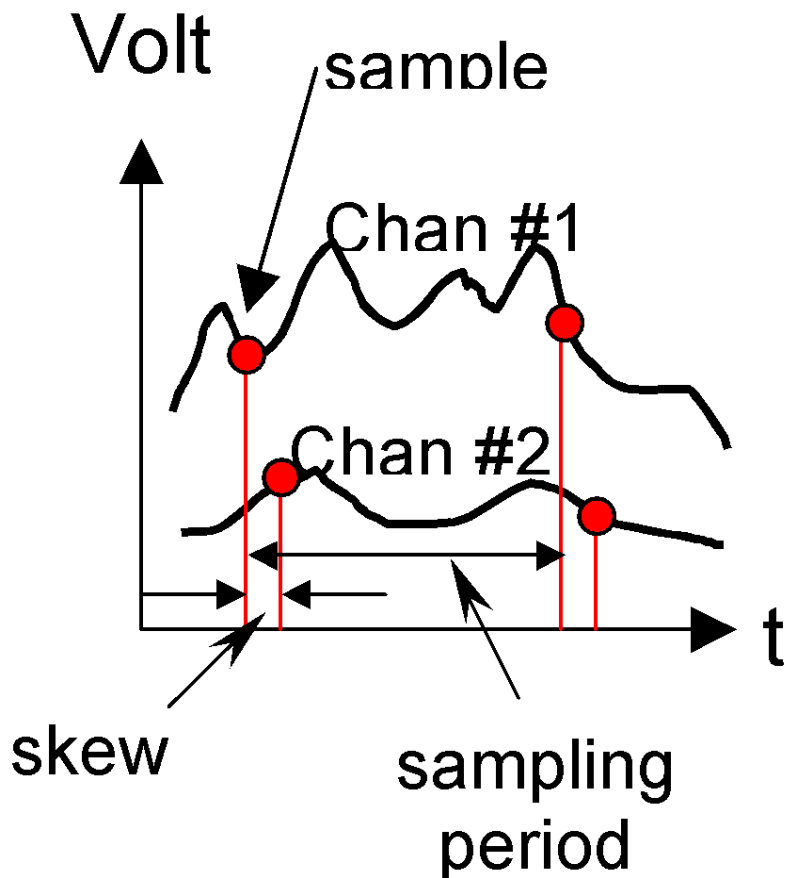
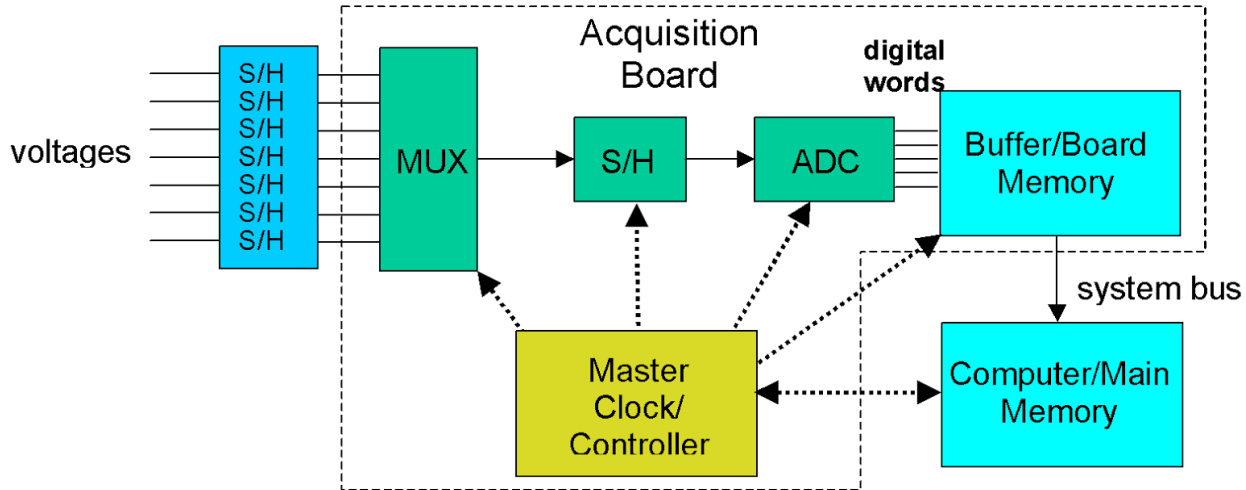


Figure 6. Time delay (skew) between successive channels in sequential sampling system.



**Figure 7.** Schematic of simultaneous sampling, computer data acquisition system.

In this lab, you control the data acquisition process through a software interface called a LabView *virtual instrument* (VI). The VI creates a display on the computer screen that lets you think of the data acquisition system as a box with “knobs”, “dials”, and other displays. For this experiment, the VI allows you to control parameters such as the minimum and maximum voltages read by the acquisition board, the sampling rate ( $f_s$ ), and the number of samples recorded.

You will also use an analog, electronic filter manufactured by Krohn-Hite. It actually contains two filters, which separately can be switched to be either low pass or high pass filters. The cutoff-frequency of each is also adjustable, using a combination of a dial and multiplier setting. You will be examining the effects of the filters on the following time-dependent signals:

[Track 1](#)

01 Track 01.m4a - 755KB

[Track 2](#)

02 Track 02.m4a - 828KB

[Track 3](#)

03 Track 03.m4a - 796KB

[Track 4](#)

04 Track 04.m4a - 717KB

[Track 5](#)

05 Track 05.m4a - 704KB

[Track 6](#)

06 Track 06.m4a - 732KB

 Track 7

07 Track 07.m4a - 926KB

 Track 8

08 Track 08.m4a - 866KB

 Track 9

09 Track 09.m4a - 740KB

 Track 10

10 Track 10.m4a - 780KB

 Track 11

11 Track 11.m4a - 242KB

## Procedure

-  If you are a remote student, or an in-person student who wishes to watch in addition to attending in person, open up the [pre-recorded lab video](#) to supplement this procedure.

1. Connect the audio player's output to the computer data acquisition system (analog input, channel 0), and *in parallel* (using a T-connector) to the oscilloscope. Locate the mp3 files containing the waveforms; you will use audio player software to play each track. Each track contains a different periodic signal. The signals include: **single sine waves**; a **sum of sine waves** (e.g.,  $b_1 \sin(2\pi f_1 t) + b_2 \sin(2\pi f_2 t)$  where  $f_1$  and  $f_2$  are different frequencies), a **product of sine waves**, and periodic waveforms that are not sine waves: **square waves**, **triangle waves**, and **ramps**. Some tracks also have "noisy" signals.
2. Start the LabView VI; use it to set the sampling rate to 22 kHz (22,000 sample/sec) and the number of samples recorded to 6000. Set the output (volume) level somewhere between its middle and high range. Make sure the VI is acquiring data.
3. View the output of each track on the oscilloscope and observe the corresponding power spectrum. Take notes that describe what you see on each track. Your goals are to identify the waveform on each track and its frequency(s). Looking at the power spectrum, it might help to note how many "peaks" show up, the approximate frequency associated with each peak, and if there are multiple peaks how their "heights" vary qualitatively. If you have time, try listening to each waveform on the speakers.
4. Find the track containing the simple harmonic waveform (a single sine wave) at  $\sim 1$  kHz. Set the sampling rate to 10 kHz. Then acquire data for at least five different record lengths (i.e., the number of samples acquired). Before you pick your record lengths, read your goals below. (Note, you might want to use the **hold button** on the VI to stop the data acquisition process each time after you change the acquisition parameters.) Observe the power spectra and the time traces of the sampled signal. For each record length, determine the

resolution and the number of data points in the spectrum (the VI plots the spectrum as straight lines connecting data points). Record sufficient data to: 1) verify the rule ***resolution = 1 / (recording time)*** where the *resolution* of the power spectrum is the spacing between points in the spectrum, and *recording time* is how long you spend taking data from when you start to the last sample in your record; and 2) determine a rule for the number of data points in a power spectrum as a function of number of samples acquired.

5. For the same ~1 kHz waveform, acquire power spectra for the following eight sampling rates: 2500, 2000, 1500, 1200, 1000, 800, 675 and 665 Hz. For each sampling rate, set the number of samples acquired to the same value (e.g., at 2000 samples/sec acquire 2000 samples). Record at what frequency the peak occurs in the Fourier spectrum (i.e., the frequency with the maximum power). You are determining how the 1 kHz peak is being **aliased**. Try to predict the frequency where the peak will show up (i.e., where it will be aliased) for at least two more additional sampling rates below 650 Hz. Then acquire data at those rates.
6. Remove the BNC cable from the oscilloscope and connect it to the input connector on the filter. Connect the output of the filter to the second analog input channel (channel 1). Set the filter to be a lowpass filter. Use the audio player controls to pick the track containing the sum of three sine waves at three frequencies. With the VI, set the sampling rate to 18 kHz (per channel) and to record both channels (0 and 1). Acquire data with the lowpass filter's cutoff frequency between 1 kHz and 10 kHz, and compare the power spectra from the filtered and unfiltered signals. The goal is to find the maximum cutoff frequency required to remove any noticeable aliasing problems.
7. Without changing the track being played, set the sampling rate to 22 kHz and the lowpass filter cutoff frequency to 10 kHz. Observe the phase plots (phase versus frequency) for the filtered and unfiltered signals. Look only at the phases for the (3) frequencies that showed peaks in the power spectrum. Record the phases at these frequencies for the filtered and unfiltered signals to see if there are any differences.
8. Use the audio player to play the track with the rapidly sweeping frequency that repeats itself a number of times). Set the sampling rate to 6 kHz and the number of samples (per channel) to 3,000. With the cutoff frequency of the filter set to 800 Hz, acquire (**and save on the computer** using the button on the VI) power spectra for both the filtered and unfiltered channels. The acquire spectra averaged over 10 measurements (the VI has an averaging control entry) and save these too. **Make sure you are displaying the power spectra with a linear scale rather than a dB (log) scale before saving the data.**
9. Remove the output of the lowpass filter from channel 1 and instead connect the filter output to the input of the second filter, and set the second filter to be a highpass filter. Then connect the output of the highpass filter to channel 1 of the computer data acquisition system. Change the track to play the waveform that contains significant amounts of noise on top of a single frequency sine wave. Vary the cutoff frequencies of the two filters and observe the effect on the data acquired. Determine what pair of cutoff frequencies is best able to reduce the noise on the signal without "hurting" the sine wave.

---

## Data to be Taken

1. A **short** description/identification of each track's waveform.
2. The number of data points (frequencies) in the Fourier Transform-based power spectrum for the different record lengths, and its resolution for the different recording times.
3. For the 1 kHz sine wave, the frequency with the peak power for each of the (at least) 10 sampling frequencies.

4. For the waveform with three frequencies (and the sampling frequency of 18 kHz), determine the maximum filter frequency that is able to produce a faithful record of the frequency content of the waveform *without aliasing*.
  5. For the waveform with three fixed frequencies (sampled at 22 kHz and the filter set to 10 kHz), the corresponding phases at each of the three frequencies for both the filtered and unfiltered channels.
  6. For the waveform with the rapidly sweeping frequency, power spectra for both the filtered and unfiltered signals, and both **spectra from a single acquisition run, and the average of 10 spectra**.  
*(Only this last item requires you to store data on the computer. However if you wish, you may store results, e.g., spectra, for other measurements you were required to take.)*
  7. The “best” bandpass filter frequencies for removing noise from the single-frequency sine wave.
- 

## Data Reduction

1. Calculate the ratio of the power spectra for the filtered data (i.e., the output from the filter) and unfiltered data (i.e., the input to the filter) recorded in step 6 of the Data to be Taken section. Thus you can find the Transfer Function of the filter (output/input at each frequency).
- 

## Results Needed for Data Report

**Note: This is a Data Report, so you must follow instructions on how to prepare the Data Report (not the FORMAL report) on the Canvas course page. Also, be sure to answer any supplemental questions listed on Canvas for this lab.**

1. A table that identifies the contents of each track of the mp3 files.
2. A data plot showing the number of points in the acquired power spectra for the different number of samples recorded, and a general equation you could use to predict the number of points as a function of the number of recorded samples.
3. A data plot showing the frequency resolution as a function of the different recording times.
4. A plot of the frequency of the peak in the power spectrum as a function of sampling frequency for the aliased simple harmonic waveform.
5. The maximum filter frequency required to prevent aliasing of the data for the waveform with three fixed frequency modes.

6. A table of the chosen “optimum” bandpass filter frequencies for removing noise from a sine wave.
  7. Plots of the single and average power spectra, filtered and unfiltered, for the waveform with the rapidly sweeping frequency.
  8. A plot of the filter transfer function described in step 1 of the data reduction, based on the average results.
- 

## Further Reading

1. R. V. Churchill and J. W. Brown, *Fourier Series and Boundary Value Problems*, 3rd ed., McGraw-Hill, 1978.
2. R. N. Bracewell, *The Fourier Transform and Its Applications*, 2nd ed., McGraw-Hill, 1978.
3. T. G. Beckwith, R. D. Marangoni and J. H. Lienhard V, *Mechanical Measurements*, 5th ed., Addison-Wesley, 1995.
4. W. H. Press, S. A. Teukolsky, W. T. Vetterling and B. P. Flanner, *Numerical Recipes - The Art of Scientific Computing*, 2nd ed., Cambridge University Press, 1992.

# Subsonic Wind Tunnels

## Objective

The primary objective of this experiment is to familiarize the student with the measurement of static and stagnation pressures, and (indirectly) velocity, in a subsonic wind tunnel. Static taps and stagnation (Pitot) probes will be used to measure pressures on the surface of a 2D airfoil, in the wake region behind the airfoil and in a boundary layer next to the wind tunnel wall. In addition, this lab demonstrates some techniques used in flow visualization, specifically tufts (attached to the airfoil) and smoke visualization (in a separate wind tunnel). Students should gain experience in observing flows and drawing conclusions about them from the observed behavior.

---

## Background

### The Aerodynamic Problems

#### i) Airfoil Surface Pressure Distribution

When a 2D airfoil is placed in a uniform subsonic freestream, the flow velocity near the airfoil is modified and, as evidenced by the Bernoulli equation, so is the local static pressure. The resulting chordwise pressure distribution on the surface of the airfoil may be calculated by various methods using an inviscid fluid model.\* At moderate angles of attack, the flow accelerates over the upper surface of the airfoil, the surface static pressure is less than freestream over most of the chord, and the pressure coefficient, which is defined as

$$C_p = \frac{p - p_\infty}{q_\infty}$$



\*From AE 3030 and Chapter 4 (Fig. 4.25) in Andersen's Fundamentals of Aerodynamics

along the airfoil upper surface has mostly negative values. Normally, there is a large suction peak (large negative value of  $C_p$ ) very near the leading edge on the upper surface, followed by a region of increasing static pressure (adverse pressure gradient) from there to the trailing edge. On the lower surface of the airfoil, there is a stagnation point near the leading edge, where  $C_p = 1.0$ , and the flow accelerates thereafter. When the two pressure coefficient distributions are plotted versus chordwise location, ( $x/c$ ), the area between the two curves is a measure of the normal force coefficient on the airfoil and hence of the airfoil lift coefficient.

As the angle of attack is increased, the suction peak on the upper surface grows larger and the adverse pressure gradient becomes larger as well. At some value of angle of attack, the adverse pressure gradient on the airfoil

upper surface becomes strong enough that the boundary layer separates from that surface. At a sufficiently high angle of attack, the oncoming freestream flow perceives a radically modified airfoil shape. The resulting effect is termed airfoil (or wing) stall, and the included area between the upper and lower pressure distribution curves collapses. The presence of stall was evident in the force measurements on the airfoil that were conducted in a previous laboratory.

The airfoil used in this experiment (see Figure 1) has an NACA 64212 section. The chord is 14 inches and it has a thickness ratio of 14%. The airfoil extends from one side wall of the wind tunnel to the other. Therefore, it should behave like a 2-d airfoil.



**Figure 1.** Two-dimensional wing showing pressure tap locations (light colored line at centerline of airfoil), red tufts used to visualize separation and tubing used to connect pressure taps to Scanivalve.

## ii) Velocity Profiles in a Boundary Layer and Wake

In the flow of a viscous fluid such as air, the flow velocity right at a solid surface is zero; i.e., the fluid can be thought of as adhering to the surface (the *no slip condition*). Within a small interval above the surface, the flow velocity increases rapidly from zero to a value that is of the order of the freestream velocity. The result is a velocity profile which exhibits a large velocity gradient in the direction normal to the surface. This velocity gradient gives rise to significant shear stresses, and the region within which this takes place is termed a **boundary layer**. Using boundary layer theory\*\* one may show that the static pressure is constant through the boundary layer in a direction normal to the surface and that the boundary layer is a region of rotational flow so that the stagnation pressure is not constant everywhere. However, the Bernoulli equation may be used locally to find the dynamic pressure distribution within the boundary layer and hence the velocity profile *if the flow is incompressible*.

(i) \*\*See your textbook from AE 2010 and 3030. It would be helpful if you review this material before coming to the lab if you do not know what the velocity profile in the boundary layer looks like.

In the case of viscous flow over an airfoil at a moderate angle of attack, the attached boundary layers on the upper and lower surfaces join at the trailing edge. The resulting viscous-dominated flow region downstream of the trailing edge is termed a **wake**, within which there is a velocity deficit compared to the freestream. This deficit is a result of the flow being retarded in the airfoil boundary layers.

## iii) Visualization of Flow Around Bodies

Aerodynamics is a difficult science because the medium with which the aerodynamicist works (air) is not visible under normal conditions. Valuable insights into the physical features or behavior of an air flow can be achieved if the entire flow field or certain regions, e.g., streamlines (or streaklines or pathlines) could be seen by the eye or by a recording device. If the flow could be made visible by some kind of flow visualization technique, then it would be possible to observe flow phenomena which are essentially inviscid (e.g., vortical flows, flows distant from surfaces) as well as those phenomena which are dominated by the effects of viscosity (e.g., **flow separation** and **wakes** behind bodies).\*\*\* Flow visualization in air may be broadly divided into surface flow visualization and off-the-surface visualization. Surface flow visualization methods include **tufts** (seen on the airfoil in Figure 1), fluorescent dye, oil or special clay mixtures that are applied to the surface of a model. Visual inspection of such tufts and coatings as a function of time, or after some time, will give valuable information on such things as the state of the boundary layer (laminar or turbulent), transition, regions of separated flow and the like. It must be remembered in such visualization that what is observed on the surface is not always indicative of what is happening away from the surface.

- ⓘ \*\*\*In addition to qualitative observations, under certain conditions it is possible to make quantitative measurements from flow visualization data as well. For example, a measurement of the distance between streamlines in a 2-D incompressible flow provides information on velocity ratios in the flowfield.

The second type of visualization is off the surface and involves the use of such tracers as smoke particles, oil droplets or helium-filled soap bubbles. The visualization medium must faithfully follow the flow pattern or it is not conveying the correct information. Smoke particles and oil droplets are very small and are light enough such that they will often follow the motion of the flow; soap bubbles are small and can be filled with helium to make them neutrally buoyant. Each of these methods requires appropriate lighting and some device for recording the image, such as the human eye or a camera. If the flowfield is illuminated in a plane by appropriate masking of the light source it is possible to examine discrete sections or slices of the flow. For example, a laser light beam can be expanded into a thin sheet by passing it through a cylindrical lens. This sheet then can be used to illuminate any cross-section of an airflow that has been seeded with particles. The laser light will reflect from the particles, but dark images will be observed where there is an absence of particles, such as in the center of a vortex. A vortex core is almost void of particles since they have been spun out by the action of centrifugal force.

## Measuring Devices

### i) Pressure Taps and Probes

The surface pressure distribution on an airfoil will be measured by means of 24 static pressure **taps**. These are small holes on the surface of the model that are connected to stainless steel tubes within the model and thence to plastic tubing. The pressure taps on the airfoil are located on the upper and lower surfaces in the chordwise direction at mid-span. The plastic tubing from these orifices is connected to a pressure transducer.

The local velocity in the boundary layer on the ceiling of the wind tunnel and in the wake behind the airfoil will be measured indirectly by traversing a Pitot\* tube through the region so as to measure local stagnation pressure; the velocity follows directly because the flow is incompressible. Since the static pressure is constant throughout the ceiling boundary layer, a single static tap on the ceiling (ideally at the measurement station) will yield the local

static pressure anywhere in the boundary layer at that station. In the wake region, the local static pressure will be approximately constant through the wake and will be equal to the freestream static pressure. This is because the wake measurement station is located sufficiently far downstream of the airfoil that the pressure disturbance due to the airfoil is negligible.



\*Named after its inventor, Henri Pitot (1695-1771), a French hydraulic engineer.

The end of the Pitot probe is made of thin stainless steel tubing with a 0.063 inch outer diameter (OD) and a small orifice, so that the Pitot pressure data is a local measurement compared to most other dimensions.

Generally Pitot probes such as ours may be oriented a few degrees (say 5-10 degrees) away from the local flow direction without any appreciable change in the measured pressure, hence a precise alignment of the probe with the local flow direction is not required. A Pitotstatic probe (a Pitot tube with a downstream static pressure tap oriented normal to the stagnation hole) located upstream of the airfoil will be used to measure freestream dynamic pressure.

## ii) Pressure Transducers

A pressure transducer is a device that converts a pressure to a quantity that may be readily measured. For example, a traditional U-tube manometer is a pressure transducer, where pressure difference is interpreted as the height of a column of liquid. This is an example of devices known as gravitational transducers. Modern electronic transducers, which convert pressure into a voltage that may be easily measured by means of a digital voltmeter or an analog-to-digital converter (ADC), are typically elastic transducers. The most common types of electronic pressure transducers use the deformation of a diaphragm or similar structural element to sense pressure. †



† A common pressure transducer for rapidly changing conditions, based on the piezoelectric effect, will be introduced in later labs.

We can categorize this type of pressure transducer by the way the deformation of the structural element is transformed into an electrical signal. The two most common approaches are *strain gage* and *capacitance* type transducers. A strain gage pressure transducer consists of a thin circular diaphragm on the bottom of which are bonded tiny strain gages wired as a Wheatstone bridge. When the diaphragm experiences a pressure on its exposed upper surface that is different from the pressure in a small cavity under the diaphragm it deflects, and the resulting bridge imbalance is a measure of the deflection. Calibration provides the constant of proportionality between bridge imbalance (interpreted as a voltage) and applied pressure. The voltage output of this type of transducer is usually in the millivolt (mV) range and requires amplification prior to measurement. Relatively inexpensive transducers can be made by using semiconductor materials. In this case, the semiconductor resistors are "written" as a bridge circuit directly onto a substrate (e.g., silicon) that acts as the diaphragm. The strain on the semiconductor results in a change in semiconductor resistance; this is known as the *piezoresistive effect*. The change in semiconductor resistance is analogous to the change in metal resistors, except in for metal resistors, the change in resistance is *primarily* due to the change in the resistor's cross-sectional area as it is strained. For

semiconductor materials, the resistance change is related to other changes in the internal structure of the semiconductor.

The capacitance-based pressure transducer has a stretched membrane clamped between two insulating discs, which also support capacitive electrodes. A difference in pressure across the diaphragm causes it to deflect, increasing one capacitor and decreasing the other. These capacitors are connected to an electrical, alternating-current (AC) bridge circuit, producing a high level of voltage output (usually 10 Volts full scale without amplification).

Strain gage transducers can be made small, hence they can be internally mounted in a wind tunnel model. Also, they have reasonably good frequency response because of the small mass of the diaphragm and the short distance between the pressure tap and the diaphragm face. Capacitance transducers usually are not well suited for internal mounting (too large) and such systems do not have a fast response. Both types of transducers can be calibrated using a primary pressure standard such as a dead-weight tester, which supplies a pressure of precisely known magnitude, or using another (already) calibrated pressure transducer. In this lab, you will use both *capacitance* type and semi-conductor *strain gage* transducers to measure pressure.

### Baratron

This is a capacitance-based transducer (of a specific brand name) to measure freestream dynamic pressure. The Baratron has internal signal conditioning electronics, with an output of 10 Volts at its maximum differential pressure, e.g., 10 Torr, which you can usually find by inspecting the Baratron's label. For this device, the differential pressure  $\Delta p$  is assumed to be related to the transducer voltage  $V$  by the relation

$$\Delta = R \times V$$

(1)

where  $R$  is the responsivity of the transducer, e.g., 1 Torr/V.

### Barocel

You will use a second capacitance transducer of a slightly different design (see Figure 2) for converting the pressure from the traversing Pitot probe. The Barocel has signal conditioning electronics that also provide an approximately 10 V full-scale signal at some maximum differential pressure. However, this maximum pressure can, in essence, be adjusted with a range switch located on the front-panel of the transducer power supply unit. The range switch, which actually controls the signal amplification, can decrease the **full-scale** differential pressure by a factor of 10,000 over the maximum pressure setting. Thus smaller pressure readings can be made to produce the full 10 V signal. Other controls on the power supply unit allow you to determine the full-scale output voltage range,  $\Delta V$  (not exactly 10 V), that corresponds to the full-scale pressure range, and to adjust the voltage output at a zero differential pressure, i.e., adjust the **zero offset** of the transducer  $V_{p=0}$ . For this transducer, we must recognize that

$$\Delta = R \times (V - V_{p=0})$$

(2)



**Figure 2.** Picture of the Barocel transducer.

### Scanivalve

This is a bank of piezoresistive pressure transducers you will used to simultaneously measure the 24 pressures on the airfoil surface. The Scanivalve system (Model DSA 3217/16PX) is composed of two units (see Figure 3), each having 16 differential pressure transducers with a maximum pressure range of 0.18 psi (or 5" H<sub>2</sub>O). The average linearity error for the pressure transducers, as determined by the manufacturer, is  $\pm 0.03\%$  of full-scale. Each unit has its own analog-to-digital converter and controller that converts the measured voltages into pressures based on a stored set of calibrations. The units are connected to our data acquisition computer via ethernet.



**Figure 3.** Picture of the two Scanivalve units.

### iii) Traverse

The Pitot probe is clamped onto a traveling nut that moves along a lead screw mounted vertically on the top of the wind tunnel test section (see Figure 4). The lead screw is driven by a stepper motor, which is a pulsed direct current (DC) motor capable of shaft rotation in either direction. Each pulse sent from a controller to the motor causes the motor to rotate 1.8 degrees (this value is specific to the stepper motor used in this lab) and stop. It is held at the new position with a holding torque. Upon command, the computer sends a signal to an interface card that then instructs the controller to send a pulse to the motor. The stepper motor used here can be pulsed at a maximum rate of 2000 steps (or equivalently, 10 revolutions) per second. The pitch of the lead screw, i.e., the number of revolutions of the lead screw needed to advance the traveling nut precisely one inch, is known. Thus, a simple calculation indicates the number of pulses needed to move the probe a required distance.

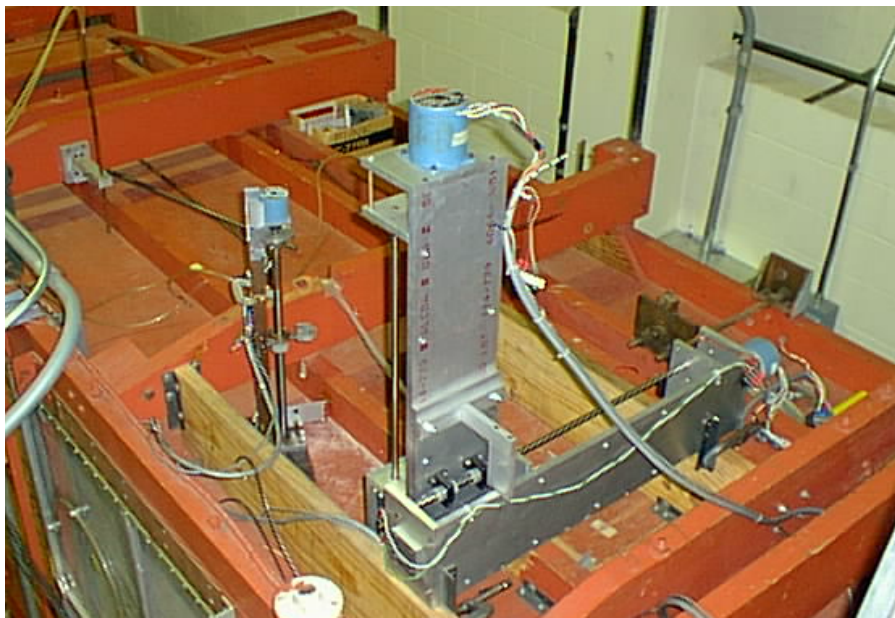


**Figure 4.** Traverse, located on top of windtunnel, used to move Pitot probe for boundary layer and wake surveys.

#### iv) Smoke Tunnel

This is a two-dimensional wind tunnel (see Figure 5) with a test section that is 48 inches high, 36 inches long, and 2.5 inches deep. The sides of the wind tunnel are made of glass. Air is pulled through the test section at a low velocity (maximum 29 ft/sec) by means of a small blower at the exhaust end of the tunnel. The test section is lit with floodlamps from the top and bottom. Smoke is generated in a reservoir, which is located in a compartment beneath the wind tunnel. Oil in the reservoir saturates a wick wrapped around a wire heating element that vaporizes the oil. An air tube, which originates from the downstream end of the blower, forces air through the reservoir and picks up the oil producing a fine smoke. The reservoir is connected to a streamlined feeder pipe that stands vertically in the middle of the flow at the upstream end of the wind tunnel test section. This feeder pipe spans the height of the test section and includes 25 small tubes spaced 3/4 inch apart that protrude from the downstream side of the feeder pipe. Smoke emerges from these small tubes and enters the main airstream, so that at the test section entrance an observer sees the flow streamlines as discrete narrow bands of white smoke. Various models may be mounted in the test section and the resulting flow patterns formed by the streaklines can be observed (or recorded by a camera). The flow velocity is kept low so that the smoke particles in the freestream will stay in layers or lamina and maintain their identity; smoke in turbulent flow tends to dissipate and makes observation difficult.

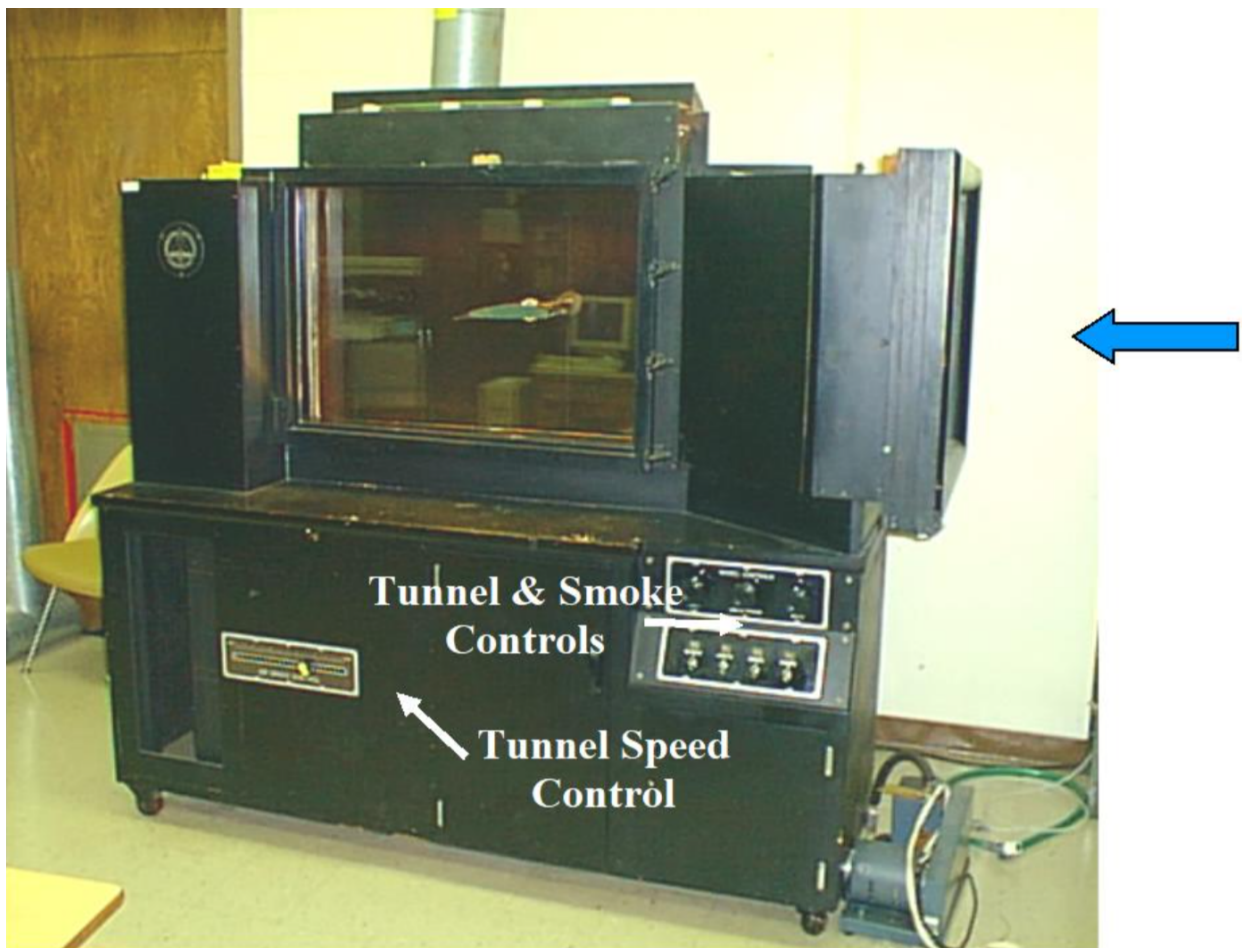


Figure 5. Smoke tunnel (flow is right to left).

## The Wind Tunnel

A wind tunnel is a duct or pipe through which air is drawn or blown.\* The Wright brothers designed and built a wind tunnel in 1901. The basic principle upon which the wind tunnel is based is that the forces on an airplane moving through air at a particular speed are the same as the forces on a fixed airplane with air moving past it at the same speed. Of course, the model in the wind tunnel is usually smaller than (but geometrically similar to) the full size device, so that it is necessary to know and apply the scaling laws in order to interpret the wind tunnel data in terms of a full scale vehicle. The wind tunnel used in these experiments is of the openreturn type (Figure 6). Air is drawn from the room into a large settling chamber (1) fitted with a honeycomb and several screens. The honeycomb is there to remove swirl imparted to the air by the fan. The screens break down large eddies in the flow and smooth the flow before it enters the test section. Following the settling chamber, the air accelerates through a contraction cone (2) where the area reduces (continuity requires that the velocity increase). The test (working) section (3) is of constant area ( $42'' \times 40''$ ). The test section is fitted with one movable side wall so that small adjustments may be made to the area in order to account for boundary layer growth, thus keeping the streamwise velocity and static pressure distributions constant. The air exhausts into the room and recirculates. The maximum velocity of this wind tunnel is  $\sim 50$  mph, and the turbulent fluctuations in the freestream are typically less than 0.5% of the freestream velocity. Thus, it is termed a "low turbulence wind tunnel."



\*Anderson, p. 123

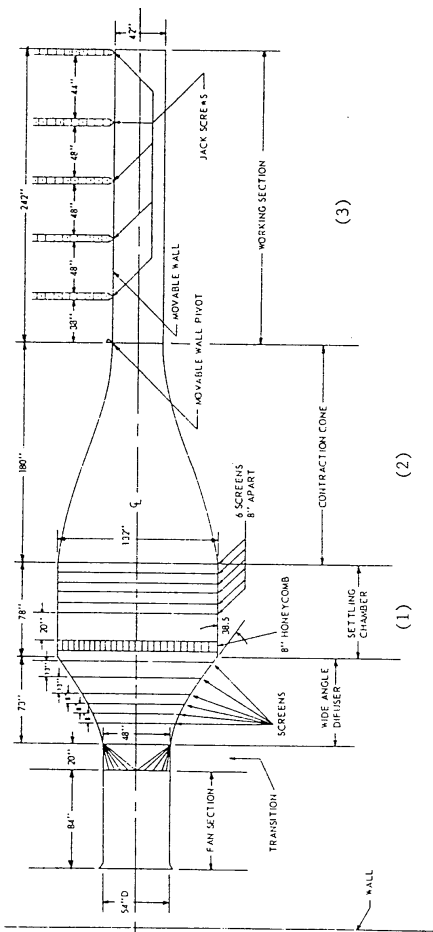


**Figure 6.** Georgia Tech low turbulence wind tunnel.

- ⓘ If you are a remote student, or an in-person student who wishes to watch in addition to attending in person, open up the [pre-recorded lab video](#) to supplement this procedure. Note: This semester, there are NO in-person labs because of health protocols (safe social distancing cannot be maintained in this lab environment of the wind tunnel).

## Low Speed Wind Tunnel Measurements

### Procedure

For all the measurements with the wind tunnel operating, you will use the same wind tunnel speed. Use a value of 35 mph, unless the TA's suggest a different value. Make sure to **record the pressure and temperature in the room** so that you can convert the dynamic pressure recorded from the Baratron to a wind tunnel velocity.

## Barocel Range Adjustment and Zeroing

1. Run the “calibration” procedure on the computer menu.
2. First, using the computer, you will determine the voltage range (“full-scale” minus “zero” voltage output) of the Barocel. The computer will instruct you to a knob on the front-panel of the Barocel’s power supply unit (located in the equipment rack).
3. Then you will set the Barocel’s amplifier (denoted “range”) to the appropriate setting – typically  $\times 0.3$  for this experiment (ask the TA if this is still the correct setting). This lets you adjust the pressure range of the Barocel to the maximum pressure difference you expect to measure in the experiment. At a gain setting of  $\times 1.0$ , the maximum voltage output from the amplifier corresponds to the maximum pressure range of the Barocel (usually recorded on the cover plate of the Barocel transducer).
4. Next you will adjust the zero offset, i.e., adjust the output voltage to be zero when the pressure difference across the Barocel is zero. To properly perform this procedure, you will **need to set up the system to produce a zero pressure difference across the Barocel input ports**. Then you can adjust the offset to zero using the needle gauge and record the value on the computer.

## Surface Pressure Distribution

1. The airfoil used in this experiment will already be mounted in the wind tunnel, and the airfoil pressure taps will already be connected to the Scanivalve system. Make sure the wall surface static pressure tap, which is on the ceiling of the tunnel and supplies the freestream pressure,  $p_x$ , is connected to both Scanivalves.
2. Use the computer data acquisition system to perform the surface pressure measurements. (*Don’t forget to turn the wind tunnel on before taking data!*) The computer will record the airfoil pressure differences a large number of times (the number of samples will be stored in the computer output file). Then the computer will calculate the average and root-mean-square (rms) of the values and store the result for a single pressure tap. You will manually set the airfoil at **three different geometric angles of attack**, one of which should be zero. (You may find it easier to change the airfoil angle with the wind tunnel off, though this is not required.) You may also wish to use observe the tufts on the airfoil to observe flow separation at the higher angles of attack – you can even use this to check whether your chosen angles of attack are “interesting.”

## Pitot Probe Surveys

1. Make sure someone has **connected the Pitot probe** and the wall surface static pressure tap to the Barocel.

*While the boundary layer survey is described first below, you may perform the wake survey first if the Pitot probe is already located in the wake region.*

1. The Pitot probe, also already mounted in the tunnel, will be traversed from the ceiling of the wind tunnel out a distance of three inches in order to **survey the ceiling boundary layer**. The boundary layer is very thick at this location since it has been growing along a considerable length from the wind tunnel settling chamber through the converging section to the measuring station. Make sure you start by manually locating the Pitot probe tip at the edge of the wall. To do this, you will adjust the location of a mechanical stop on the lead screw/Pitot probe system. This is the location the computer denotes as “y=0”.
2. Use the data acquisition program to traverse the probe and take data. After the probe has been moved to a new location away from the wall, denoted  $y$ , the software allows a short time for the pressure to settle out and then record a number of samples (storing the number of samples, the average and rms in the output file)

to evaluate the Pitot pressure. In order to take a data point it is necessary to input the desired value of  $y$ . Start by taking data with the probe tip nearly at the edge of the wall, i.e., at  $y=0$ .

3. You need to make measurements at a total of 18  $y$  values: 16 unique  $y$ 's and 2 *repeats*. Your lab group should agree on these values. The first value, as noted above should be next to the wall and there should also be some values near 3.0 in., since this is known to correspond roughly to the edge of the boundary layer. As the data are being taken, the computer screen will show a plot of the velocity and position that is updated every time a data point is taken. The two repeat values are taken so that you can observe the repeatability of the data. *Make the two repeat measurements at the end of the boundary layer survey.* One of the repeat points should be near the inner edge of the boundary layer (somewhere near, but not necessarily at, the wall) and one should be closer to the outer edge of the boundary layer.
4. The probe also will be traversed to **survey the wake region behind the airfoil**. First, manually set the airfoil at 8 degrees angle of attack. You will need to adjust the connection between the Pitot tube and lead screw/stepper motor in order to lower it (from its position near the wall) for the wake survey. When the probe is at its highest point, check that the probe is on a horizontal line that passes through the airfoil trailing edge when the airfoil is at an angle of attack of 8 degrees. This will be where the computer (arbitrarily) denotes  $_y=_0$ .
5. Use the data acquisition program to perform the wake survey. The required values of  $y$  are pre-programmed (16 points in all), starting at a  $_y=_0$  and extending 3 inches. **Perform the complete wake survey a total of two times**, that is run the survey once, then go back and choose the wake survey option again. (Do not forget to check the starting position of the probe.)

## Data to be Taken

1. **Surface Pressure Distribution** - The lab computer will record the measurements acquired by the Scanivalve systems, which will be measuring the differential pressure between each wing pressure tap and a freestream static pressure (in mm Hg). The pressure results are stored in a file versus the chordwise location of the pressure tap nondimensionalized by the airfoil chord length. The wind tunnel dynamic pressure (mm Hg) will also be recorded by the computer (remember to record the atmospheric pressure and temperature to convert this to a wind tunnel velocity).
2. **Pitot Probe Survey of a Boundary Layer** - The Barocel will measure the pressure difference between the Pitot probe pressure and the wall surface static pressure on the ceiling of the wind tunnel at the measurement station. The data acquisition program will output to disk the pressure difference (mm Hg) versus the distance (in.) from the surface. The survey begins with the probe (nearly) touching the ceiling. If it was just touching the wall, and since the Pitot probe is 0.063 inches in outside dimension, this first position (which the computer denotes as  $y=0$ ) would actually correspond to the distance to the middle of the probe. You will record 16 locations away from the wall, and then repeat two measurement locations.
3. **Pitot Probe Survey of a Wake** - The Barocel in this application will measure the pressure difference between the Pitot pressure in the wake and the wind tunnel freestream static pressure. The acquisition software will output the value of the streamwise component of the dynamic pressure (mm Hg) versus the vertical distance location (in.). You should record the wake profile twice.
4. **Tubing Schematic** - Make a sketch indicating how a typical airfoil pressure tap is connected to the pressure transducer. Also sketch the tubing hookup to the transducer used during the boundary layer and wake surveys. Finally, sketch the tubing hookup used in the measurement of wind tunnel dynamic pressure with the Pitotstatic probe.

## Data Reduction

1. **Surface Pressure Distribution** - Convert the measured pressure differences and free stream dynamic pressures to local pressure coefficients.
2. **Pitot Probe Surveys** - For the boundary layer results, apply the Bernoulli equation locally to convert the dynamic pressure to local streamwise velocity component. From the result, select a value of  $\delta$  and  $u_{edge}$ , defined respectively as the height above the surface where the velocity becomes *essentially* constant and the value of that velocity. Then calculate the nondimensional quantities  $y/\delta$  and  $u/u_{edge}$ . For the wake profile, again calculate the velocity from the pressure differences.

## Results Needed for Report (for part "Low Speed Wind Tunnel Measurements")

1. Make a four-part tubing schematic figure showing all connections necessary for the measurement of (a) the airfoil static pressures, (b) the boundary layer velocity profile, (c) the wake velocity profile and (d) wind tunnel dynamic pressure. Indicate what each tube is connected to at both of its ends and label each tube as to what pressure it contains. The figure subtitles for each tubing hookup should describe to which of the different experiments it corresponds.
2. Plot two figures showing the chordwise pressure coefficient distribution on the airfoil versus nondimensional chordwise position,  $x/c$ , where  $c$  is the airfoil chord. The standard aerodynamics format is to plot  $C_p$  as the ordinate, negative upward. On both figures plot the distribution at zero angle of attack as a standard. Then, plot one distribution at the smaller angle of attack on the first figure and the other distribution at larger angle of attack on the second. Plot data points only; do **NOT** draw lines or smooth curves between them.
3. Plot a figure showing the shape of the nondimensional boundary layer profile  $u/u_{edge}$  versus  $y/\delta$  with distance as ordinate. Again, plot data points only (not connected with curves).
4. Plot a figure showing the variation in streamwise velocity component  $u$  through the wake behind the airfoil with  $y$  as ordinate. Plot data points only.
5. Plot the normalized velocity profile,  $u/u_\infty$ , where  $u_\infty$  is the wind tunnel velocity simultaneously recorded with each wake velocity measurement, again with vertical position as the ordinate.

---

## Smoke Tunnel Visualizations

### Procedure

1. The room is supplied with a high quality CCD Fokus color camera. To use the camera, you need to run the FGControl software located on the computer's desktop.
2. On the front panel, turn the main power **on**, then turn **on** the power for the lights and smoke. Allow the smoke generator to start producing the smoke (~5-10 seconds), then turn the blower **on**.\* To start, set the speed control about halfway - you will *not* need to know the air velocity, but it varies approximately linearly with the setting of the speed control with a maximum velocity of 29 ft/sec.

**i** \*If needed (if the smoke flow begins to disappear so much you can not see it), you can routinely turn the blower off to allow the smoke generator time to regenerate smoke. Only do this if the smoke flow is hard to see; otherwise, you will just end up filling the room with smoke.

1. Before opening the front door/window of the test section, turn the smoke generator and blower **off**. † Open the front door of the test section and mount the following models in turn on the attachment disk. Observe the flow patterns in each case; take notes and draw rough sketches documenting what is observed; do **not** rely on your memory - keep a careful log as the laboratory progresses.

**i** † Again, if the smoke flow is hard to see, you can leave the smoke generator on when you turn the blower off.

1. a cylinder;
2. a symmetrical airfoil without flap - at a minimum, vary the angle of attack from a small value through stall;
3. an airfoil with flap (the flap angle is controlled by turning the knob marked *Aux 1* on the front panel) - at a minimum, set the airfoil at a moderate angle of attack and vary the flap angle from 0 to 45 degrees;
4. a finite wing - set at a moderate angle of attack before installation; and
5. a 3-D wing tip.

This is a flow visualization experiment. That means you should feel free to adjust the wind tunnel speed and geometry of the models in order to "see" what happens as you change conditions. **Please note:** make sure you make sufficient observations to address the issues listed below in the Results Needed for Report section.

1. When the observations have been completed, turn **off** the smoke first, then the lights. Allow the blower to run for about five minutes to clear the smoke out of the tunnel, then turn **off** the blower and the main power.

## Data to be Taken

Just the sketches or digital images of the flowfields for the various models at the appropriate conditions.

## Data Reduction

Since no quantitative data will be taken, no data reduction is required.

## Results Needed for Report

You need to provide results that help answer the list of discussion questions below; you should address these questions in your report. This will, in part, require that certain flow features be observed during the experiments described in the Pressure Experiments. These questions are in addition to any that might be listed in the supplemental handout (Canvas). Each answer to the questions below must be based on a figure (introduced in

the appropriate part of the Results and Discussion section of your report). The figures should be digital images or sketches (freehand is okay, but carefully done) of the flow patterns that were observed. Therefore, carefully observe the major flow features and take notes during the experiment.

**Specific questions (for Smoke Visualization) to be answered in the report for this lab:**

1. **Cylinder** - Contrast what was observed as the airflow went around the cylinder with the potential flow prediction for the flow around a cylinder. Why is there a difference? What is the effect of this difference on the aerodynamic performance of a cylinder?
2. **Symmetrical airfoil without flap** - Describe the flow behavior you observe as the angle of attack is increased from a small value to a value above the stall point. Pay particular attention to the behavior of the streamlines nearest the body as a function of angle of attack.
3. **Airfoil with flap** - With the airfoil set at a moderate angle of attack, vary the flap angle from zero to 45 degrees and describe the changes in the flow around the airfoil/flap combination that are observed as a function of flap deflection angle.
4. **Finite wing at angle of attack and 3-D wing tip** - Describe the behavior of the streamlines near to tip of the wing and downstream of the wing. What does this behavior represent physically?

# Digital Image Correlation

## Objective

One object of this experiment is to explore the displacement and strain behavior of structures using the digital image correlation technique. In addition, you will explore the interesting response of polypropylene, a material that exhibits different moduli in tension and compression. The experiment consists of two tests: 1) a four point bending test of a polypropylene specimen from which you will estimate the elastic moduli of polypropylene; and 2) a tension test of a second polypropylene specimen with a hole cut in it, from which you can determine the strain and stress concentrations caused by the hole. The loading for both tests will be accomplished using an Instron load frame.

---

## Background

### Digital Image Correlation

In the context of structural testing, Digital Image Correlation (DIC) is a method for tracking the point-wise displacements of a structure (typically a surface of the structure) using a series of images of the structure undergoing deformation. DIC is a non-intrusive measurement technique since nothing has to be mounted to the specimen directly. Furthermore, DIC can measure real structural component geometries in real world conditions. The DIC measurements are primarily limited by image resolution, such that higher resolution images produce more accurate results. Alternatively, a higher-resolution displacement field can be captured by zooming the camera's field of view to a smaller portion of the specimen of interest. To use DIC, it is usually necessary to prepare the specimen by painting a high-contrast speckle pattern on the surface so that subsequent pre- and post-deformation images can be analyzed to accurately determine the displacement field on the structural surface.

There are some requirements and rules-of-thumb for producing good speckle patterns. First, the pattern should be "random"; a highly organized and repeatable pattern would produce ambiguity in the displacement measurement. Second, the size of the speckles (or high contrast objects) should be roughly the same as (or slightly larger than) a 3x3 pixel region on the digital image for optimal tracking of the displacement. If the speckles are smaller than this, the image magnification can be changed to meet this criterion. Finally, the "density" of speckle features should be sufficient to have an average of 3-4 such features in a 10x10 pixel region. DIC does not rely on correlating a single speckle features, but rather multiple features to get an average displacement in a (multi-pixel) sub-region of the image.

DIC has its origin in speckle imaging approaches used in solid mechanics, and correlation-based analysis methods developed in the 1980's for object tracking in image processing applications and particle-based velocimetry measurements in fluid mechanics. In fact, DIC is very similar to a common velocity-field measurement approach used in fluid mechanics, Particle Image Velocimetry (PIV). In both DIC and PIV, the individual displacements of many small subregions of an imaged area are obtained by comparing images before and after the displacement has occurred. For each subregion, the "before" (pre) and "after" (post) images are cross-correlated, sometimes using Fast Fourier Transform (FFT) algorithms. The displacement for that subregion is the one that provides the best correlation between the two images. In DIC, the displacement is the desired

quantity. In PIV, this displacement is divided by the (short) time between the two images to obtain the local velocity.

This analysis process is typically performed after recording a sequence of images. In DIC, after the displacement field is calculated, the strain field can be determined. The two-dimensional surface displacement field is characterized as  $u(x,y)$  and  $v(x,y)$ , where  $u$  and  $v$  are the displacements in the  $x$  and  $y$  directions for a point originally at location  $(x,y)$ . With  $u$  and  $v$  determined, we can obtain the surface strain field using the strain-displacement relationships

$$\varepsilon_x = \frac{\partial u}{\partial x} \quad \varepsilon_y = \frac{\partial v}{\partial y} \quad \gamma_{xy} = \frac{\partial u}{\partial y} + \frac{\partial v}{\partial x}$$

(1)

Note that differentiating the displacement data amplifies the noise in the data; so advanced analysis software like the package used here<sup>1</sup> employ additional processing approaches such as sophisticated smoothing to find the strain field from the displacement data.<sup>2</sup>

 <sup>1</sup> In this lab, we will use the Aramis analysis software package.

<sup>2</sup> You will also export the Aramis DIC data so you can analyze the full-field data.



**Figure 1.** The 3D DIC imaging systems, with two cameras mounted in a stereoscopic configurations and two light sources.

DIC (and PIV) systems come in different flavors. For example, the measured displacements of a thin region can be two-dimensional (2D) or three-dimensional (3D). In this lab, we will use a 3D DIC system (shown in Figure 1) that enables us to capture displacements in all three coordinate directions, including out-of-plane deformations. A 3D system provides more information than the more common 2D systems by adding an additional measurement. The 2D system requires only one camera (or equivalently, only camera imaging view point). To capture out-of-plane deflections, the 3D DIC system uses two cameras in a stereoscopic configuration. It is important to reiterate that 3D DIC (and PIV) systems provide three components of displacement (or velocity) from a surface (or thin planar region). There are also *volumetric* DIC and PIV approaches that provide 3D results for each location within a three-dimensional volume.

Our 3D DIC system, which employs two 5-megapixel cameras, will measure the displacements within a test volume that is centered on the test specimen. While the 3D DIC system provides accurate 3D displacement fields, it requires additional calibration effort compared to a simple, single-camera 2D system. The cameras are calibrated by orienting a thermally balanced plate with calibrated markings on it within the test volume.<sup>3</sup>



<sup>3</sup> The Aramis software will guide you through the calibration.

## Four-Point Flexure Testing

The four-point flexure or bending test is designed to test the flexural response of a slender beam. The goal of the four point bending test is to create a state of pure bending. Pure bending is a stress state where the bending moment is constant and the shear resultant is zero everywhere. The diagram on the left in Figure 2 illustrates a pure bending condition in which only opposing bending moments are applied to either end of the beam. Unfortunately, it is difficult to generate a pure bending moment in a real experiment. Instead, we will use opposing off-set point loads that generate a couple at either end of a beam. This configuration is shown on the right diagram in Figure 2. The advantage of this loading condition is that over the central span there are no shear loads and the beam is subject only to a bending moment.

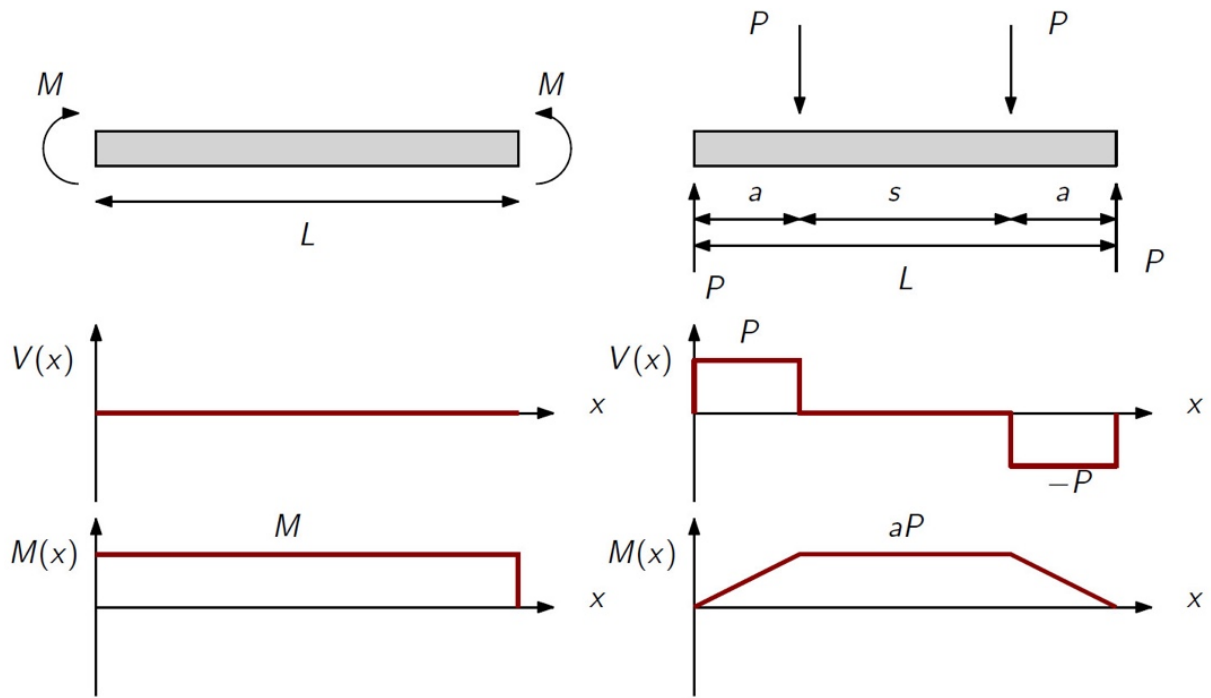


**Figure 2.** Idealized pure bending load (left); four point bending test load (right).

Figure 3 illustrates the setup of the test apparatus for the four point bending test. The test specimen is placed on rollers which are placed below and above the specimen. The load frame applies a compressive load to the experimental apparatus which transmits point loads to the top and bottom of the beam. Rollers are used to ensure that simple support conditions are imposed.

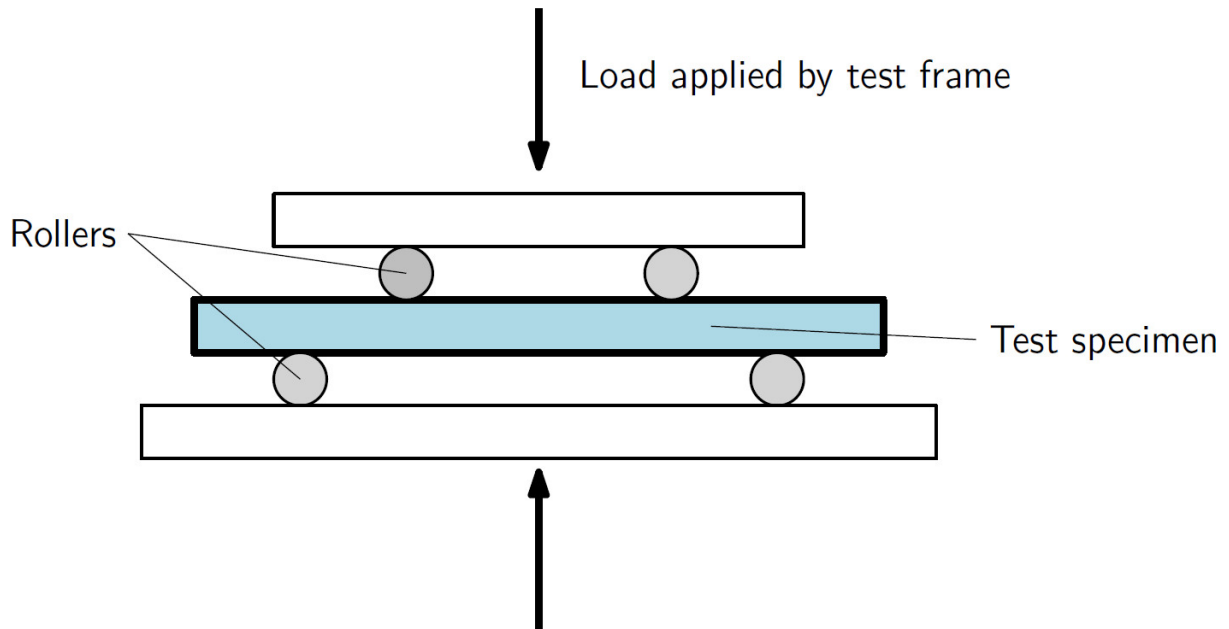


**Figure 3.** Apparatus schematic for a four point bending test

**Under ideal conditions in pure bending,** the strain in the beam should be linear through the thickness:

$$\varepsilon_x = -\kappa y$$

(2)

Furthermore, if the material is linear elastic and isotropic, then Hooke's law applies and the bending moment can be calculated as follows:

$$M = - \int_A \sigma_x y dA = - \int_A E \varepsilon_x y dA = \int_A E \kappa y^2 dA = EI\kappa$$

(3)

where  $I$  is the second moment of area of the beam, which is given as

$$I = \frac{wh^3}{12}$$

(4)

In Eq. (4),  $w$  is the width of the beam, and  $h$  is its depth. Therefore, if we impose  $M$  through a four point bending test, and can estimate from the digital image correlation results, we can infer the elastic modulus from

$$E = \frac{M}{I\kappa}$$

(5)

Polypropylene, however, exhibits different elastic moduli under tension and compression. As a result, the neutral surface is not at the geometric centroid of the cross-section and we have to use a composite beam analysis technique to find the elastic modulus under tension and compression. The measured strain will be offset from the geometric centroid, i.e., Eq. (2) has to be modified as follows:

$$\varepsilon_x = -\kappa y - b$$

(6)

where  $b$  is a strain offset.

The through-thickness stress distribution is shown in Figure 5. The  $y$ -location of the neutral surface can be found as  $y_N = -b/\kappa$ . The bending moment can be found by a similar integration as that in Eq. (3), except using Eq. (6) for the strain and integrating separately on either side of the neutral surface, i.e.,

$$M = - \int_{-w/2}^{w/2} \int_{-h/2}^{y_N} -E_T(\kappa y^2 + by) dy dx - \int_{-w/2}^{w/2} \int_{y_N}^{h/2} -E_C(\kappa y^2 + by) dy dx$$

(7)

Integrating Eq. (7) yields

$$M = wE_T \left( \kappa \left( \frac{y_N^3}{3} + \frac{h^3}{24} \right) + \frac{b}{2} \left( y_N^2 - \frac{h^2}{4} \right) \right) + wE_C \left( \kappa \left( \frac{h^3}{24} - \frac{y_N^3}{3} \right) + \frac{b}{2} \left( \frac{h^2}{4} - y_N^2 \right) \right)$$

(8)

Substituting our expression for  $y_N$  in (8) and simplifying gives

$$\begin{aligned} M &= wE_T \kappa \left( \frac{h^3}{24} + \frac{b^3}{6\kappa^3} - \frac{bh^2}{8\kappa} \right) + wE_C \kappa \left( \frac{h^3}{24} - \frac{b^3}{6\kappa^3} + \frac{bh^2}{8\kappa} \right) \\ &= \frac{w}{24} E_T \kappa \left( h - \frac{2b^2}{\kappa} \right) \left( h + \frac{b}{\kappa} \right) + \frac{w}{24} E_C \kappa \left( h + \frac{2b}{k} \right)^2 \left( h - \frac{b}{\kappa} \right) \end{aligned}$$

(9)

Next, we know from equilibrium that there cannot be an internal axial load in the beam. Therefore, the axial resultant ( $N$ ) must be zero:

$$\begin{aligned} N &= 0 = \int \sigma_x dA \\ &= \int_{-w/2}^{w/2} \int_{-h/2}^{y_N} -E_T(\kappa y + b) dy dx + \int_{-w/2}^{w/2} \int_{y_N}^{h/2} -E_C(\kappa y + b) dy dx \end{aligned}$$

(10)

Integrating Eq. (10) and replacing  $y_N$  with  $-b/\kappa$  yields

$$0 = E_T \left( \frac{2b}{\kappa} - h \right)^2 - E_C \kappa \left( \frac{2b}{\kappa} + h \right)^2$$

(11)

Now combining Eq. (11) and Eq. (9) for the bending moment, eliminating  $E_C$  and using our expression for the 2nd moment of area, Eq. (4), results in

$$M = \frac{wh}{12} E_T \kappa \left( h - \frac{2b}{\kappa} \right)^2 = E_T \kappa I \left( 1 - \frac{2b}{h\kappa} \right)^2$$

(12)

Eq. (12) can be solved for the modulus under tension, giving

$$E_T = \frac{M}{I \kappa \left( 1 - \frac{2b}{h\kappa} \right)^2}$$

(13)

Inserting this into Eq. (11) provides an expression for the compressive modulus

$$E_C = \frac{M}{I \kappa \left( 1 + \frac{2b}{h\kappa} \right)^2}$$

(14)

## Stress Concentrations

Stresses around defects and sudden changes in a structure can be significantly higher than the average stress in the structure. These sharp increases in stress are called **stress concentrations**. A good example of a stress concentration is the behavior of the stress near a circular hole in a structure subject to uniform tension or compression. For an infinite plate loaded in-plane, the tangential stress around the edge of the hole has an analytic solution

$$\sigma_{\theta\theta} = \sigma_{av}(1 - 2\cos 2\theta)$$

(15)

where the coordinate  $\theta$  runs circumferentially around the circular hole and  $\sigma_{av}$  is the average stress in the specimen far away from the hole. The direction  $\theta=0$  is aligned with the loading direction, or the  $x$ -axis in our geometry. The maximum value of the stress (due to the hole) normalized by  $\sigma_{av}$  is known as the stress concentration factor.

The stresses in planar cylindrical coordinates (i.e.,  $\sigma_{rr}$ ,  $\sigma_{\theta\theta}$ , and  $\sigma_{r\theta}$ ) can be calculated from Cartesian stresses (i.e.,  $\sigma_x$ ,  $\sigma_y$  and  $\gamma_{xy}$ ) using standard coordinate transformations, for example

$$\sigma_{rr} = \sigma_x \cos^2 \theta + \sigma_y \sin^2 \theta + \sigma_{xy} 2 \sin \theta \cos \theta$$

(16)

$$\sigma_{\theta\theta} = \sigma_x \sin^2 \theta + \sigma_y \cos^2 \theta - \sigma_{xy} 2 \sin \theta \cos \theta$$

(17)

In this lab, you will measure displacements and strains in a polypropylene test specimen (Figure 6) with a circular cutout subject to tension. The DIC system will enable us to visualize the distribution of strains around the hole and observe the stress and strain concentration.

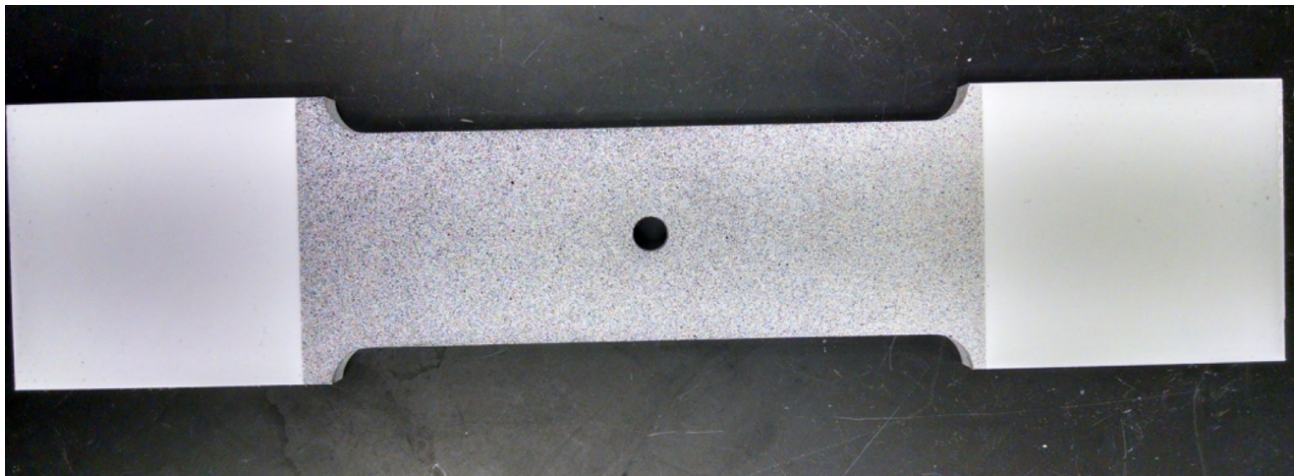


**Figure 6.** Photograph of test specimen with hole.

## Procedure

Normally an important step in a DIC experiment is to prepare the surface to be measured. Proper preparation of the surface is crucial to obtaining high quality data. For this lab, the specimens have already been prepared, so the steps below are for your enlightenment.

- First the surface was sanded using sandpaper on a sanding block to remove any loose material particles produced from cutting the specimen. Only the rough edges were sanded and as little material was removed as possible. The bars were then wiped clean.
  - Next, a very light coat of white paint was applied to one entire cut side. The smooth sides should not be painted. The paint was allowed to dry for 2 minutes, then another light coat of paint was applied. This procedure was repeated a few times until the white paint coats the specimen evenly and completely.
  - Finally, a toothbrush is used to apply black paint. The toothbrush is dipped into the black paint and excess paint is tapped off. The toothbrush is used to “spray” black paint onto the white painted surface in a “uniform” distribution of small speckles. The “spraying” is repeated until the specimen is covered with ~50% black speckles.
1. Calibrate the 3D DIC system using the Aramis software, which will lead you through the calibration procedure. During and after the DIC system calibration, **it is very important that the cameras are not moved - or even touched, otherwise the entire calibration procedure will have to be repeated.**
  2. Measure the thickness and width of the beam for the four-point bending test.
  3. Measure the thickness and width of the open hole test specimen, and the hole diameter.

## Four-Point Bending Test

	Value
$a$ (in.)	4
$s$ (in.)	4
$L$ (in.)	12

**Table 1.** Four-point loading parameters to be used in experiment (defined in Figure 2)

1. Position the beam in the test fixture using a 12-inch lower support length and a 4-inch upper support length. Place the roller locations to produce the four-point bending parameters listed in Table 1.
2. Take an un-loaded reference image, and then a second unloaded image.
3. Use the Aramis software to select your target area and perform an analysis. Extract the full field information. If you are satisfied with your results, move on – if not, you may need to recalibrate.
4. Take an un-loaded reference image.
5. Apply the load to the Instron test fixture. Choose a load not exceeding a total of 166 lb  $f$ .
6. Take the deformed image and unload the specimen.
7. Use the Aramis software to select your target area and perform the analysis. Extract the full field information.
8. If you are satisfied with your results, remove the specimen from the Instron.

## Open-Hole Tension Test

1. Position the specimen with the hole in the test fixture.
  2. Take an un-loaded reference image, and then a second unloaded image.
  3. Use the Aramis software to select your target area and perform an analysis. Extract the full field information.  
If you are satisfied with your results, move on.
  4. Take an un-loaded reference image.
  5. Load the test specimen with a load not exceeding 2.5 kN.
  6. Take the deformed image and unload the specimen.
  7. Use the Aramis software to select a target area and perform the analysis. Extract the full field information for the area selected.
  8. If you are satisfied with your results, repeat steps 4-7 for a second loading value that is lower than your previous measurement.
  9. If you are satisfied with your results, remove the specimen from the Instron.
- 

## Data to be Taken

1. Thickness and width of the beam, and load value used in the four-point bending test.
  2. Displacement and strain data from the Aramis software for the four-point bending test.
  3. Thickness and width of the specimen, hole diameter, and load value used in the open-hole tension test.
  4. Two sets of displacement and strain data from the Aramis software for the open-hole tension test.
- 

## Data Reduction

1. Using a best linear fit for the appropriate region of your  $\varepsilon_x(y)$  plots from the four-point bending test, compute the slope ( $\kappa$ ) and intercept ( $b$ ) relative to a coordinate axis centered on your specimen.
  2. From your experimental data, determine the tensile and compressive moduli ( $E_T$  and  $E_C$ ) for polypropylene.
  3. From your plots of transverse normal strain  $\varepsilon_y$  divided by the axial strain  $\varepsilon_x$ , determine a value for Poisson's ratio ( $\nu$ ) for polypropylene.
  4. For the open-hole tension test, compute the stresses in your specimen based on the measured strains and the appropriate *measured* modulus of elasticity for polypropylene.
- 

## Results Needed for Data Report

1. Table of beam dimensions and load value used in the four-point bending test.
2. Table of specimen dimensions, hole size and load value used in the open-hole tension test.
3. "Image graphs" or "full-field color plots"<sup>1</sup> of the axial (horizontal) and transverse (vertical) displacement field for the field of view analyzed by the Aramis software in the bending test. Choose your color scaling wisely to accentuate any important gradients. Be sure to also include color bars showing how your colors map to the values of displacement.



<sup>1</sup> Here an "image" means a false-color image, where each displacement (or strain) measurement location is like a pixel in the false-color image, and the color of the pixel corresponds to the value being shown (axial displacement in this case). You can do this, for example, with the image function in Matlab

1. Images of  $\epsilon_x$ ,  $\epsilon_y$  and  $\gamma_{xy}$  for the field of view imaged and analyzed by the Aramis software in the bending test, with color bars.
2. For the four-point bending test, plots of the axial and transverse normal strain fields as a function of  $y$  (with the  $y$ -axis as defined in Figure 5), at three axial locations between the two inner load points (i.e., within the constant moment region). One of these should be the center axial location.

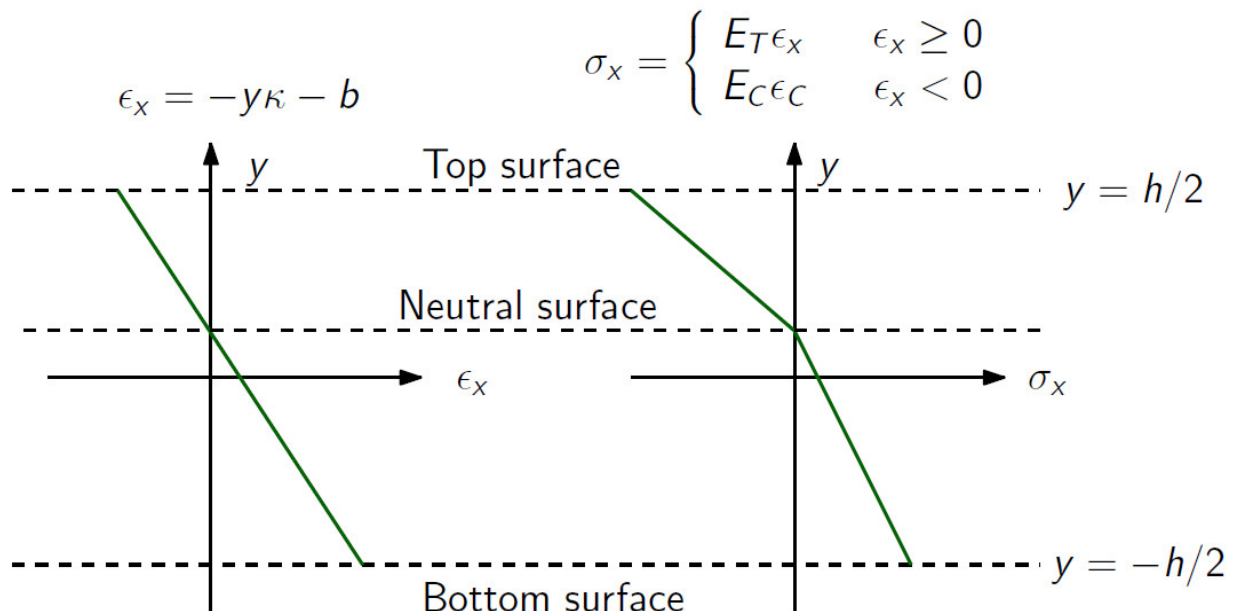


**Figure 5.** Through-thickness stress-strain distribution for material with different moduli in compression and tension.

1. Plot of the transverse normal strain  $\epsilon_y$  divided by the axial strain  $\epsilon_x$  along the center line used for Result 5.
2. Table of measured values of  $\kappa$ ,  $b$ , and the polypropylene properties  $E_T$ ,  $E_C$ , and  $\nu$ . Include in your table the published values for the polypropylene properties (include your source for those values).

3. Images of the axial strain ( $\varepsilon_x$ ) and transverse strain ( $\varepsilon_y$ ) fields for the region analyzed by the Aramis software in the open-hole tension test, with color bars, for both loadings.
4. Images of the axial ( $\sigma_x$ ) and transverse stress ( $\sigma_y$ ) fields based on your measured strains and measured modulus of polypropylene, with color bars, for both loadings.
5. Images of the normal radial stress ( $\sigma_{rr}$ ) and normal tangential stress ( $\sigma_{\theta\theta}$ ) fields for the open-hole tension tests, with color bars, for both loadings.
6. A single graph containing plots of the tangential stress along a line perpendicular to the length dimension of your specimen that passes through the center of the hole, for each loading.
7. A single graph containing plots for each of the loadings of the tangential stress (normalized by its value far from the hole) as a function of angle around the hole, close to the edge of hole.

# Pressure Vessel

## Objective

This experiment will allow you to investigate hoop and axial stress/strain relations for a pressurized thin-walled cylinder. This is an opportunity to examine a system with a biaxial state of stress, as opposed to the primarily uniaxial stress systems of earlier labs. Furthermore, you will be analyzing transient (as well as steady-state) strain readings from a rosette strain gauge in response to a dynamic event. Finally, you will be able to determine the internal pressure within the vessel from your wall stress measurements and cylindrical pressure vessel relations.

---

## Background

Many components of aerospace vehicles have an internal pressure higher than the surrounding pressure. Perhaps the most obvious examples are the fuselages of manned aircraft and the crew-compartments of spacecraft, which maintain internal pressures close to one atmosphere in low pressure environments. In other applications, the internal pressure can be significantly higher than 1 atm. For example, pressurized structures are required for many gas and liquid storage systems, e.g., propellant tanks in spacecraft, and for the propulsion engines used in aircraft and spacecraft.

We can characterize many of these structures as thin-wall pressure vessels, where the wall is essentially a membrane because its thickness is much less than other characteristic dimensions of the vessel, such as its length or radius.<sup>1</sup> In an ideal thin-wall pressure vessel, the stresses are uniform across the thin wall and the bending stresses are negligible over much of the structure. The vast majority of thin-wall pressure vessels are nearly spherical or cylindrical in shape (or composed of combinations of these two geometries). A sphere provides the advantage of minimizing stresses for a given volume and storage pressure compared to other shapes, i.e., it is structurally efficient. While cylinders are not as efficient and have larger stresses at the ends, which require additional structural reinforcement, they often have significant manufacturing and implementation advantages compared to spheres (imagine the drag induced by a spherical aircraft fuselage).



<sup>1</sup> Structures such as vacuum tanks and submarine hulls may also be characterized as thin-walled pressure vessels, through with internal pressures below the external pressure. For those cases, one must consider wall buckling as a failure mode.

## Wall Stress and Pressure Relations

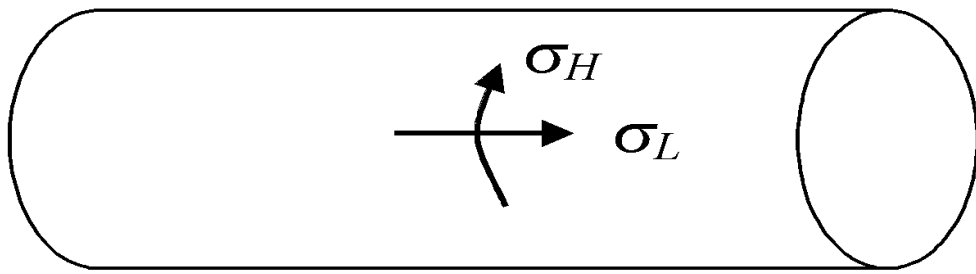


Figure 1. Direction of hoop and longitudinal stresses in a cylindrical thin-wall pressure vessel.

There are two principal stresses for a cylindrical thin-wall pressure vessel (Figure 1): a **longitudinal stress** in the axial direction ( $\sigma_L$ ) ; and a **hoop stress** ( $\sigma_H$ ) in the circumferential direction. This is a **biaxial-stress state** since there are two non-zero stress components. For a sufficiently long cylinder, we can relate these stresses to the difference between the internal pressure and the external pressure ( $\Delta p$ ) , sometimes referred to as the gauge pressure.

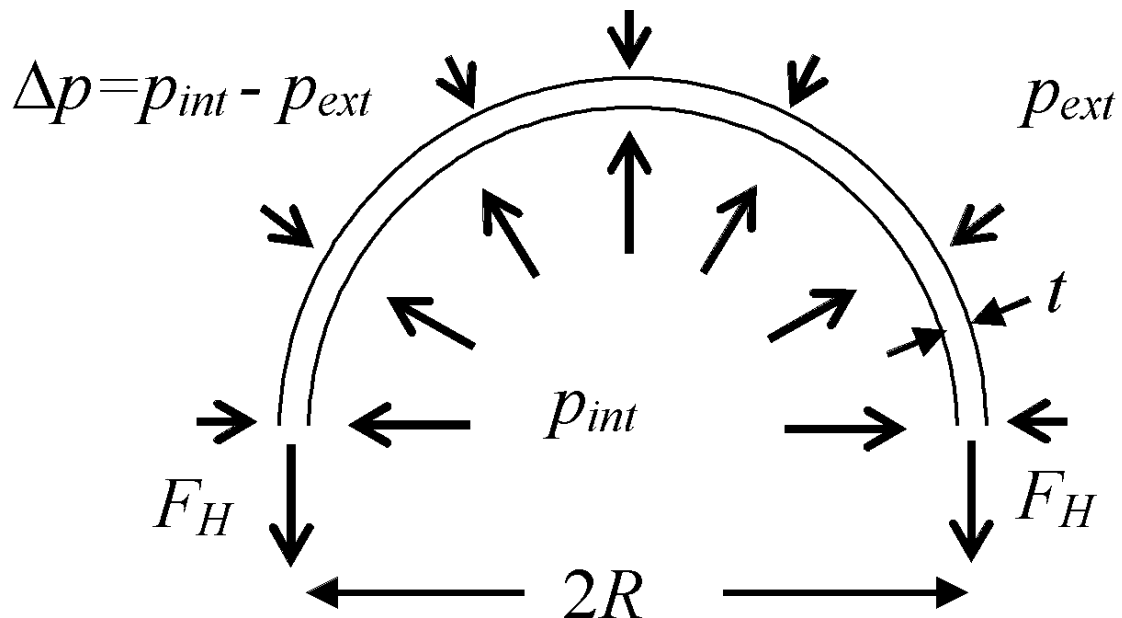


Figure 2. Section of cylindrical thin-wall pressure vessel of radius  $R$  and wall thickness  $t$ , subject to a pressure difference  $\Delta$ .

Ignoring the ends, we can calculate the hoop stress by considering the top half of the cylinder (a section of this is shown in Figure 2). We can use a free body diagram to get the necessary relationships for a cylinder of length  $L$ , radius  $R$  and wall thickness  $t$ . First, from the definition of stress, we have

$$F_H = tL\sigma_H$$

(1)

The wall must support the difference in (vertical) forces on the inner and outer sides of the wall due to the pressure difference, so

$$2F_H = \int_0^\pi \Delta p LR \sin \theta d\theta = LR2\Delta p$$

(2)

Combining (1) and (2), gives us a relation between the hoop stress and the gauge pressure.

$$\sigma_H = \frac{R}{t} \Delta p$$

(3)

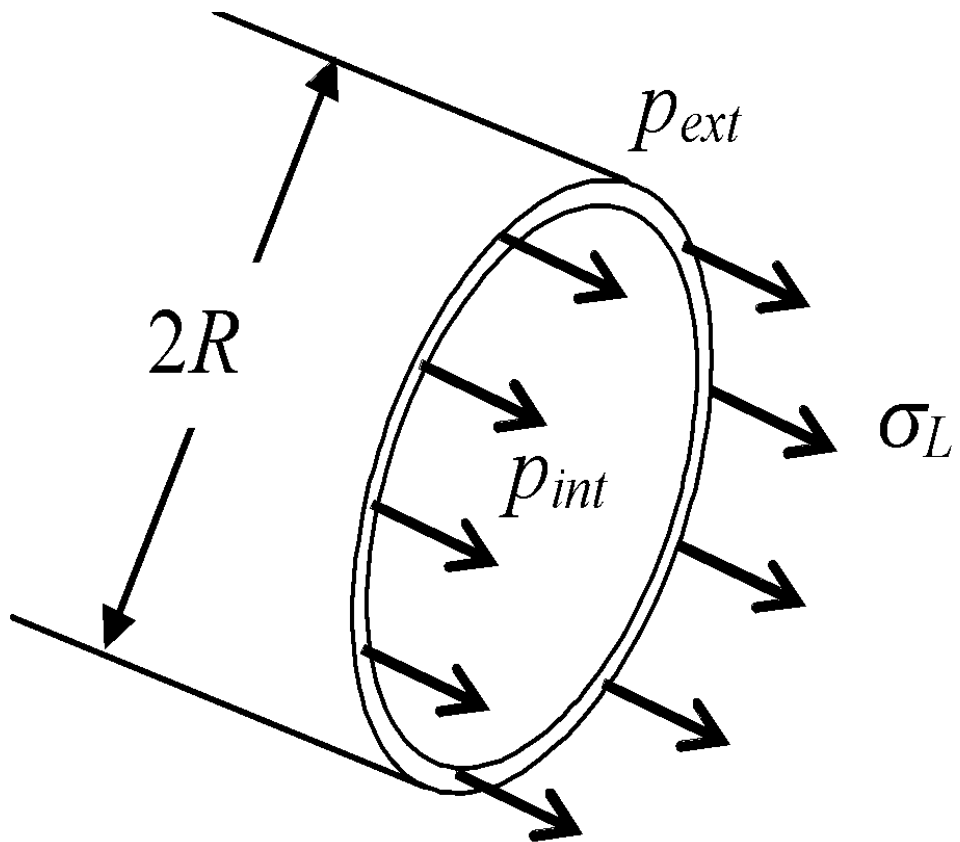


Figure 3. Apparatus schematic for a four point bending test.

A similar process looking at a cross-sectional cut normal to the longitudinal axis (Figure 3), where the longitudinal force in the wall must balance the pressure difference across the end of the cylinder, gives

$$F_L = 2\pi R t \sigma_L = \Delta p \int_0^{2\pi} \int_0^R r dr d\theta = \pi R^2 \Delta p$$

(4)

Solving (4) for the longitudinal stress gives

$$\sigma_L = \frac{R}{2t} \Delta p$$

(5)

So ideally, the longitudinal stress is one-half the hoop stress for a cylindrical vessel, or  $\sigma_H = 2\sigma_L$ .

## Stress-Strain Relations

As you will be measuring strains in our thin-wall vessel, you will need to convert them to stresses. As usual, this relationship is provided by Hooke's Law for strain, e.g.,

$$\varepsilon_x = \frac{\sigma_x}{E} - \nu \frac{\sigma_y}{E} - \nu \frac{\sigma_z}{E} \quad \text{and} \quad \varepsilon_y = -\nu \frac{\sigma_x}{E} + \frac{\sigma_y}{E} - \nu \frac{\sigma_z}{E}$$

(7)

For our geometry, we have  $\sigma_x = \sigma_H$ ,  $\sigma_y = \sigma_L$  and  $\sigma_z = 0$ . Thus we can simplify (7) to

$$\sigma_H = \frac{E}{1 - \nu^2} (\varepsilon_H + \nu \varepsilon_L)$$

$$\sigma_L = \frac{E}{1 - \nu^2} (\varepsilon_L + \nu \varepsilon_H)$$

(8)

Including our stress results for the ideal cylindrical vessel ( $\sigma_H = 2\sigma_L$ ) gives

$$\varepsilon_H + \nu\varepsilon_L = 2(\varepsilon_L + \nu\varepsilon_H)$$

or

$$\sigma_H = \frac{2E}{2 - \nu}\varepsilon_H$$

$$\sigma_L = \frac{E}{1 - 2\nu}\varepsilon_L$$

(9)

## Transients

In this lab, you will record the wall strains in your pressure vessel as a function of time while the vessel is depressurized. The strains in the wall will go from one steady-state condition (fully pressurized) to another (depressurized). One way to characterize a transient system like this, moving from an initial state to a final state, is the “rise” or “fall” time, i.e., the time required for a chosen state variable to go from 10% to 90% of the difference from its final value, i.e.,  $t_{rise} = t_{90} - t_{10}$ , where  $t_{10}$  is the time required for state variable  $y$  to meet the condition  $y(t_{10}) = y_{initial} + 0.1(y_{final} - y_{initial})$ . An example of this is shown in Figure 4.

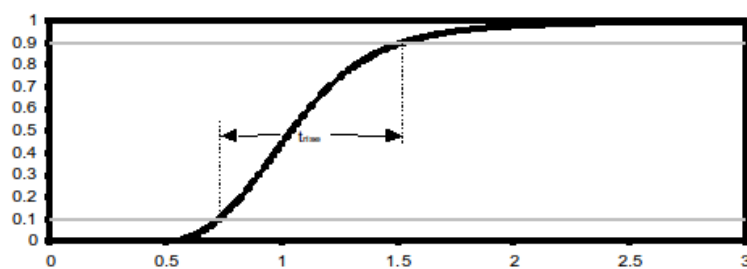


Figure 4. Example of rise time based on a state variable transitioning from an initial zero value to a final value of one.

## Experimental Equipment

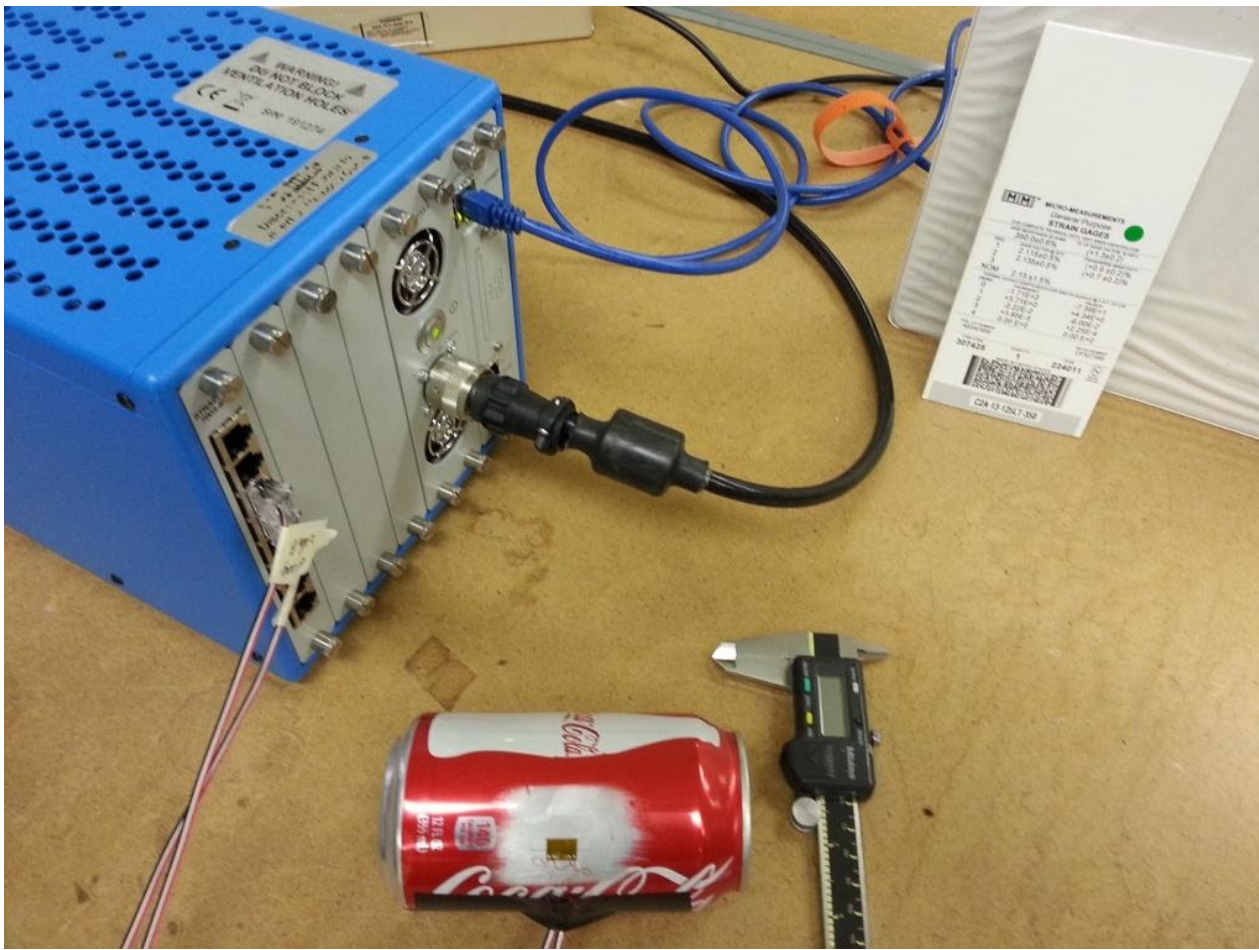


Figure 5. Equipment used in transient thin-wall strain-stress measurements.

The equipment used in this lab are pictured in Figure 5. The pressure vessel you will investigate is the common soda can. You will mount on the can either a rectangular rosette strain gauge, which measures strain along three directions, or a T-rosette gauge, which measures the strain along two perpendicular directions. You will use the Vishay 7000 acquisition system to record the reading from the strain gauge. Care must be exercised when handling the soda can. Be careful not to indent or drop the can or shake it so as not to increase the internal pressure. Be sure not to excessively strain the lead wires connected to the T-rosette gauges.

## At Home Before the Lab

Look up some common aluminum alloys used to manufacture soda cans. Find values for the modulus of elasticity, Poisson's ratio, and 0.2% offset yield stress for these alloys (you might try [www.matweb.com](http://www.matweb.com)).

## Procedure

1. Measure the diameter of the can using digital calipers. Zero the calipers with the jaws in the fully closed position. Measure the diameter of the can by laying the calipers over the top of the can with the can standing upright. Carefully close the caliper jaws around the can being sure not to squeeze the can. Iterate between

- locating the diameter and allowing the jaws to contact the walls of the can. Conduct a total of 3 diameter measurements and record these values.
2. Measure the thickness of the soda can Aluminum material from the provided cutout sheet. Be careful not to close the calipers too tightly and deform the material plastically. Collect a total of 3 thickness measurements and record these values.
  3. Note the precise designation of the strain gauges you will use so that you can look up relevant parameters associated with this gauge such as the gauge factor  $S_g$  and the transverse sensitivity factor  $K_t$ . Note for T-rosette or rectangular gauges there is a value of  $K_t$  assigned to each grid.

## Transient Can Opening Test

1. Mount the strain gauge on your soda can.
2. *If you are using a T-rosette gauge*, it should be bonded so that one grid is aligned with the longitudinal axis of the can and the other grid is aligned with the hoop direction. It is best to scribe perpendicular lines on the sanded region of the can to facilitate the alignment of the gauge with the axial and radial directions.
3. *If you are using a rectangular rosette gauge*, you should bond the gauge in such a way that none of the 3 grids are aligned with the longitudinal and hoop directions.<sup>1</sup>
4. Properly connect the strain gauge wires to the strain gauge card in the Vishay 7000.
5. Configure the Vishay 7000/Strain smart software interface. Be sure to supply the appropriate values for the strain gauge and transverse sensitivity factors - assign the correct values for the appropriate strain gauge grid. Set the data sampling rate to the maximum possible value (2048 samples/second). The fast sampling rate will allow you to capture some data points associated with the early, sharply rising portion of the strain gauge record when the pressure suddenly changes.
6. The individual strain gauges will already be configured to their respective 1/4-bridge circuits. Zero each 1/4-bridge circuit and perform standard shunt calibrations.
7. Shake the can carefully, being sure not to accidentally damage the strain gauge, or the lead wires.
8. **WITHOUT OPENING THE CAN**, carefully and gently pry up the soda can tab just a bit so that you will be able to easily get your finger underneath when you are ready to crack open the can.
9. Trigger the Vishay 7000 to start recording data. Grab the top of the can with two fingers while you open the can with your other hand. You should avoid squeezing the can during this step!<sup>2</sup> Stop recording data and save the strain data to the hard drive.
10. Be sure to note down which strain gauge grid corresponds to each recorded strain gauge signal. This is especially important in the case of the 3-element rectangular rosette gauge if that is the type of gauge you are using in your experiment.

 <sup>1</sup> The whole point is to apply the strain transformation formulas in order to recover the principle strain directions (maximum and minimum) along with the principle angle ( $\varphi_p$ ). Once you calculate these three quantities you should of course recover the hoop and axial directions of the can.

<sup>2</sup> You should see the dynamic strain change associated with the hoop and axial strain components on the live computer display. Your curves should feature a sharp change in strain, which then levels off at a steady value.

## Data to be Taken

1. Can diameter and can wall material thickness.
  2. Gauge factors  $S_g$  and transverse sensitivity factors  $K_t$  for each of the strain gauges used in your test.
  3. Strain gauge outputs for the transient can opening test.
  4. Displacement rate and the digital sampling rates for the Vishay system
  5. Axial loads and bending strains for loading and unloading runs for short beam-column.
- 

## Data Reduction

1. If you used a rectangular rosette for the transient can experiment (and misaligned it as you were supposed to), then you need to transform the measured strains to the principal strains (maximum and minimum) and corresponding principal strain angles using a similar approach to that used in the cantilever beam bending lab. The principal strains should turn out to be the hoop and longitudinal strains.
  2. Determine the rise times for the hoop and longitudinal strain (magnitudes) that occurred as the can was first opened.
  3. Estimate the dynamic strain rates  $d\varepsilon/dt$  by dividing the respective change in strain during the 10% to 90% interval by your rise time estimate. Do this for both the hoop and longitudinal strain signals.
  4. Use the value of the Poisson ratio that you found from the material database in the at home exercise and estimate the radial strain in the can wall. Combine with the measured can wall thickness to estimate the change in wall thickness when the can was pressurized.
  5. From your hoop and axial strain versus time profiles, identify the steady state portions of each curve (before opening the can and afterwards where the strain finally levels out to a nearly constant value). Use data from each steady state portion to estimate the overall change in hoop and longitudinal strains experienced by the can.
  6. Using the material database values of  $E$  and  $\nu$ , use the Hooke's Law Equations (8) to determine the changes in the can's  $\sigma_H$  and  $\sigma_L$  corresponding to the strain changes determined in Step 7.
  7. Using the material database values of  $E$  and  $\nu$ , use the simplified Hooke's Law expressions for an ideal thin-wall cylinder (Equations (9)) to determine the changes in the can's  $H$  and  $L$  corresponding to the strain changes determined in Step 7.
  8. Using the appropriate results for  $\sigma_H$  and  $\sigma_L$  estimate, from Equations (3) and (5), the gauge pressure within the soda can before it was opened.
- 

## Results Needed for Report

1. Table of can dimensions.
2. Table of gauge factors and transverse sensitivity factors for each of the strain gauge.
3. Combined plot of measured strains (in microstrain) as function of time (in seconds) for the can-opening experiment.
4. Plot of maximum principal stress angle as function of time for the can-opening experiment.<sup>1</sup>

-  <sup>1</sup> The plot should exhibit a chaotic and unstable variation during the first several seconds followed by a level, steady state value of  $\theta p$ . The “average” value of  $\theta p$  during the steady region should coincide with the expected direction for a hoop stress.

1. Combined plot of hoop and axial strains (in microstrain) as a function of time (in seconds). You may truncate your plots in time as required – but be sure to clearly display the transient and steady state of your data.
2. Table of estimated rise times (in units of  $\mu\text{s}$ ) and strain rates (in units of  $\text{s}^{-1}$ ) for both hoop and longitudinal strain signals.
3. Table of overall changes in hoop and longitudinal strains and stresses (reported in MPa) from the initial can state to the final state. Provide stress results using both the full (Equations (8)) and simplified (Equations (9)) Hooke’s Law relations.
4. Table of estimated can gauge pressure values (in psi) using each of your results for  $\sigma_H$  and  $\sigma_L$  (note, you will be reporting at least two pressure estimates).

# Bending and Buckling

## Objective

In this laboratory, students will experimentally investigate the behavior of beams and columns subject to externally applied forces and displacements. First, students will explore the force-deflection and displacement-deflection behavior of a cantilever beam through surface strain measurements. Data from a rectangular rosette strain gauge will be used to determine the state of strain on the surface of a thin rectangular beam. Specifically, rosette strain analysis (strain transformation) theory can be used to determine the principal strain components of a beam under pure bending. Experiments will examine two types of boundary conditions: load-controlled, where prescribed loads are applied at the free end of the beam; and displacement-controlled, where known displacements (measured here with a precision micrometer) are applied to the free end. The measured beam behavior can then be compared to elementary Euler-Bernoulli beam theory predictions to determine Young's modulus, Poisson's ratio, and effective beam stiffness. Second, students will explore the buckling and post-buckling behavior of slender columns loaded axially along their length. This part of the experiment includes two tests: a long column and a short column buckling test. Each test will explore the change in critical buckling strength caused by changes in geometry and loading conditions. In addition, students will gain familiarity with buckling analysis techniques such as the Southwell plot.

---

## Background

### Simple Beam Theory

A beam is a structure whose length is much larger than its other two principal dimensions. In many cases, aircraft structures such as wings and fuselages can be treated as thin-walled beams. Simple beam theory is based on the Euler-Bernoulli assumptions (thus, simple beam theory is also known as Euler-Bernoulli beam theory). Specifically, those assumptions are: 1) the beam cross-section is rigid and does not (significantly) deform under the applied axial or transverse load; 2) the cross-section remains plane after deformation; and 3) the cross-section remains normal to the deformed axis of the beam. These assumptions have been extensively validated for long, thin beams formed from isotropic materials with solid cross-sections, as well as many other beams under "small" deflections

Applying these assumptions allows us to describe the behavior of the beam under load as a one-dimensional function, i.e., solely as a function of the distance along the beam length. For example, the deflection of a beam under an applied load is just a function of the load distribution, the Young's modulus ( $E$ ), and the geometry of the cross-section of the beam. The predictions of simple beam theory are available in numerous references, e.g. the text by Bauchau and Craig<sup>1</sup>.



<sup>1</sup> O. Bauchau and J. Craig, Structural Analysis: With Applications to Aerospace Structures, Springer, 2009.

## Strain Transformation Theory

In this lab, we will study a cantilever beam that is subjected to applied loads and applied displacements. A rectangular rosette strain gauge will be used to measure the components of strain on the beam surface near the root in a reference frame that is not aligned with the beam axis. Therefore, it will be necessary to consider a transformation of the components of strain between coordinate frames. If we look at the stresses and strains in a beam subject to transverse load, as shown in **Figure 4(a)**, a good approximation is that only the longitudinal (axial) components of stress exist along the length of the beam. If we use the coordinate frame defined in **Figure 4(a)**, then the axial components of stress correspond to  $\sigma_x$ .

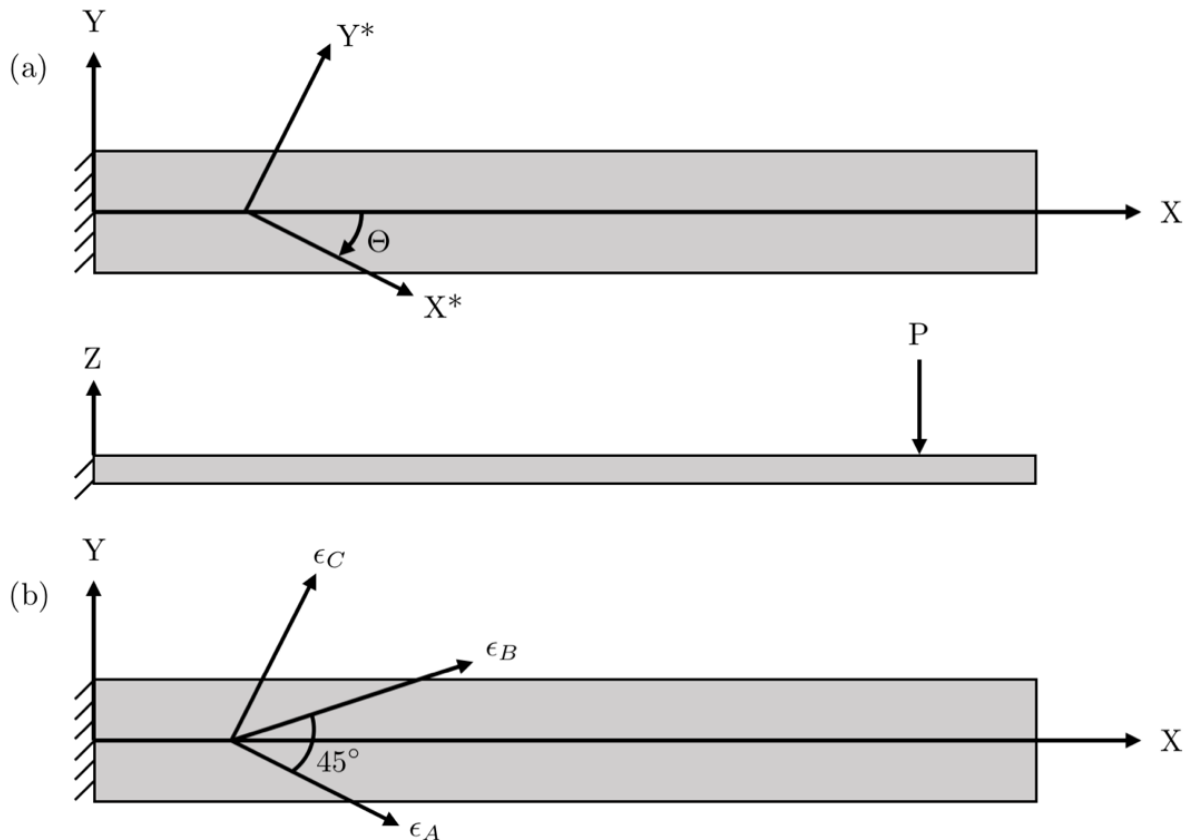


**Figure 4.** Cantilever beam schematic.

Using Hooke's law for an isotropic material, the non-zero observed components of strain, also with respect to the  $X-Y-Z$  coordinate frame defined in the figure, should be:

$$\epsilon_X = \frac{\sigma_x}{E}$$

$$\epsilon_Y = -\nu \frac{\sigma_x}{E}$$

$$\epsilon_Z = -\nu \frac{\sigma_x}{E}$$

(1)

where  $E$  is the elastic modulus and  $\nu$  is the Poisson ratio. However, the rectangular rosette strain gauge that is used for these experiments will not be aligned with the X-Y-Z frame. Instead, it will be oriented at an angle. Looking at the beam, we will measure strains in the transformed coordinate system X\*-Y\*-Z\*, shown in **Figure 4(a)**, where we note that the Z axis is shared between the two coordinate frames, and the coordinate system is rotated about the Z axis by an unknown angle  $\theta$ .

To relate the components of strain in these two coordinate frames, we will use strain transformations. The components of strain in the rotated reference frame X\*-Y\*-Z\* are given as a function of the components of strain in the X-Y-Z frame through

$$\epsilon_X^* = \frac{\epsilon_X + \epsilon_Y}{2} + \frac{\epsilon_X - \epsilon_Y}{2} \cos(2\theta) + \frac{\gamma_{XY}}{2} \sin(2\theta)$$

$$\epsilon_Y^* = \frac{\epsilon_X + \epsilon_Y}{2} + \frac{\epsilon_X - \epsilon_Y}{2} \cos(2\theta) - \frac{\gamma_{XY}}{2} \sin(2\theta)$$

$$\frac{\gamma_{XY}^*}{2} = -\frac{\epsilon_X - \epsilon_Y}{2} \sin(2\theta) + \frac{\gamma_{XY}}{2} \cos(2\theta)$$

(2)

The strain components in the rotated frame X\*-Y\*-Z\* can be determined with a rectangular strain rosette. For example, **Figure 5.** shows a strain gauge rosette mounted on the top surface of a beam, with the three gauges separated by 45° from each other.

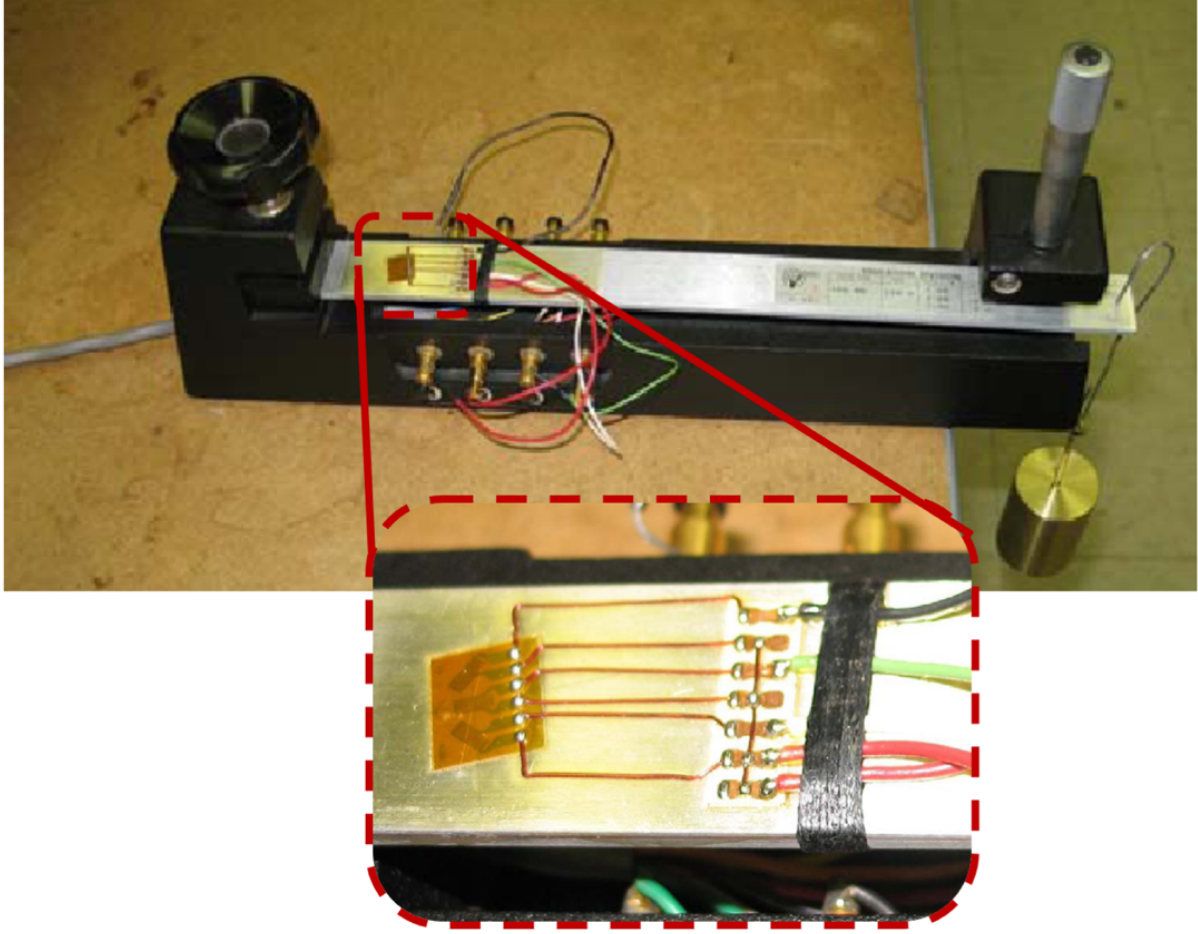


**Figure 5.** Photograph of cantilever beam experimental configuration.

Labeling the gauges as A, B, and C as in **Figure 4(b)**, the rosette can thus measure strain in these three directions. If we consider that the frame X\*-Y\*-Z\* is aligned with the rosette such that X\* is in the  $\epsilon_A$  direction, then  $\epsilon_X^*$  and  $\epsilon_Y^*$  are simply given by  $\epsilon_X^* = \epsilon_A$  and  $\epsilon_Y^* = \epsilon_C$ . To find  $\gamma_{XY}^*$  we can use the strain gauge in the  $\epsilon_B$  direction. We consider then a rotation of the X\*-Y\*-Z\* frame to a frame that is aligned in the  $\epsilon_B$  direction, and using equation (2) yields

$$\epsilon_B = \frac{\epsilon_X^* + \epsilon_Y^*}{2} + \frac{\epsilon_X^* - \epsilon_Y^*}{2} \cos(2 \cdot 45^\circ) + \frac{\gamma_{XY}^*}{2} \sin(2 \cdot 45^\circ)$$

or

$$\epsilon_B = \frac{\epsilon_X^* + \epsilon_Y^*}{2} + \frac{\gamma_{XY}^*}{2}$$

Finally, solving for  $\gamma_{XY}^*$  and using  $\epsilon_X^* = \epsilon_A$  and  $\epsilon_Y^* = \epsilon_B$ , we can relate the strains measured from the gauges in the strain gauge rosette to the components of strain in the X\*-Y\*-Z\* frame through

$$\epsilon_X^* = \epsilon_A$$

$$\epsilon_Y^* = \epsilon_C$$

$$\frac{\gamma_{XY}^*}{2} = \epsilon_B - \frac{\epsilon_A + \epsilon_C}{2}$$

(3)

With the strains known in the rotated frame X\*-Y\*-Z\*, we can compute the strains in the reference frame aligned with the beam, that is the X-Y-Z frame. If the misalignment angle  $\theta$  between the rosette and the beam was known, we could simply use the rotation equations (2). However, it is not necessary to know the misalignment angle since we can recognize that in the beam aligned X-Y-Z frame, all shear strain components are zero, and the strains are principal strains! That is  $\epsilon_X$ ,  $\epsilon_Y$ , and  $\epsilon_Z$  are principal strains under the Euler-Bernoulli beam bending assumption used here. For a two-dimensional state of strain, the principal strains can be computed from the strains in any arbitrary reference frame through

$$\epsilon_1 = \frac{\epsilon_X^* + \epsilon_Y^*}{2} + \left[ \left( \frac{\epsilon_X^* - \epsilon_Y^*}{2} \right)^2 + \left( \frac{\gamma_{XY}^*}{2} \right)^2 \right]^{1/2}$$

$$\epsilon_2 = \frac{\epsilon_X^* + \epsilon_Y^*}{2} - \left[ \left( \frac{\epsilon_X^* - \epsilon_Y^*}{2} \right)^2 + \left( \frac{\gamma_{XY}^*}{2} \right)^2 \right]^{1/2}$$

(4)

where  $\epsilon_1$  and  $\epsilon_2$  are the principal strains, and the angle from the given reference frame and the principal reference frame is given by

$$\tan(2\theta_p) = \frac{\gamma_{XY}^*}{\epsilon_X^* - \epsilon_Y^*}$$

(5)

We note again that the components  $\epsilon_X^*$ ,  $\epsilon_Y^*$ , and  $\gamma_{XY}^*$  could be with respect to any Cartesian reference frame.

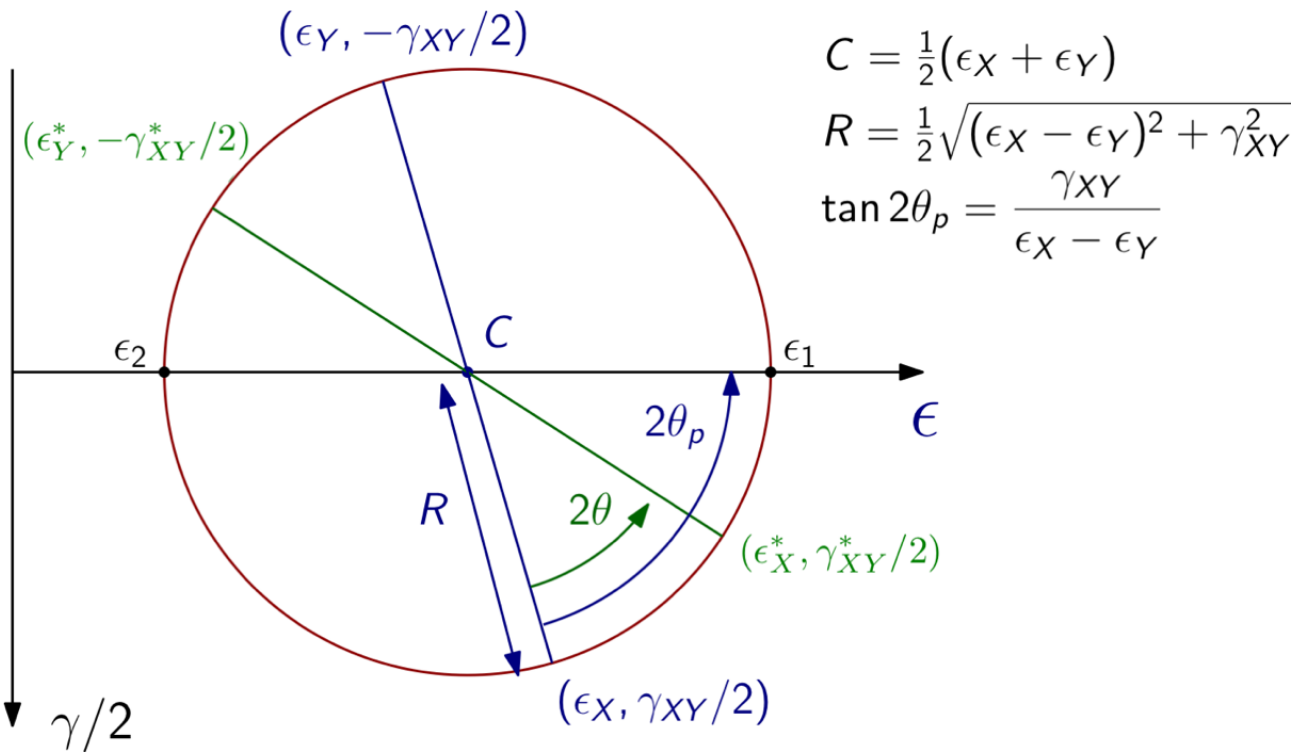


**Figure 6.** Mohr's circle for strain.

The strain transformation relations (2) can be visualized using Mohr's circle as shown in **Figure 6**, which is a convenient graphical technique for transforming strains (and can also be applied to transforming stresses). All the components of strain in any rotated reference frame lie on Mohr's circle, where a rotation  $\theta$  in physical space corresponds to a rotation of  $2\theta$  on Mohr's circle. In Mohr's circle, the shear strain axis is drawn in the reverse direction such that positive axis points downward. Similar to the equations in (2), Mohr's circle can be used to transform strain components  $(\epsilon_X, \epsilon_Y, \gamma_{XY})$  in a X-Y coordinate frame to the corresponding components  $(\epsilon_X^*, \epsilon_Y^*, \gamma_{XY}^*)$  in an X\*-Y\* coordinate frame, which is rotated about a common Z-axis by an angle To perform the transformation, first draw the points  $(\epsilon_X, \gamma_{XY}/2)$  and  $(\epsilon_Y, -\gamma_{XY}/2)$ . Since all the strain states lie on the circle, straightforward geometry can be used to solve for the strain components in the rotated reference frame. Mohr's circle also shows us graphically how one can rotate to a particular strain state where the shear strain is zero and there are two principal stresses  $\epsilon_1$  and  $\epsilon_2$ .

## Structural Instability

Slender structures, like beams or columns, that are subject to compressive loads often exhibit elastic instabilities. One type of elastic stability is known as buckling. Aerospace structures are often slender and are subject to compressive loads. Therefore, understanding structural instability in general and buckling in particular is required for aerospace structural design.

Structural instability is a fundamentally nonlinear phenomena, therefore to predict buckling we must model the structural nonlinearity. The most common structural instabilities are due to geometric nonlinearity rather than nonlinear material behavior. Geometric nonlinearity accounts for the effect of deformation within an equilibrium analysis rather than assuming infinitesimal structural deflections.

## Buckling of a Perfect Column (Euler Buckling)

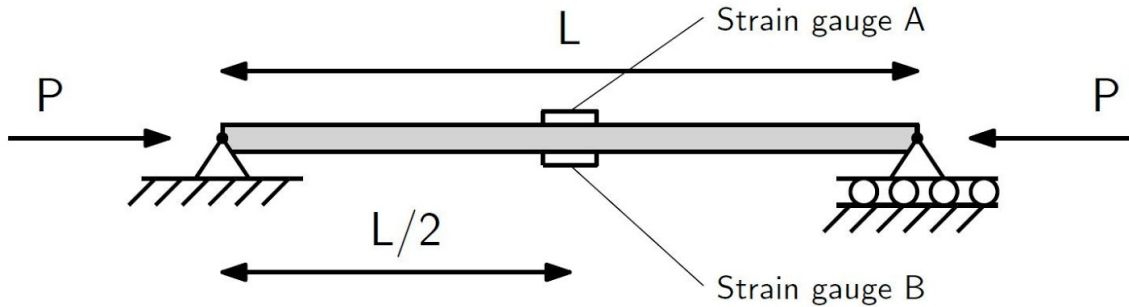


Figure 1. Euler-Bernoulli beam subject to a compressive load,  $P$ .

Consider the buckling of a column loaded by opposing axial loads as shown in Figure 1. We can model this using an extension of Euler-Bernoulli beam theory. Using this theory, the transverse deformation,  $w(x)$ , of a beam is governed by the equation (1)

$$EI \frac{d^4 w}{dx^4} + P \frac{d^2 w}{dx^2} = q(x)$$

(1)

where  $E$  and  $I$  are the elastic modulus and second moment of area,  $P$  is the axial compressive load and  $q(x)$  is the distributed load. At first glance, this equation may not appear to be nonlinear, however, the second term  $P(d^2 w / dx^2)$  is, in fact, a nonlinear term. If we consider a beam that is only subject to a compressive load, with  $q(x)=0$ , then the governing equation can be rewritten as

$$\frac{d^4 w}{dx^4} + k^2 \frac{d^2 w}{dx^2} = 0$$

(2)

where  $k^2 = P/EI$ .

Note that the governing equation (2) is now an eigenproblem. Using simply supported boundary conditions for the ends of the beam, we find the eigenvalues of (2) are given by equation (3).

$$k_n L = n\pi \quad \text{for } n = 1, 2, 3, \dots$$

(3)

Rearranging this expression gives the following equation for the loads corresponding to these eigenvalues

$$P_n = n^2 \frac{\pi^2 EI}{L^2}$$

(4)

We are most interested in the lowest load for which the beam becomes unstable, i.e., the critical load. This corresponds to the case with  $n = 1$ , i.e., .

$$P_{cr} = \frac{\pi^2 EI}{L^2}$$

(5)

The critical load based on this theory is often referred to as the Euler buckling load. Using this load, we can compute the axial stress in the beam when it buckles

$$\sigma_{cr} = \frac{P_{cr}}{A} = \frac{\pi^2 EI}{L^2 A}$$

(6)

where  $A$  is the cross-sectional area of the beam. This critical stress is often written in terms of the radius of gyration ( $R_g$ ) of the column about its weak axis, which is defined as  $R_g \equiv \sqrt{I/A}$ . With this definition, the critical buckling load stress and strain from this theory are given by

$$\sigma_{cr} = \left( \frac{\pi R_g}{L} \right)^2 E$$

$$\varepsilon_{cr} = \left( \frac{\pi R_g}{L} \right)^2$$

(7)

## Buckling of an Imperfect Column and the Southwell Plot

The model of Euler buckling is flawed. In particular, the beam is not perfectly straight and the axial compressive load is not applied through the center of the beam. As a result, the beam does not suddenly buckle at  $P_{cr}$  but more gradually buckles in a direction determined by the imperfections in the beam. Such an imperfect beam is shown in Figure 2. Even though these imperfections can be quite small, they can have a large effect on the response of the structure. This is called imperfection sensitivity.

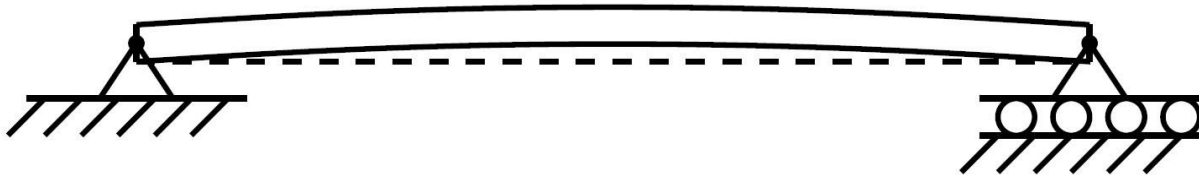


Figure 2. Imperfect Euler beam with initial curvature.

A more sophisticated analysis that takes into account an initial imperfection of the beam, where the imperfection causes an initial displacement with the form  $a_1 \sin(\pi x/L)$ , results in the following expression for the transverse deflection of the beam at its mid-point ( $x = L/2$ ) as a function of the Euler buckling load.

$$\delta = \frac{Pa_1}{P_{cr} - P}$$

(8)

This relationship forms the basis of the **Southwell plot**. Rearranging this relationship, one can create an expression for the deflection normalized by the load, i.e.,

$$\frac{\delta}{P} = \frac{\delta}{P_{cr}} + \frac{a_1}{P_{cr}}$$

(9)

A Southwell plot consists of a series of measurements plotted on a graph of  $\delta/P$  versus  $\delta$ . The slope of a linear fit to the data then provides  $P_{cr}$  and the y-intercept provides a measure of the initial displacement magnitude (see Figure 3a).

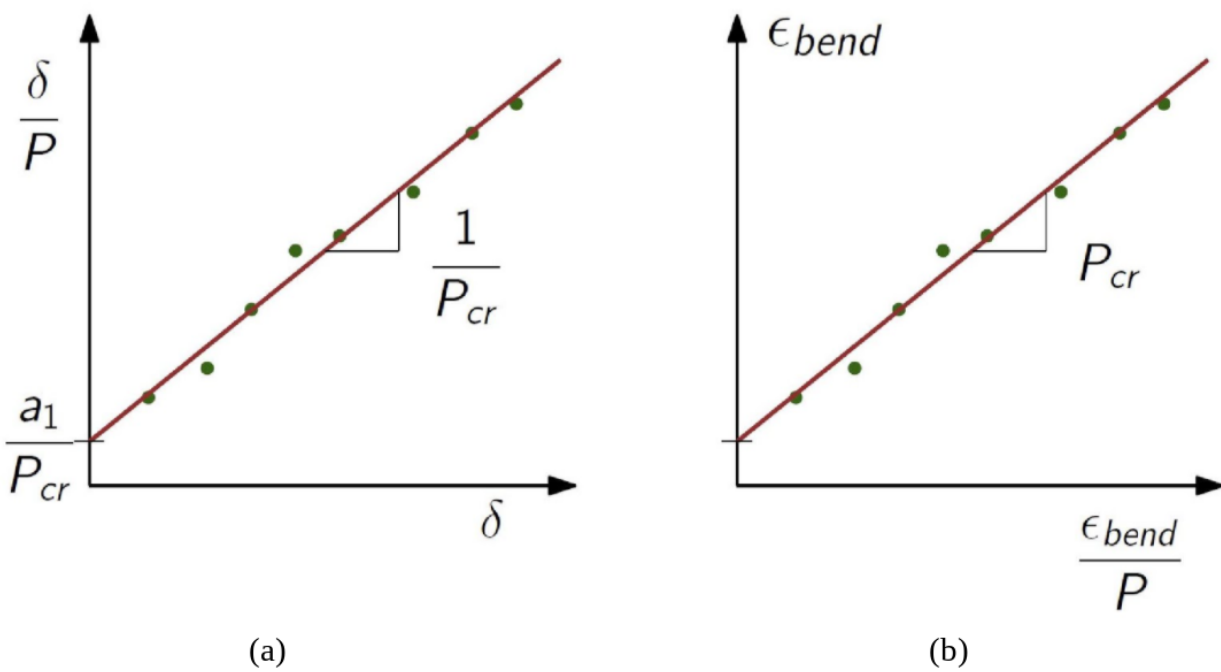


**Figure 3.** Southwell plots for determining the critical load: (a) Southwell plot in original form, (b) Southwell plot for strain. The figures are not drawn to scale, and the slopes on the two graphs are the reciprocal of one another.

In this lab, however, we will only be able to measure the bending strains using the strain gages mounted to the specimen. Therefore, we will modify the classical Southwell plot to use our strain measurements as follows. First, we note that the bending moment at the mid-point of the beam is  $M = \delta P$ . With the expression for the bending strain,  $\varepsilon_{bend} = -yM/EI$ , the deflection of the beam at the mid-span is

$$\delta = \frac{2EI}{Ph} \varepsilon_{bend}$$

(10)

where we have used  $y = -h/2$  as the bending moment. Substitution of this value for  $\delta$  into (9) yields

$$\varepsilon_{bend} = \frac{\varepsilon_{bend}}{P} P_{cr} - a_1 \frac{Ph}{2EI}$$

(11)

This version of the Southwell plot for strain (see Figure 3b) is the one you will use for data reduction in this lab.

## Experimental Setup: Cantilever Beam

The experiment involves a cantilever beam approximately 12 inches long, which is mounted within a support fixture, see **Figure 5**. Beam dimensions will be measured with a precision digital caliper. In general, calipers are devices used to measure thicknesses or distances between surfaces, usually having a screw-driven or sliding adjustable piece.

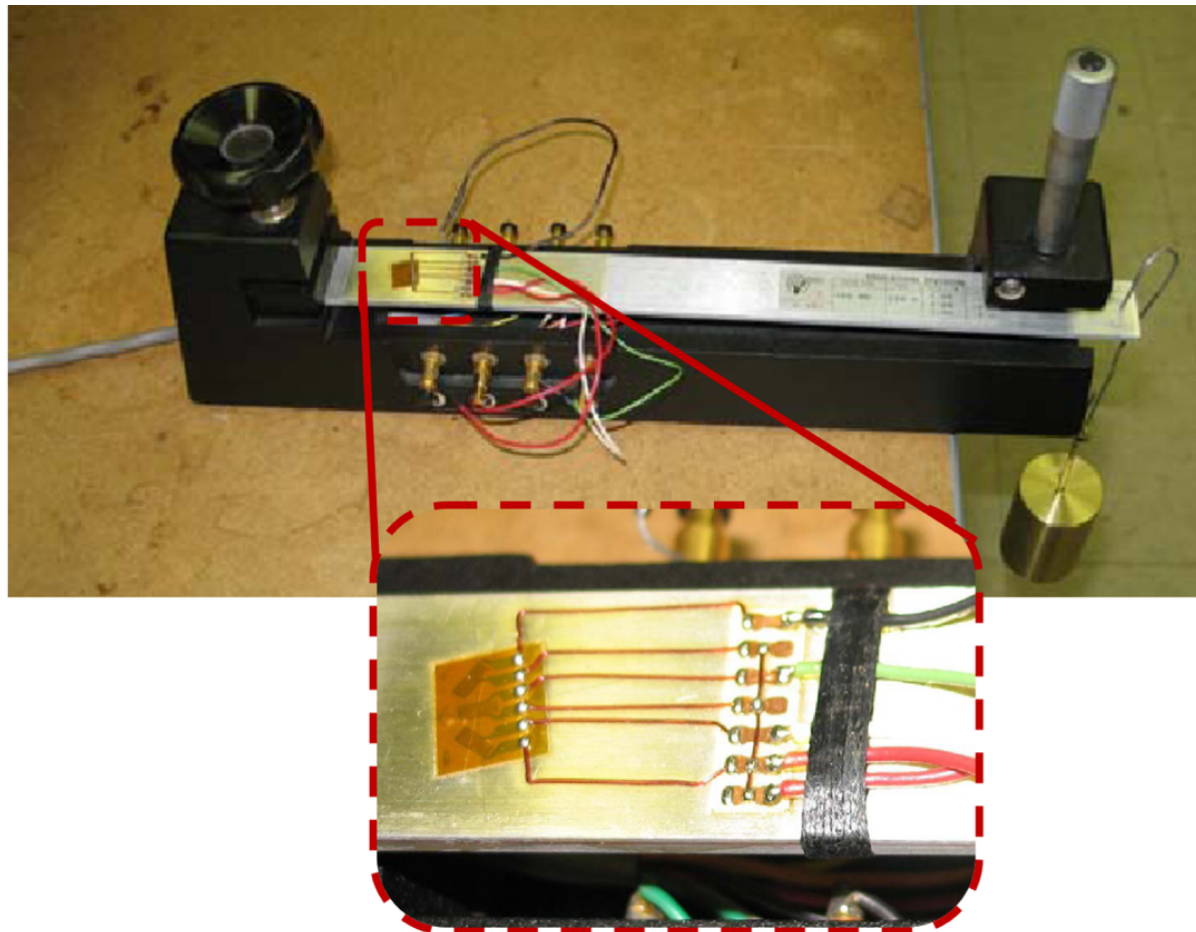


**Figure 5.** Photograph of cantilever beam experimental configuration.

The set-up allows either an applied load at the free end of the beam (by hanging dead weights) or a prescribed deflection of the beam using a precision micrometer (shown at right side of **Figure 5**). Precision micrometers typically use a finely threaded screw to accurately measure a linear distance. Turning the outer thimble moves a central rod, called the spindle. A given angular rotation corresponds to a linear distance traveled by the spindle based on the pitch of the screw. The distance the end of the spindle moves can be read from combined scales: a low-resolution length scale on the sleeve and a high-resolution rotating scale on the thimble (see **Figure 7**). On some micrometers, the readable resolution of the rotating scale is increased by the addition a fine vernier scale on the sleeve.

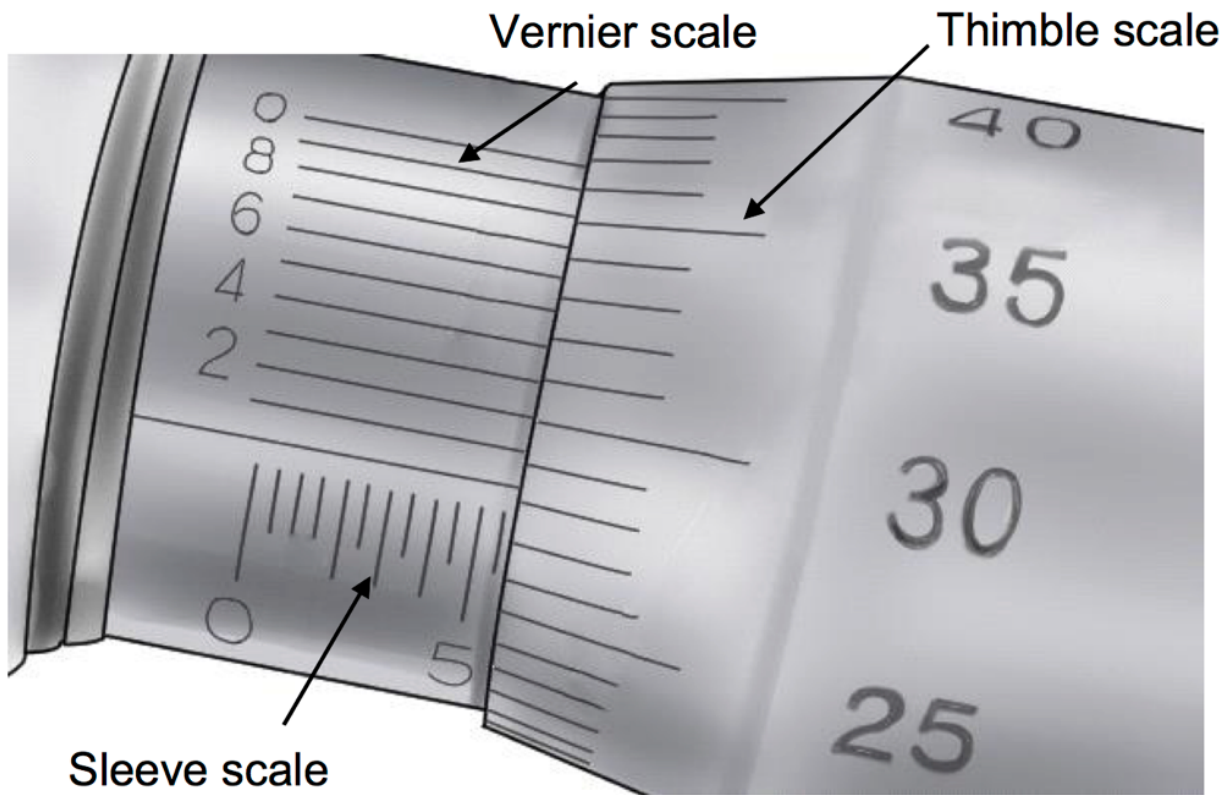


**Figure 7.** Micrometer scale.

A rectangular rosette strain gauge rosette is bonded on the top surface near the root of the beam (**Figure 5**). Each of the three individual grids in the rosette strain gauge will be connected to a dedicated 1/4 bridge circuit within the Vishay 7000 data acquisition system.

### Experimental Setup: Column buckling

All the test subjects are composed of 2024-T3 aluminum. Each column will only be tested in the elastic regime to ensure accurate results with the strain gages and so as not to permanently deform the columns. There are two test specimens: a long and a short column; both have rectangular cross-sections (see Table 1 for dimensions).

	Long Column	Short Column
Length (in.)	29	24
Width (in.)	0.75	0.75
Thickness (in.)	0.50	0.50

**Table 1.** Dimension of aluminum columns.

When pure axial loads are applied to the nominally perfect columns, we have no advance knowledge of any preferential buckling direction; thus it is difficult to correctly place any lateral displacement gage. As a result, the columns are fitted with two strain gages at mid-span mounted on the top and bottom surfaces of the beam.

Assuming that the strain varies linearly through the beam, the axial strain measured at the top ( $\varepsilon_a$ ) and bottom ( $\varepsilon_b$ ) surfaces of the beam would be

$$\varepsilon_a = \varepsilon_{axial} + \varepsilon_{bend}$$

$$\varepsilon_b = \varepsilon_{axial} - \varepsilon_{bend}$$

(12)

where  $\varepsilon_{axial}$  is the strain from the axial deformation and  $\varepsilon_{bend}$  is the strain due to bending. To find these two strains, we could combine the measured strains to produce

$$\varepsilon_{axial} = \frac{1}{2}(\varepsilon_a + \varepsilon_b)$$

$$\varepsilon_{bend} = \frac{1}{2}(\varepsilon_a - \varepsilon_b)$$

(13)

Due to the fact that the direction of buckling is unknown, the strain reading may either be positive or negative.

Note that the bending strain is also given by

$$\varepsilon_{bend} = -\frac{h}{2}K = -\frac{hM}{2EI}$$

(14)

---

## Procedure

### Cantilever beam

1. Measure the beam dimensions: thickness ( $h$ ) and width ( $b$ ) using the precise electronic caliper.
2. Measure the length  $L_1$ , from the application position of the micrometer to the clamped end of the beam, as well as the length,  $L_2$ , from the point of application of the dead load to the clamped end (see Figure 8).

Determine the distance  $X_g$  between the end of the beam and the rosette center-line. Note that the accuracy of the distances  $L_1 - X_g$  and  $L_2 - X_g$  are critical to your data reduction.

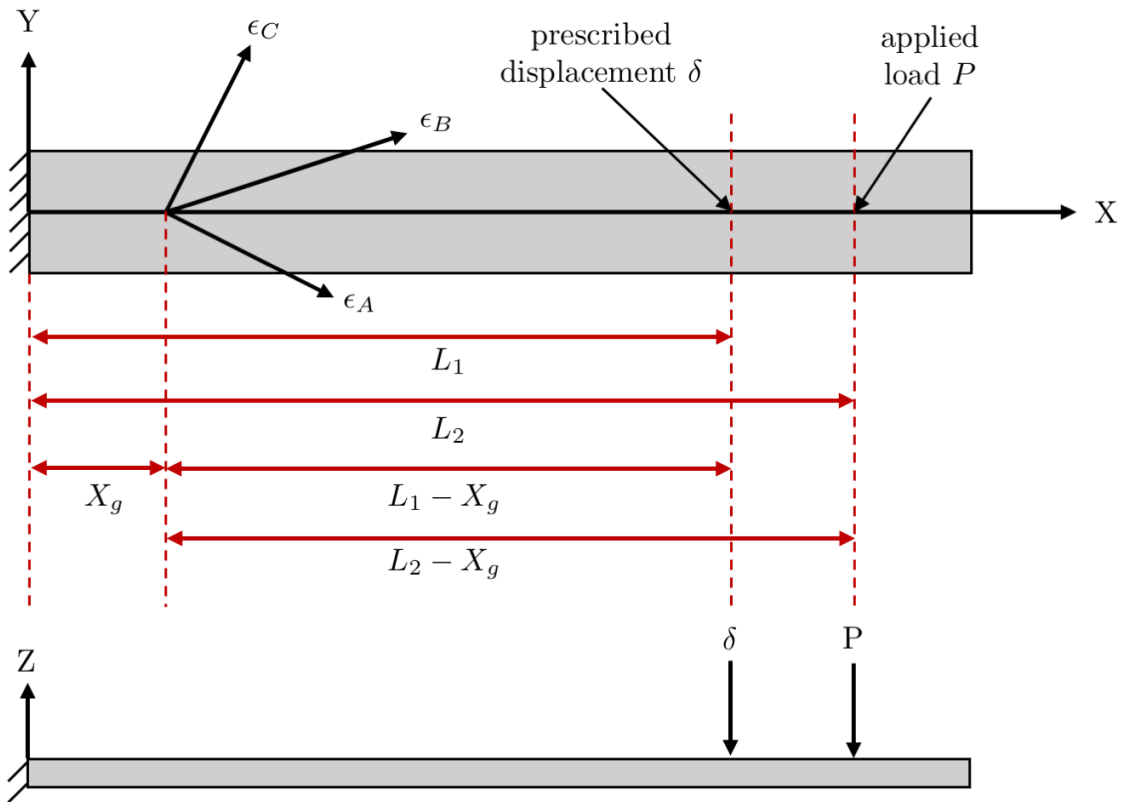


Figure 8. Cantilever beam dimensions.

*3. Load-control tests:* Apply prescribed loads ( $P$ ) by hanging dead weights from the point labeled "Applied load" in Figure 8. Record the strain readings indicated by each gauge within the rectangular rosette gauge in response to a set of applied loads ranging from 0 to 1000 grams.

*4. Displacement-control tests:* Apply prescribed displacements using the precision micrometer used to measure the beam deflection  $\delta$ . Record the strain readings indicated by each gauge within the rectangular rosette gauge in response to prescribed displacements at the free end of the beam from 0 to 0.6 in.

## Column buckling

- Locate the test fixture to be used to connect the beams to the Instron Load Frame. The fixture consists of two small round vee-grooved inserts that will be located in the small holes in the two aluminum plates attached to the lower crosshead and upper load cell extension in the Instron Load Frame.

### Long Column Tests

- Mount the long column between the vee-groove adapters.

2. Load the column under manual load control from 100lbf to 900lbf. Use five different load settings. For each setting record load and bending strain readings.
3. Again using manual load control, record the load and bending strains as you unload the beam. For the unloading run, use five loadings; repeat one of the intermediate loadings from Step 3, but choose different loadings for the other four points.

### Short Column Tests

1. Remove the long column and mount the short column between the vee-groove adapters.
  2. Load the column under manual load control from 500lbf to 1300lbf. Use five different load settings. For each setting record load and bending strain readings.
  3. Using manual load control, record the load and bending strains as you unload the beam; again, repeat one of the intermediate loadings from Step 6, but choose different loadings for the other four points.
- 

## Data to be Taken

1. Cantilever beam dimensions and locations of rosette, micrometer and load along beam.
  2. Strain readings for known loads from the cantilever experiment.
  3. Strain readings for known deflections from the cantilever experiment.
  4. Axial loads and bending strains for loading and unloading runs for long column buckling.
  5. Axial loads and bending strains for loading and unloading runs for short column buckling.
- 

## Data Reduction

### For the load-controlled experiments:

1. Using the rectangular rosette strain gauge data, determine the strains  $\epsilon_X^*$ ,  $\epsilon_Y^*$ , and  $\gamma_{XY}^*$  and that resulted from each of the applied loads.
2. Based on  $\epsilon_X^*$ ,  $\epsilon_Y^*$ , and  $\gamma_{XY}^*$  estimate for each of the applied loads: the maximum and minimum principal strains ( $\epsilon_1$  and  $\epsilon_2$ ).
3. Determine the slope of the best fit linear relationship between  $\epsilon_1$  and  $P$  and use it, along with cantilever beam theory for the relationship between the axial strain  $\epsilon_X$  and  $P$  at the free end of the beam, to estimate the elastic modulus  $E$  in MPa of the cantilever beam material. This relationship will also depend on the geometric quantities  $(L_2 - X_g)$ ,  $b$  and  $h$

### For the displacement-controlled experiments:

1. Using the rectangular rosette strain gauge data, determine the strains  $\epsilon_X^*$ ,  $\epsilon_Y^*$ , and  $\gamma_{XY}^*$  that resulted from each of the applied deflections.
2. Based on  $\epsilon_X^*$ ,  $\epsilon_Y^*$ , and  $\gamma_{XY}^*$ , estimate for each applied deflection: the maximum and minimum principal strains ( $\epsilon_1$  and  $\epsilon_2$ ).
3. Determine the slope of the best fit linear relationship between  $\epsilon_1$  and  $\delta$ , and use it, along with the relationship between  $P$  and the beam deflection  $\delta$  from cantilever beam theory to estimate the “effective bending spring stiffness” (in N/m) of the cantilever beam. To accomplish this, you will also need to use your estimate of  $E$  from the load-controlled data

### **For the column buckling experiments:**

1. Using a Southwell plot for each of the columns, determine the column's buckling load and buckling (axial) stress.
  2. Calculate the theoretical buckling load and stress for each column based on beam theory.
- 

## **Results Needed for Data Report**

1. Table of measured rosette strains ( $\epsilon_A, \epsilon_B, \epsilon_C$ ) and inferred local strains ( $\epsilon_X^*, \epsilon_Y^*, \gamma_{XY}^*$ ) for each of the applied loads.
2. Table of measured rosette strains ( $\epsilon_A, \epsilon_B, \epsilon_C$ ) and inferred local strains ( $\epsilon_X^*, \epsilon_Y^*, \gamma_{XY}^*$ ) for each of the applied deflections.
3. A combined plot of  $\epsilon_X^*$ ,  $\epsilon_Y^*$  and  $\gamma_{XY}^*$  as a function of the applied load (in Newtons).
4. A combined plot of  $\epsilon_X^*$ ,  $\epsilon_Y^*$  and  $\gamma_{XY}^*$  as a function of the applied deflection  $\delta$  (in meters).
5. Plot of  $\epsilon_1$  as a function of  $P$  (in Newtons), including the best-fit line.
6. Plot of  $\epsilon_1$  as function of  $\delta$  (in meters), including the best-fit line.
7. Table of linear proportionality constants for  $\epsilon_1$  vs.  $P$  and  $\epsilon_1$  vs.  $\delta$ , and inferred beam elastic modulus and effective bending stiffness.
8. Table of measured strains for each of the applied (measured) axial loads for long column.
9. Table of measured strains for each of the applied (measured) axial loads for short column.
10. Individual Southwell plots for each of the columns.
11. Table of experimentally determined and predicted buckling loads for each column.

# Turbine Engine

## Objective

This laboratory introduces the measurement of gas temperature and explores the performance of a jet engine. First, the operation and proper use of thermocouples is explored. Then, thermocouples are used to measure gas temperatures at various locations in the jet engine. In addition, engine pressures are measured with piezoresistive transducers.



**NOTE: All combustion experiments are potentially hazardous. Please follow all precautions outlined in the safety section and given during the lab.**

## Background

### Temperature Measurements

There are a number of devices used for the measurement of temperature. Most rely on the effect temperature has on some other *measurable* property of a substance. One of the oldest types is the expansion thermometer, which relies on the change in volume of a substance (usually a liquid) as the temperature varies. An example is the glass tube, mercury-filled thermometer, in which the height of the mercury column becomes a measure of temperature. While easy to manufacture, expansion thermometers are not easily implemented as small, compact electronic sensors.

Various electronic temperature sensors have been developed, including thermocouples, resistance thermometers and quartz resonance thermometers. In a quartz resonance thermometer, temperature is determined by its influence on the resonant frequency of a quartz crystal. Since frequency can be determined to great accuracy, these devices have potential for high resolution. Resistance temperature detectors (RTDs) rely on the change in resistance of a material with temperature; thus measurement of resistance is converted to a temperature measurement. There are two basic types of RTDs: metal based devices and semiconductor devices (also known as *thermistors*). While quite accurate temperature measurements can be obtained with RTDs and crystal thermometers,\* they are usually limited to “low temperature” operation. For example, platinum resistance thermometers can operate only up to  $\sim 1000^{\circ}\text{C}$ , while thermistors are generally limited to a few hundred degrees Celsius. Thermocouples, on the other hand, can provide reasonably accurate measurements at temperatures up to at least 2600 K with proper choice of materials.



\*Quartz resonance thermometers and RTDs can have precisions better than  $10^{-4}^{\circ}\text{C}$ .

### Thermocouple Principles

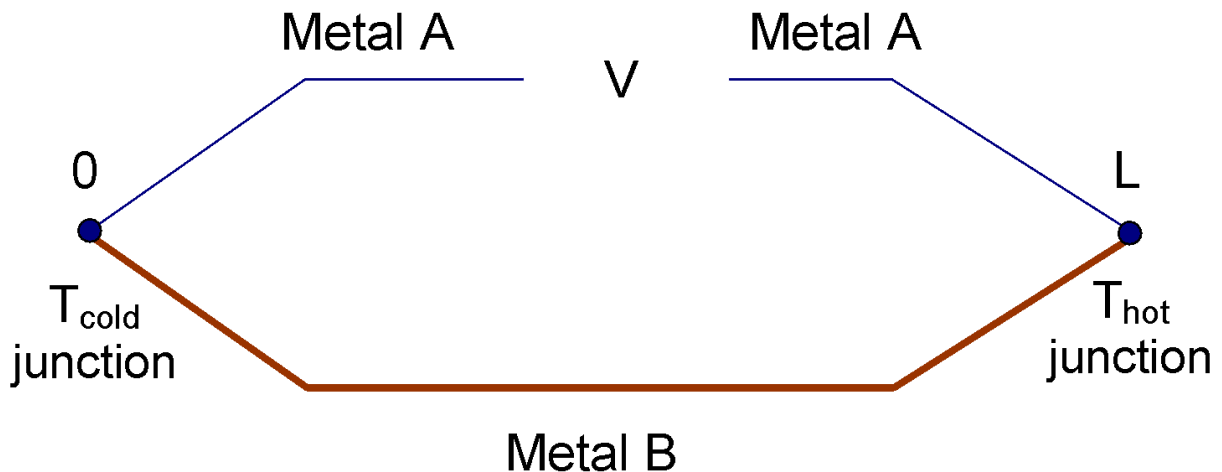


**Figure 1.** Simple (open) thermoelectric thermocouple circuit.

Thermocouples rely on the voltage produced by a temperature difference between two junctions formed between thermoelectrically dissimilar metals (see Fig. 1). In other words, a thermocouple is simply two different types of metals, usually in the form of wires, connected together. The voltage is produced because a temperature gradient in a metal conductor also induces a gradient in electron density in line with the temperature gradient. It can be shown that the voltage produced between the two junctions of the Fig. 1 circuit is given by:

$$V = \int_0^L \varepsilon_A \frac{dT_A(x)}{dx} + \int_L^0 \varepsilon_B \frac{dT_B(x)}{dx} dx$$

(1)

where  $T(x)$  is the temperature distribution along each wire, and  $\varepsilon$  is called the thermoelectric power of the material.<sup>†</sup> Thus it can be seen that the **voltage difference is generated throughout the length of the wires**, and is due to the local temperature gradient.

ⓘ <sup>†</sup> Equal to the sum of the Thomson coefficient and temperature derivative of the Peltier coefficient for the metal.

When the wire is perfectly uniform in composition, such that  $\varepsilon$  is not a function of position, and the two wires are connected between  $T_{cold}$  and  $T_{hot}$ , the integrals in equation (1) become,

$$V = \int_{T_{cold}}^{T_{hot}} \varepsilon_a dT + \int_{T_{hot}}^{T_{cold}} \varepsilon_B dT = \int_{T_{cold}}^{T_{hot}} (\varepsilon_A - \varepsilon_B) dT$$

(2)

In this case, one can think of the voltage produced in a thermocouple as strictly due to the temperature difference between the junctions. It is important to remember that this holds only for the above **uniformity assumption**. In fact, some descriptions of thermocouples erroneously state that the voltage is produced "at the junction", when in fact it is produced wherever there is a temperature gradient in the metal. The thermocouple circuit that will be considered the "ideal" circuit is shown in Fig. 2. The difference between it and the circuit of Fig. 1 is simply that the voltage is "measured" at the reference junction, instead of midway through one of the legs of the thermocouple. Note, both points in the reference junction must be at the same temperature (*isothermal*) to be equivalent to the circuit of Fig. 1.

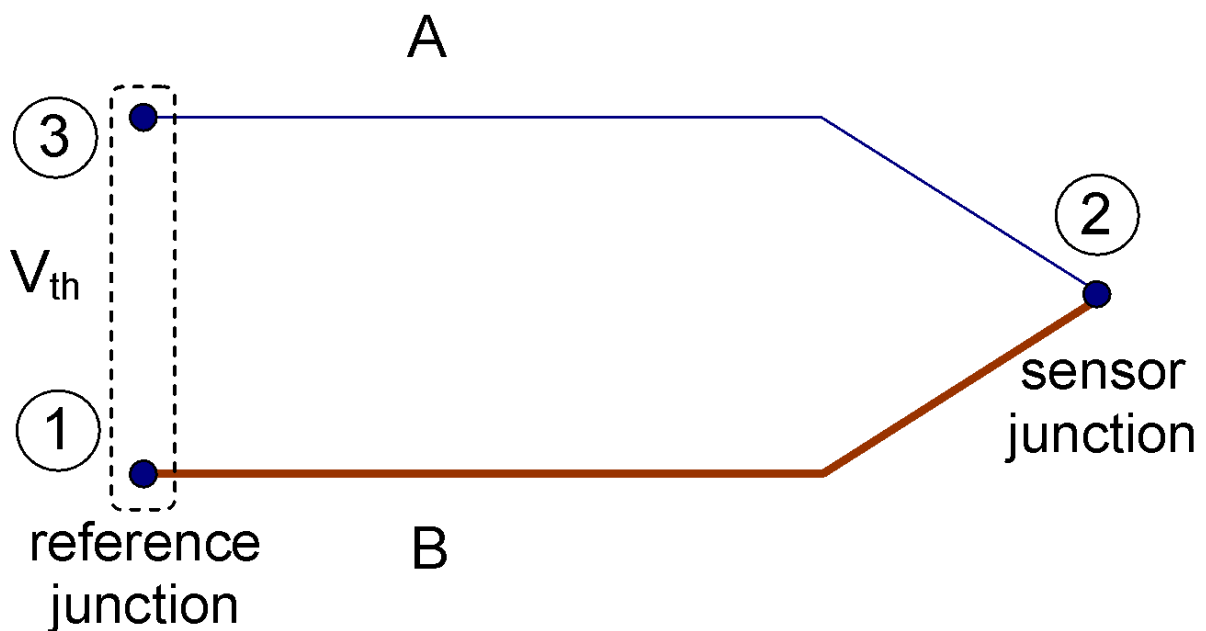


**Figure 2.** Ideal thermoelectric circuit, with the thermocouple voltage measured across the *isothermal* reference junction.

While any two metals with different  $\epsilon$  can be used to produce a thermocouple,\*\* a small number of metals (both pure and alloys) have been identified for their stability, linearity, reproducibility, and high temperature capability. Table 1 lists some common pairs of thermocouple materials, including their approximate limiting operating temperature. Some of these are sufficiently common that they are considered standards and are denoted simply by a letter. For example, a chromel/alumel †† device is called a "type K" thermocouple, and it has a nearly linear temperature sensitivity (see Fig. 3). The pairs of metals listed in Table 1 were also chosen for their good temperature sensitivity, which is normally achieved by picking materials that have  $\epsilon$  with different signs. Figure 4 shows the voltage that would be generated along a single, homogeneous wire of various materials as a function of the temperature difference between its two ends. For the type K thermocouple, the chromel and alumel alloys produce voltages of opposite sign for the same temperature gradient.

**i** \*\*In fact, there have been a number of applications where the operating temperature of a machinery part has been measured using the machine structure itself as part of the thermoelectric circuit.

†† Chromel is a nickel-chromium alloy; alumel is a nickel-aluminum alloy

Material	**** T <sub>max</sub> °C (°F)	ANSI Type	Allowable atmosphere	Avg Output mV/100°C
Tungsten/ tungsten 26% rhenium	2320/4210	-	inert, H <sub>2</sub> (nonoxidizing)	1.7
Tungsten 5% rhenium/ tungsten 26% rhenium	2320/4210	-	inert, H <sub>2</sub> (nonoxidizing)	1.6
Platinum 30% rhodium/ platinum 6% rhodium	1820/3310	B	oxidizing, inert	0.76
Platinum 13% rhodium/ platinum	1770/3200	R	oxidizing, inert	1.2
Platinum 10% rhodium/ platinum	1770/3200	S	oxidizing, inert	1.0
Chromel/alumel	1370/2500	K	oxidizing, inert*	3.9
Chromel/constantan	1000/1830	E	oxidizing, inert*	6.8
Iron/constantan	1200/2193	J	reducing, inert, vacuum †	5.5
Copper/constantan	400/750	T	mild oxidizing, reducing vacuum, inert	4.0

\*Limited use in vacuum or reducing environments

† Limited use in oxidizing at high temperature

**Table 1.** Some standard thermocouple materials and their properties.

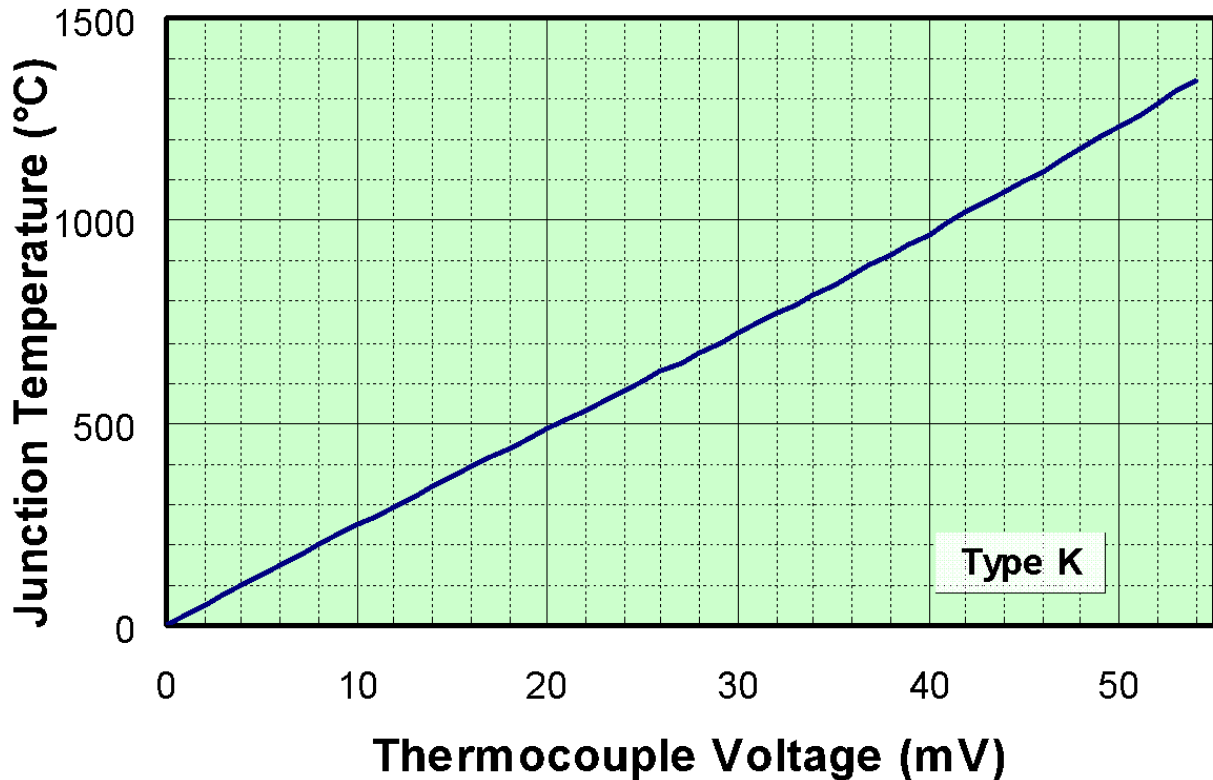


**Figure 3.** Sensitivity of a standard type-K thermocouple, based on ITS-90 inverse polynomial fit. The millivolt output is based on a reference temperature of 0°C.

The temperature behavior shown in Fig. 4 can be used to explain what happens in a thermocouple circuit like that of Fig. 2. Consider a type-J thermocouple connected between a reference junction at  $T_{\text{ref}}$  and a junction at higher temperature,  $T_{\text{probe}}$ . As shown in Fig. 5, the voltage that would be produced is found by starting at the reference temperature, following a line with a slope equal to  $\varepsilon_{\text{iron}}$  up to  $T_{\text{probe}}$ , and then switching to a line with the slope of  $\varepsilon_{\text{constantan}}$  back to  $T_{\text{ref}}$ . Thus the constantan end of the reference junction will be at a higher voltage than the iron. If the temperature at the probe junction is raised, the thermocouple voltage increases. The reason that two dissimilar materials must be used is also evident in Fig. 5. If iron was used for both legs of the thermocouple, the voltage developed in the first leg of the circuit would be canceled as the temperature drops in the other leg, i.e., we would follow the iron curve upward to  $T_{\text{probe}}$ , and then back down to  $T_{\text{ref}}$  with no net voltage induced.

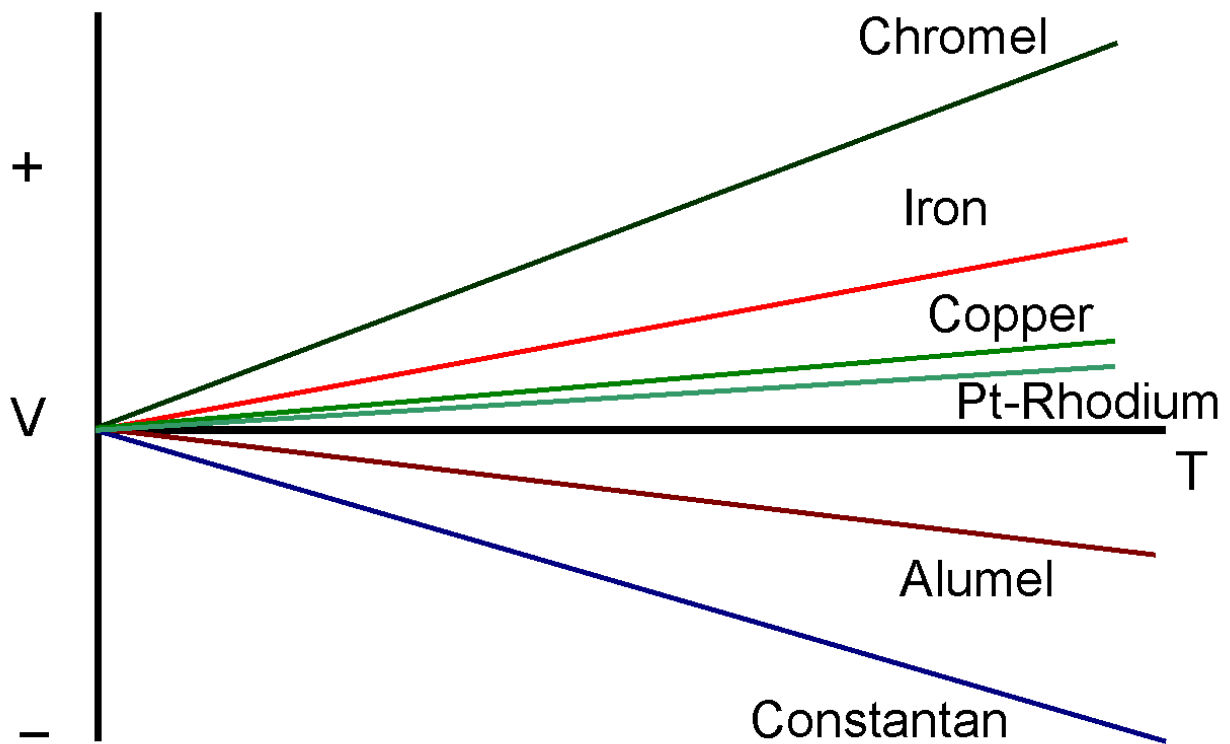


**Figure 4.** Voltage–temperature response for several metals.

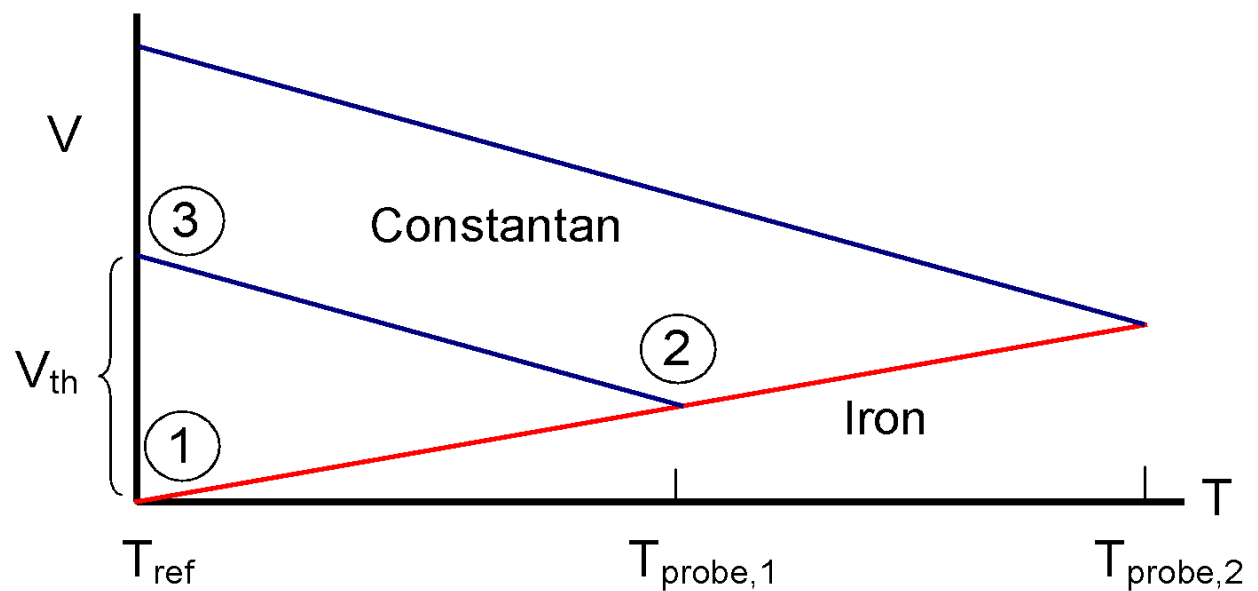


**Figure 5.** Development of the voltage difference across the thermocouple,  $V_{th}$ , in a thermocouple circuit, like that of Fig. 2, formed by two metals.

While the circuit of Fig. 2 is ideal, it is usually not practical. First, thermocouple wire can be somewhat expensive. Thus it becomes costly if the measuring device needs to be located remotely from the experiment. Also, it is not uncommon to connect multiple thermocouples to a single measurement device through some sort of switching circuit. Finally, the measurement device may have wires and connectors of its own, which effectively become part of the thermocouple circuit. Therefore, it is important to consider modifications to the ideal circuit. For example,

Fig. 6 shows a circuit in which the reference junction is connected to the measurement device through copper wires. As seen in Fig. 7, the voltage difference across the device junction ( $V_{15}$ ) is identical to the reference junction voltage ( $V_{24}$ ) if the copper wires are identical, and if the device connections (1 and 5) are both at the same temperature. In this case the voltage developed in leg 1-2 is counteracted by the voltage produced in leg 4-5.

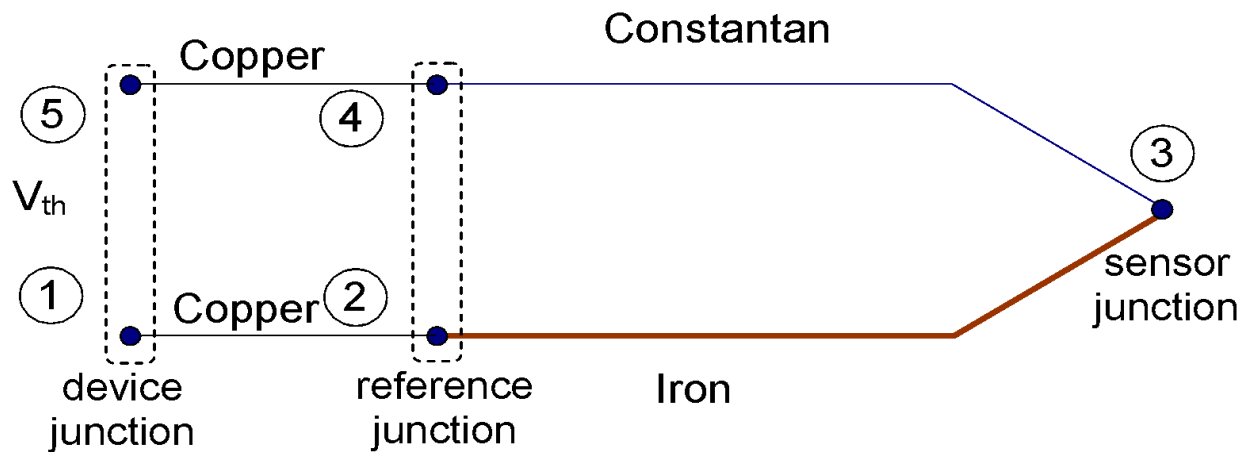


**Figure 6.** Modified circuit; copper extension wires connect the thermocouple to the measuring device, and the device connections are at the same temperature.

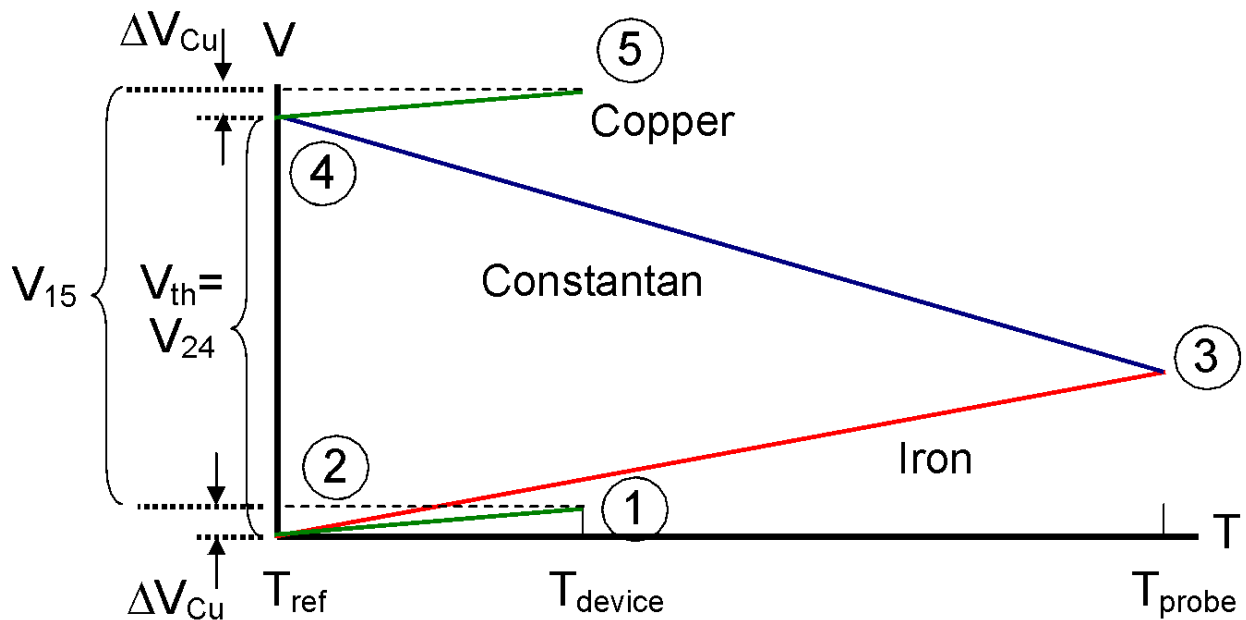


**Figure 7.** Development of the thermocouple voltage difference for the thermocouple circuit shown in Fig. 6. If the wires connecting points 1 to 2, and 4 to 5 are identical, and the temperatures  $T_1$  \*\*and  $T_{ref}$  are the same, then the voltage measured across the device ( $V_{15}$ ) is equal to the voltage that would be produced by the ideal thermocouple circuit ( $V_{th} = V_{24}$ ).

### Thermocouple Referencing

So far we have explored the thermocouple voltage that is produced between a junction at an unknown temperature  $T_{\text{hot}}$  and another junction at  $T_{\text{ref}}$ . To convert the thermocouple voltage to the unknown  $T_{\text{hot}}$  requires us to know two things: 1) the change in voltage associated a given temperature change, i.e., the temperature sensitivity of the thermocouple materials, and 2)  $T_{\text{ref}}$ .

First, consider ways to determine  $T_{\text{ref}}$ . There are two basic approaches: 1) create a situation where  $T_{\text{ref}}$  is fixed by some physical condition, and 2) measure  $T_{\text{ref}}$  with another device. A known temperature can be produced using a phase point of a material, for example 0°C can easily be produced to within 0.01°C accuracy by a bath of liquid water and ice, *if the ice and water are both present and allowed to come to equilibrium* (this generally requires crushing the ice to small size and putting the mixture in an insulated container). If the reference junction (or points 2 and 4 in Fig. 6) are place in the ice bath, then  $T_{\text{ref}}$  will essentially be 0°C. In many situations, however, it is impractical to require access to ice. Therefore, a popular approach is to measure the reference junction's temperature with a thermistor or similar device that can provide accurate, absolute temperature measurements, *though at low temperatures*.

With  $T_{\text{ref}}$  known, all that remains is to convert the thermocouple voltage to temperature. Standard thermocouple materials have been extensively studied at the National Institute of Standards and Technology (NIST), and the voltage produced by a thermocouple at  $T_{\text{hot}}$  is generally reported for  $T_{\text{ref}} = 0^{\circ}\text{C}$ , and the values are available in tables, graphs (such as Fig. 3) or polynomial fits (see Table 2). If one is using a 0°C reference junction, then you simply look up the measured thermocouple voltage in the table (or graph or fit) and find the corresponding temperature. If you are using a different reference temperature, you must first add an offset voltage to your measured voltage. The offset is the voltage would be produced by a thermocouple at your measured  $T_{\text{ref}}$  referenced to 0°C. Electronic ice reference circuits exist to do just this, the add the proper offset voltage to account for  $T_{\text{ref}} \neq 0^{\circ}\text{C}$ .

Temperature Range	0-500 °C	500-1372 °C
Voltage Range	0-20,644 µV	20,644-54,886 µV
$a_0$	0.000000	$-1.318058 \times 10^2$
$a_1$	$2.508355 \times 10^{-2}$	$4.830222 \times 10^{-2}$
$a_2$	$7.860106 \times 10^{-8}$	$-1.646031 \times 10^{-6}$
$a_3$	$-2.503131 \times 10^{-10}$	$5.464731 \times 10^{-11}$
$a_4$	$8.315270 \times 10^{-14}$	$-9.650715 \times 10^{-16}$
$a_5$	$-1.228034 \times 10^{-17}$	$8.802193 \times 10^{-21}$
$a_6$	$9.804036 \times 10^{-22}$	$-3.110810 \times 10^{-26}$
$a_7$	$-4.413030 \times 10^{-26}$	-
$a_8$	$1.057734 \times 10^{-30}$	-

**Table 2.** ITS-90 thermocouple inverse polynomials for type K thermocouples; two polynomial fits are listed, for separate temperature/voltage ranges. The reference junction is assumed to be at 0°C, and the polynomials are of the form,  $T = \sum a_i V^i$ , with  $T$  in degrees Celsius and  $V$  in microvolts.

### Gas Temperature

Strictly speaking, a thermocouple sensor measures the temperature of the thermocouple junction itself, which of course is not what we usually want to know. Rather, we wish to determine the temperature of the body in which the thermocouple is embedded. For gas temperature measurements, the “body” of interest is the gas. As shown in Fig. 8, there are two basic thermocouple probe arrangements: one in which the thermocouple junction is immersed in the gas (*unshielded probe*); and one where the junction is inside some housing material (usually a metal), and the housing is immersed in the gas (*shielded probe*). The former provides a better measure of the gas temperature and a better time response; the latter approach protects the thermocouple from damage or exposure to incompatible gases (see Table 1). For high speed flows, there are also shielded *stagnation probes*, which are designed to slow the flow down to a very low velocity before it contacts the thermocouple junction (see Fig. 8 for a simple example).

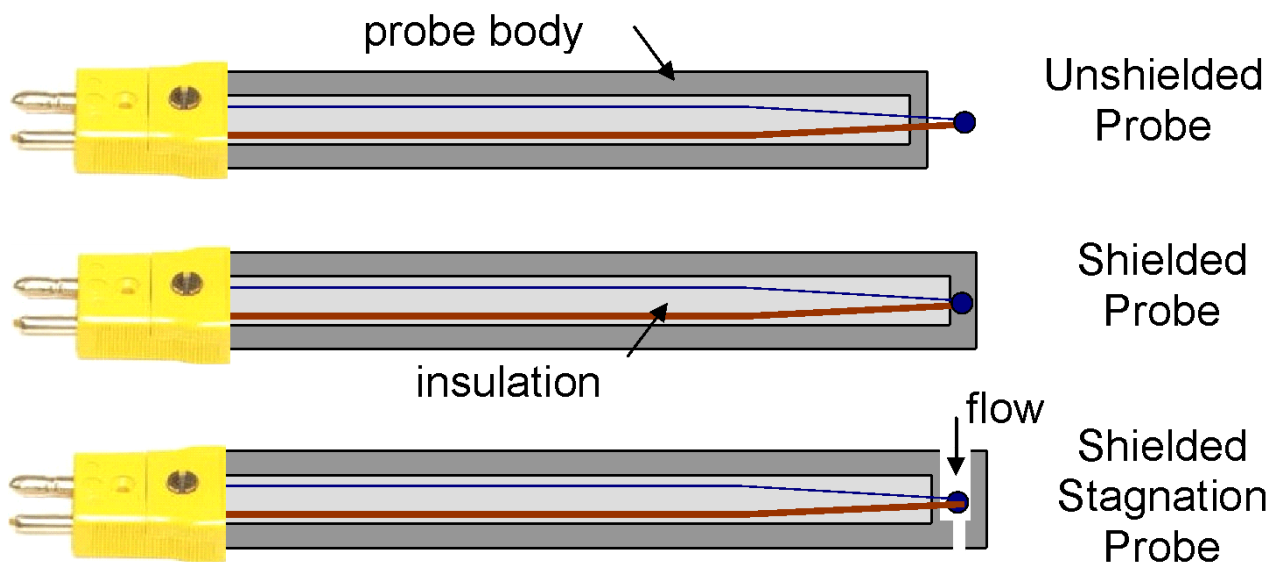


**Figure 8.** Examples of unshielded, shielded and stagnation thermocouple probes.

In general, the thermocouple temperature can not exactly equal the gas temperature due to heat losses. Assuming the gas is the hotter material, it will heat up the initially colder thermocouple junction. If the thermocouple had no way of losing energy, then it would eventually heat up to the gas temperature. However, the thermocouple can lose heat; either by thermal conduction from the junction down through the thermocouple wires, or by radiation. Therefore even in steady-state operation, the thermocouple will tend to be at a lower temperature than the surrounding (hot) gas in low speed flows. For high speed flows, the thermocouple temperature will also be affected by the conversion of the flow's kinetic energy to thermal energy in the region in front of the probe.

Therefore in high speed flows, the thermocouple temperature will generally exceed the freestream static temperature.

## Pressure Measurements

You will also be making pressure measurements in this lab with a transducer that is something like the Barocel/Baratron type transducers used in a previous lab, i.e., a differential pressure is determined from the movement of a thin diaphragm exposed to the pressure difference. Instead of the capacitance based approach of the Barocel/Baratron devices, the sensors used in this lab consist of a miniature diaphragm and strain sensors composed of semiconductor material and manufactured using MEMS (Micromachined Electro-Mechanical Systems) technology. The sensors are described in more detail in a following lab.

## Turbine Engines

In most cases, with the exception of civil aviation, modern aircraft are powered by turbine engines (also called gas turbines). While piston engines are efficient for low power applications, their power (or thrust) to weight ratio drops significantly as engine power increases. This makes them unsuitable for large aircraft that require high power engines. Gas turbine engines are also used in a number of other applications including marine propulsion, operating gas pipeline compressors, and most notably, the generation of electric power.

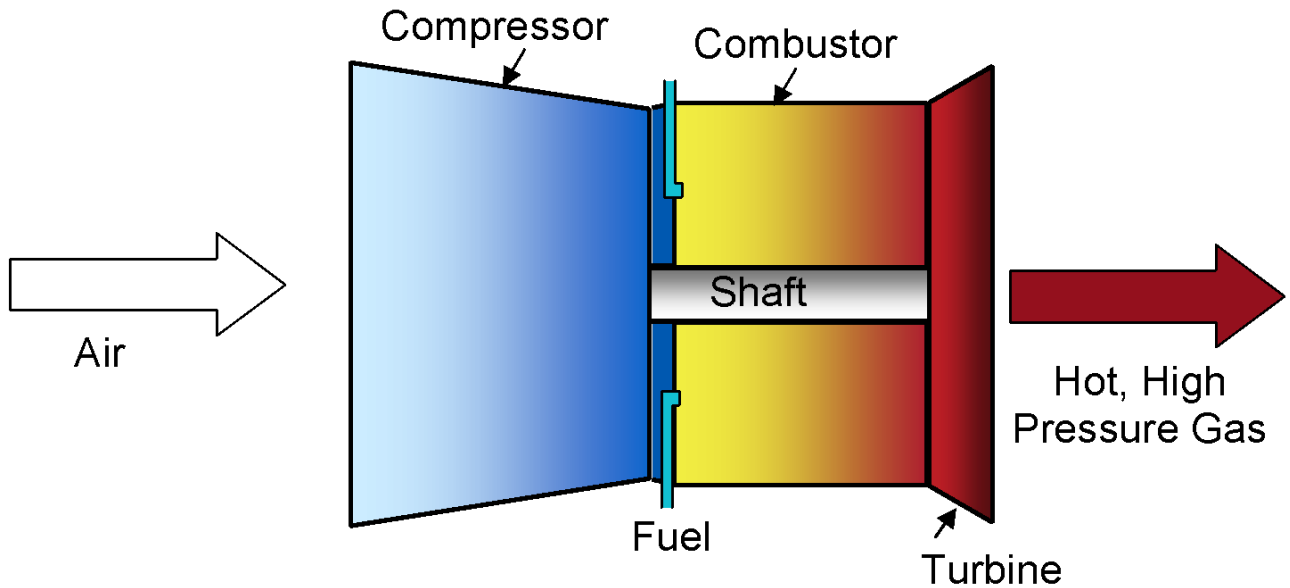
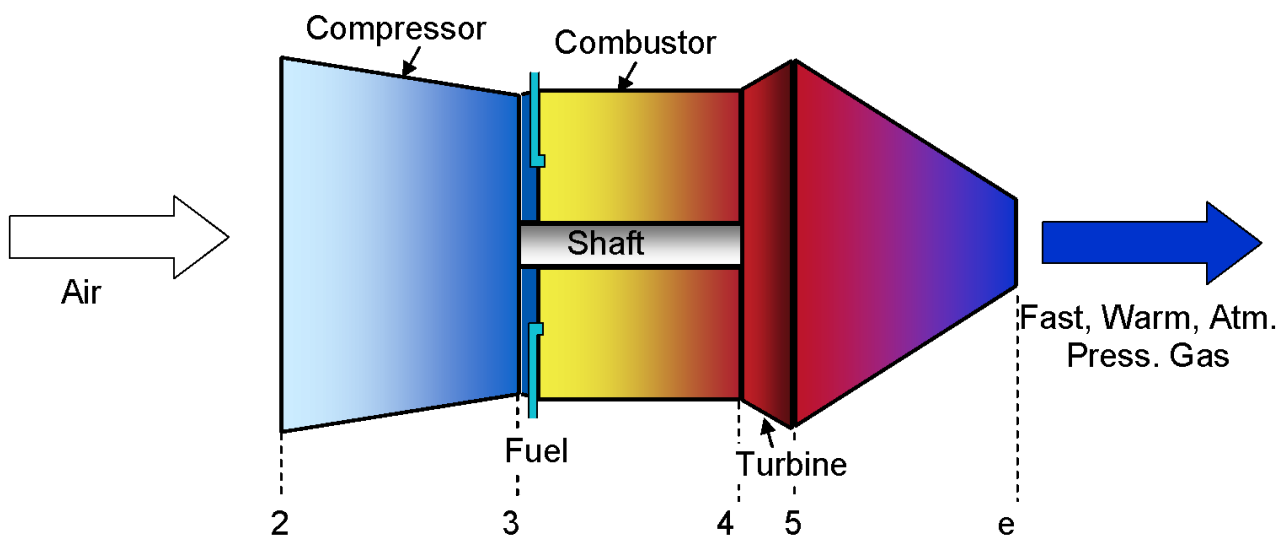
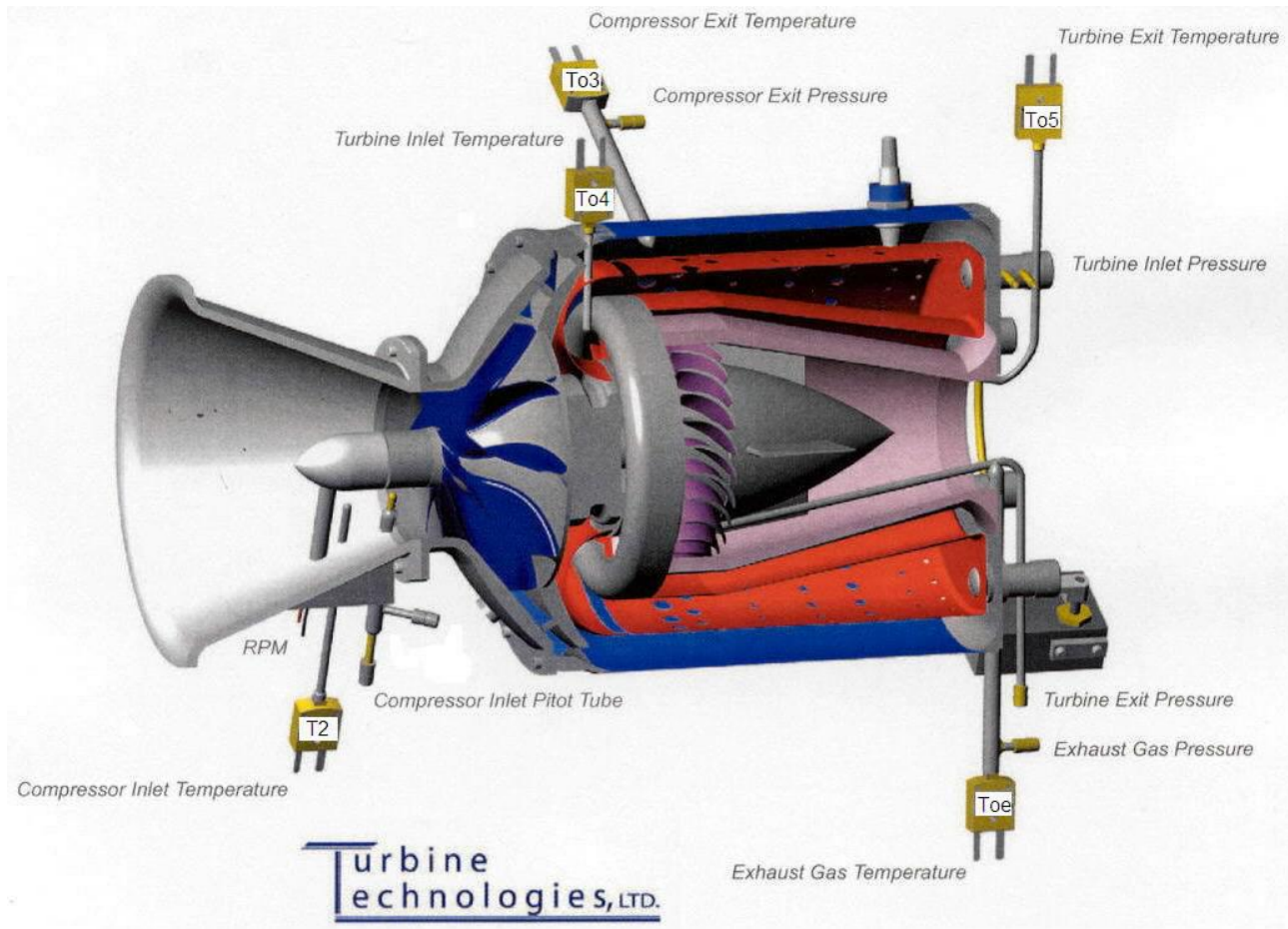


Figure 9. Basic components of a gas turbine engine.



**Figure 10.** Basic components of a gas turbine engine.

The components of a basic gas turbine system are shown in Fig. 9. Air enters the engine (through an inlet not shown) and passes through a rotating compressor that raises the air pressure. Next, the high pressure air enters the combustor where it is mixed with fuel and burned without much change in pressure. The hot products then pass through a rotating turbine that extracts work from the flow and sends it to the compressor via a rotating shaft. The exhaust of the turbine is a hot, high pressure gas. In a **turbojet**, the exhaust is expanded through a nozzle (Fig. 10), which converts the thermal energy to kinetic energy, i.e., it accelerates the gas in order to produce thrust. On the other hand in a **turboshaft** engine, the hot, high pressure gas exiting the first turbine is expanded through a following power turbine that converts the thermal energy to shaft power, which can be used to run a rotor in a helicopter engine or to turn an electric generator in an aircraft's auxiliary power unit (APU) or in a ground power station. In this lab, you will operate and perform measurements on an SR-30 turbojet manufactured by Turbine Technologies, Ltd. (Fig. 11), operating on Jet-A fuel.



**Figure 11.** Schematic of the gas turbine system to be used in this lab.

### Thermodynamic Analysis

The following is a brief description of the thermodynamic expressions used to analyze a jet engine.\*\*\* The processes that occur in a turbine engine can be modeled, *in the ideal case*, ††† by a Brayton cycle. As shown in Fig. 12, the ideal compressor ( $2 \rightarrow 3$ ), turbine ( $4 \rightarrow 5$ ) and nozzle ( $5 \rightarrow e$ ) can be modeled as isentropic processes (constant entropy,  $s$ ). The ideal combustor ( $3 \rightarrow 4$ ) is modeled as a constant pressure heat addition, where the “heat” comes from burning the fuel, and the heat release rate is given by

$$\dot{Q} = \dot{m} \times HV$$

(3)

where  $\dot{m}_f$  is the fuel mass flow rate and  $HV$  is the heating value of the fuel ( $\sim 45\text{MJ/kg}_{\text{fuel}}$  for most liquid jet fuels).

ⓘ \*\*\*A more detailed development can be found in the text for AE 4451, Hill and Peterson's Mechanics and Thermodynamics of Propulsion.

††† Meaning each component of the engine is reversible and has no heat losses

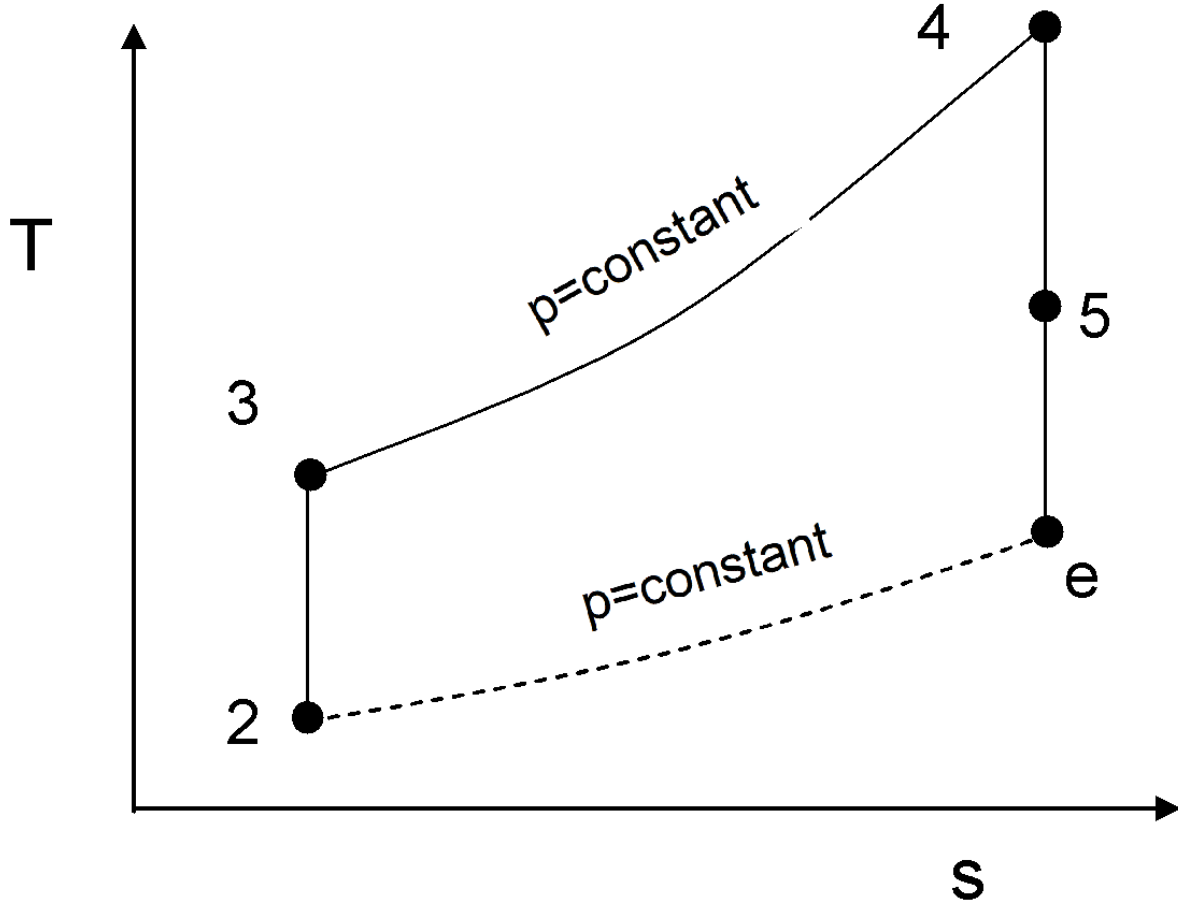


**Figure 12.** Ideal Brayton cycle; stations 2-e correspond to the numbering scheme shown in Fig. 10.

For the three isentropic processes, we can find a relationship between the ratios of temperature (absolute, i.e., in Kelvin or Rankine units) and pressure (absolute, not gauge pressure) across each device from the entropy state equation for a perfect gas, i.e., for an isentropic process going from state a to state b,

$$0 = S_b - S_a = \int_{T_a}^{T_b} c_p \frac{dT}{T} - R \ln \frac{p_b}{p_a} \Rightarrow \frac{p_b}{p_a} = e^{\int_{T_a}^{T_b} \frac{c_p}{R} \frac{dT}{T}}$$

(4)

Assuming that the gas is also calorically perfect ( $c_p = \text{constant}$ ),

$$\frac{p_b}{p_a} = \left( \frac{T_b}{T_a} \right)^{\frac{c_p}{R}} = \left( \frac{T_b}{T_a} \right)^{\frac{\gamma}{\gamma-1}}$$

(5a)

or equivalently for stagnation properties,

$$\frac{p_{ob}}{p_{oa}} = \left( \frac{T_{ob}}{T_{oa}} \right)^{\frac{\gamma}{\gamma-1}}$$

(5b)

where  $\gamma$  is the ratio of specific heats ( $\gamma = c_p/c_v$ ).

There is also a relationship between the stagnation temperature change across the compressor and turbine. Since the turbine is used to power the compressor, the output power of the turbine should equal the power input to the compressor (assuming steady operation and no shaft losses, which are typically less than 1% of the shaft power). Therefore from conservation of energy (*and for adiabatic conditions*),

$$\dot{W}_T = (\dot{m}_a + \dot{m}_f) c_{p,T} (T_{o4} - T_{o5}) = \dot{m}_a c_{p,C} (T_{o3} - T_{o2}) = \dot{W}_c$$

(6)

where  $\dot{m}_a$  is air mass flow rate entering the engine, and  $c_{p,T}$  and  $c_{p,C}$  are the (average) specific heats of the gases passing through the turbine and compressor. Similarly, the velocity at the nozzle exit can be found from

$$u_e = \sqrt{2c_{p,N}(T_{oe} - T_e)}$$

(7)

where  $c_{p,N}$  is the (average) specific heat of the gas passing through the nozzle, and  $T_{oe} = T_{o5}$  (again *assuming the nozzle is adiabatic, i.e. no heat losses*). For the combustor, again using energy conservation, we can calculate the expected change in temperature caused by burning the fuel:

$$T_{o4} = (T_{o3} + f HV)/c_{p,Combustor}/(1+f)$$

(8)

where  $f$  is the fuel-air ratio  $\dot{m}_f / \dot{m}_a$ .

If the compressor, turbine and nozzle are not ideal, i.e., they are not reversible (*but still adiabatic*), the temperature and pressure ratios across each component are related by the adiabatic component efficiencies:\*\*\*

$$\eta_{compressor} = \frac{(p_{o3}/p_{o2})^{\frac{\gamma-1}{\gamma}} - 1}{(T_{o3}/T_{o2}) - 1}$$

(9)

$$\eta_{turbine} = \frac{1 - (T_{o5}/T_{o4})}{1 - (p_{o5}/p_{o4})^{\frac{\gamma-1}{\gamma}}}$$

(10)

$$\eta_{nozzle} = \frac{1 - (T_e/T_{o5})}{1 - (p_e/p_{o5})^{\frac{\gamma-1}{\gamma}}}$$

(11)

Note, if the nozzle is truly adiabatic, then  $T_e/T_{o5} = T_e/T_{oe} = (p_e/p_{oe})^{\frac{\gamma-1}{\gamma}}$ .

We can also define an overall thermal efficiency of a static (stationary) turbojet engine, which is given by,

$$\eta_{th} = \frac{\text{Output Kinetic Power}}{\text{Input Heat Rate}} = \frac{(\dot{m}_f + \dot{m}_a)u_e^2/2}{\dot{m}_f HV}$$

(12)

If the turbojet is ideal (and  $c_p$  is assumed constant throughout the engine), it can be shown that the thermal efficiency should solely be a function of the cycle pressure ratio:

$$\eta_{th} = 1 - \frac{1}{(p_3/p_2)}^{\frac{\gamma-1}{\gamma}}$$

(13)

Thus as pressure ratio of the compressor increases,  $\eta_{th}$  of the engine should increase.

---

## Safety Considerations

As with any combustion experiment **safety is a primary concern**. Improper operation of the jet engine can damage the engine, and pose a hazard to those nearby. Carefully follow all the safety instructions presented during the lab concerning startup, operation and shutdown of the engine. Do not operate the engine without direct supervision by the lab technician. Do not place any part of your body, or any objects in the inlet or exhaust regions. **All students working in the lab MUST WEAR safety glasses/goggles in the lab and hearing protection when the engine is operating** (both will be supplied to you).

---

## Preliminary

*The following items must be turned in at the start of your lab session.*

1. Using the information supplied in Table 2, determine the thermocouple voltage you would expect to measure if the type-K thermocouple junction was at room temperature (~74°F) and the reference junction was placed in an ice bath.
  2. Bring a modified copy of the equation you developed in the earlier labs that relates dynamic pressure to velocity of a gas, and the ambient pressure and temperature. You need to **modify** the **equation** to use **dynamic pressure in psi** rather than mm Hg.
- 

## Procedure

1. Locate the electronic barometer/thermometer and record the ambient pressure and temperature.
2. Locate the type K, unshielded thermocouple probe (it has a yellow base). Connect the probe to the color-coded type K thermocouple extension wire. Then connect the extension wires to the standard electrical wire using the strip screw terminal according to the diagram of Fig. 14. Record the thermocouple voltage with the thermocouple exposed to the ambient air, and any other systems you can measure (e.g., an ice bath or boiling water).

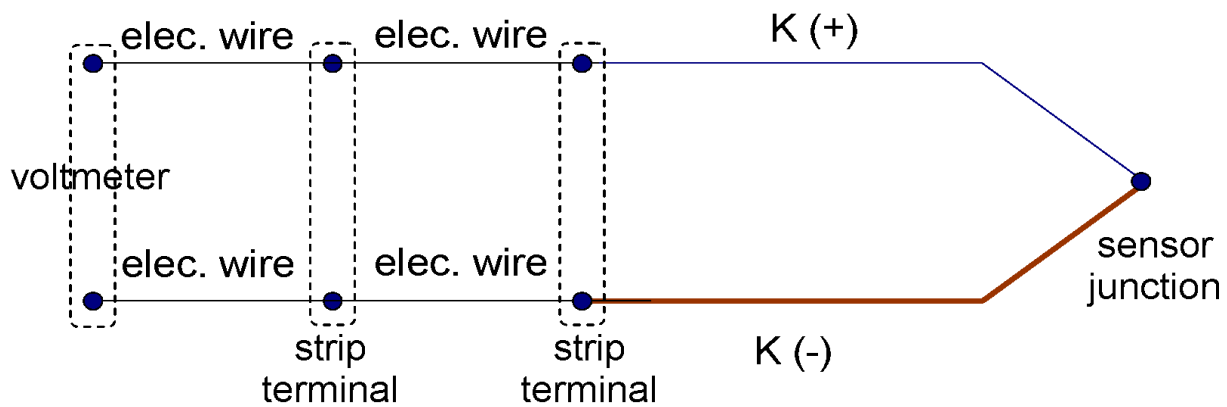


**Figure 14.** Thermocouple circuit to be used in this lab.

1. Again record the thermocouple voltage with the thermocouple exposed to the ambient air, except this time raise and lower the temperature of the screw terminal junctions. You should do this: a) where the thermocouple extension wires connect to the first set of electrical wires and b) again where the first and second set of electrical wires are connected. You can also try to change the temperature of a single connector or both connectors in each junction. Record the measured voltage for each of these various cases.
2. Disconnect the extension wires from the probe, and connect the probe to the electronic ice point module (small rectangular yellow box). Connect the module to the voltmeter, and switch on the ice point module (be careful not to rotate the switch all the way to the ON mark; make sure the voltage reading changes after you turn the module on). Record the thermocouple voltage with the thermocouple exposed to the ambient air and any other systems you wish.
3. Turn off the ice point module.
4. Take a tour of the turboshaft engine cutaway in the Combustion Lab foyer.
5. Familiarize yourself with the flowpath through the SR-30 turbojet engine.
6. Review the safety, startup, and engine shutdown procedures with the lab TA's and with the lab technician who will oversee the engine operation.
7. Determine the cross-sectional area of the flow where the inlet velocity is measured.
8. Ask the lab technician to start the engine (the technician may ask students to help, but the engine should be started only under the supervision of the lab technician).
  
11. Acquire data for *at least 5 RPM* conditions (change RPM by changing the throttle – which changes the fuel flowrate). DO NOT EXCEED 82,000 RPM. The data acquisition program will allow you to continuously monitor the engine RPM, pressures and temperatures. When you decide to acquire data at some RPM, the software will sample all the probes, and update graphs of engine conditions vs. RPM. Each time you acquire the data, the computer will pause until you are ready to return to the real-time display. **NOTE:** it will be very hard to hear while the engine is running. Make sure your group has discussed what conditions you are looking for and work out some hand signals to identify when you want to take data and when you want to return to the real-time display.

1. When you are finished, ask the technician to shutdown the engine.

**i** The efficiency compares an actual process to an isentropic one that has the same starting condition and same pressure ratio

## Data to be Taken

1. Ambient pressure and temperature.
2. Voltages from the type-K thermocouple probe connected to the voltmeter under the different connection and temperature cases described above.
3. Cross-sectional area of the compressor inlet.
4. Values of: 1) dynamic pressure and  $T_2$  at the compressor inlet, 2)  $T_{o3}$  and  $p_{o3}$  (gauge) at the compressor exit, 3)  $p_{o4}$  (gauge) and  $T_{o4}$  at the turbine inlet, 4)  $p_{o5}$  (gauge) and  $T_{o5}$  at the turbine exit, 5)  $p_{o6}$  (gauge) and  $\sim T_{o6}$  at the nozzle exit, and 6) pressure drop (a voltage signal) in the fuel system at various RPM settings.

## Data Reduction

1. Unshielded thermocouple probe temperatures reduced from the measured voltages (without heating or cooling the strip terminal junctions).
2. Air mass flowrate (from dynamic pressure at the compressor inlet).
3. Fuel mass flowrate (from fuel pressure reading and calibration, see Table 3).

Voltage (Volts)	Flowrate (cc/min)
1.7	175
2.2	227
2.8	255
3.0	300

**Table 3.** Calibration data for fuel flowrate

1. Compressor efficiency.
2. Exit static temperature determined from the nozzle exit  $p_{o6}$  (which is measured as a gauge pressure here) and the exit stagnation temperature  $T_{oe}$ .
3. Nozzle exit velocity.
4. An estimate of the heat loss rate from gas to the nozzle (based on the difference in stagnation temperature across the nozzle).
5. Compressor and turbine powers (assuming adiabatic operation).
6. The actual engine thermal efficiency.

## **Results Needed for Report**

1. Tables of the thermocouple voltages and reduced temperatures for the different cases.
  2. Tables of the raw and reduced engine conditions at each operating RPM.
  3. Plot of the compressor pressure ratio versus air mass flowrate.
  4. Plot of the compressor efficiency versus air mass flowrate.
  5. Plot of the heat loss in the nozzle rate versus air mass flowrate.
  6. Plot of the engine thermal efficiency versus compressor pressure ratio.
- 

## **Further Reading**

1. Philip Hill and Carl Peterson, *Mechanics and Thermodynamics of Propulsion*, 2nd edition, Prentice-Hall, 1992.

\*\*\*\*

# Laser Doppler Velocimetry

## Objective

In this lab, you will learn the basic principles of laser Doppler velocimetry – which is a standard technique for measuring instantaneous, spatially resolved flow velocities. You will then use a laser Doppler velocimeter to explore the flowfield of a jet in a coflow. The jet is produced by the exhaust of a round pipe centered in a small, low-speed wind tunnel.



**Please note the following safety precautions very carefully:**

1. Your eyes, and your friends' and instructors' eyes, can get hurt by lasers. Take no chances or shortcuts: laser beams travel a lot faster than you can react! To ensure safety, no one who has not read the instructions thoroughly can be allowed near the experiment. Anyone disobeying safety rules will be ordered out of the lab immediately.
2. Remove all rings and watches when working in the vicinity of lasers.
3. Do not go to the back side of the test section unless directly supervised by a TA.
4. Do not lean over the laser beam, or stick your head between the laser transceiver and the test section when the laser is on.
5. Do not touch the laser or fiber optic coupler, whether the laser is on or off. If they go out of alignment, the TA will realign the system. Also, do not touch the transceiver unless instructed to.
6. Be very careful where you move the traverse: you must know clearly where all the reflections are (if any)!

## Background

Rapid fluctuations in velocity occur in most flows of practical interest. Examples are: the boundary layer above wings and fuselage surfaces, the wakes behind obstacles in flows, jets from the nozzles of rockets and gas-turbine engines, and flows inside engine components. These fluctuations have profound effects on such things as drag, surface shear stress, boundary layer separation, mixing between fuel and air in engines, and vibrations of turbomachines and control surfaces. To understand such phenomena, we must be able to measure velocity fluctuations accurately.

There are several difficulties in making such measurements. First, we must find a method that has a measurable change in output for small changes in velocity (*good signal sensitivity* or resolution), and which will work in the unsteady environment of a fluctuating flowfield (*robust*). Second, the device must respond faithfully, and perhaps without any time lag, to rapid fluctuations (*good temporal resolution* or *good high frequency response*). Third, the device must respond only to the velocity in a very small, and precisely known, region (*good spatial resolution*).

While the Pitot probe used in earlier experiments can measure mean velocities, it is not suited to measuring fluctuation velocities. There is another well-known probe, the hot wire (also known as a constant temperature

anemometer) that is suited to this task (under certain limitations). Its small, almost "microscopic" size gives it good spatial resolution and high frequency response. In addition, it has good signal sensitivity to velocity in constant temperature gas flows. The sensing element is a long circular cylinder, typically a tungsten or platinum wire of diameter in the range of 5 to 20  $\mu\text{m}$  ( $2.8 \times 10^{-4}$  inches). Slightly more rugged are hot-film sensors, which use glass rods,  $\sim 50 \mu\text{m}$  in diameter, with platinum films, typically 10 Å thick (Å = Angstrom =  $10^{-10}$  m), coated on the surface. In either case, the wire or the glass rod is fixed to two gold-plated steel needles which serve as the electric contacts to the sensor. The wire or film is kept heated by an electric current, to temperatures of 200 to 300 °C (and sometimes up to 800 °C). When air flows over the wire, energy in the form of heat is carried away by the much colder air stream (*forced convection*) because of the temperature difference between the (hot) sensor and (cold) air.

In many cases, however, probe-based approaches should be avoided so that the measurement not interfere with the flowfield (*nonintrusive*), else it change the quantity being measured. In addition to altering the flowfield, there may be several other reasons for using a nonintrusive technique. First, it may be physically difficult to design a probe that can survive in the flow to be measured. For example, consider the problem of measuring velocity inside the passages between the blades of a jet engine compressor while the engine is operating. Also it can be useful when several properties are varying simultaneously, as in a turbulent flame (e.g., inside an engine combustion chamber). For example, the velocity, pressure, and temperature may all be changing from one instant to the next. Most probes, such as Pitot tubes and hot-wires, respond to changes in several of these properties, and so it may be quite difficult to separate out the part due to velocity alone. Still another problem arises in two-phase flows (e.g., not all gas): there may be liquid droplets or solid particles that can clog or even instantly destroy sensitive probes. Examples of such applications include injection of liquid propellants or fuels sprays in rocket and aircraft propulsion systems, and water droplets and ice particles flowing around wings.

The laser Doppler velocimeter (LDV, also known as a laser Doppler anemometer - LDA) is a non-intrusive measurement device that is sensitive only to velocity. Thus, it is one of just a few techniques that can be used in complex flowfields to measure velocity. This is why, despite the greater cost and difficulty usually involved in making measurements with this technique, laser velocimeters are highly regarded instruments.

## Principles of Operation of LDV

When electromagnetic waves are scattered from moving objects, the scattered light has a frequency which is different from that of the incident waves. This is similar to the phenomenon that we have all observed: The horn of an oncoming car changes pitch suddenly as it passes us. The difference in frequency is known as the Doppler shift, and is proportional to the relative velocity between the moving object and the observer (or receiver). This principle is also used in radar and laser speed detection.

A laser is a source of radiation that *generally* has most of the following properties; it is: 1) well-collimated, which means the beam will not diverge or change in size much; 2) highly coherent, meaning its electromagnetic wavefronts are all in phase; and 3) nearly monochromatic, which means that the radiation is composed of a very narrow range of wavelengths. Thus, it is ideal for making measurements of Doppler shift; you can precisely and easily calculate what the shift should be for a given velocity. Unfortunately, the frequency of light is very high, and the Doppler shift caused by the kinds of velocity that we encounter is extremely small by comparison. So, if one were to shine a laser beam at a moving object, measure the incident light frequency and the scattered frequency, and try to find the difference, one would probably find that one's measuring instrument cannot make out the slight difference between these frequencies. The solution to this problem is to find the difference in Doppler shift

caused by two beams, hitting the same object at slightly different angles. If one tries to measure only this difference, one can get good accuracy. This is the principle of the dual-beam interferometer-type LDV that is widely used today (see Figure 1).

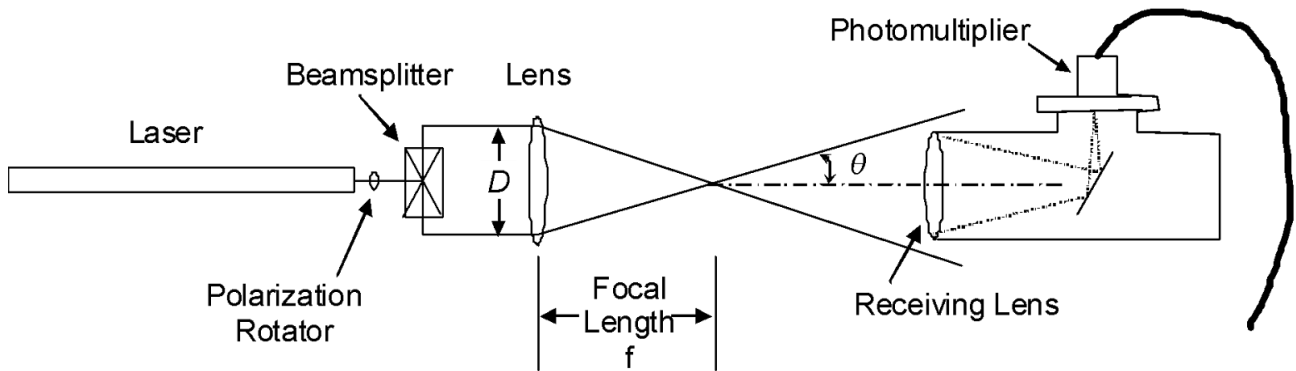
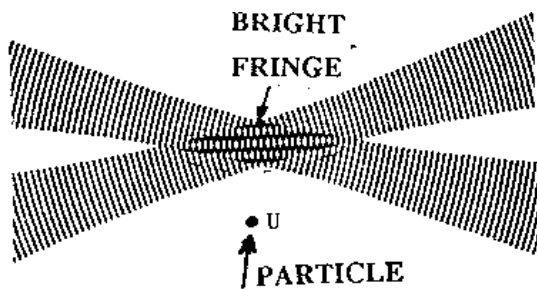


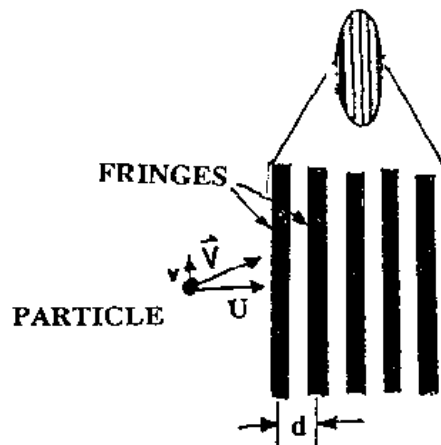
**Figure 1.** Schematic of a basic 1-component LDV system in forward-scattering mode (plan view).

### DualBeam Laser Velocimeter

When two laser beams of the same frequency cross in a small region, stationary interference fringes are formed, as shown in Figure 2. This is because light behaves as a kind of wave, with an amplitude and a phase. At some points, the two beams are in phase and the amplitudes add together; there the light's amplitude is large. At other points, the amplitudes cancel each other out (out-of-phase), and you get nothing at all. Thus, fringes are formed, with each bright fringe being a thin disc inside which the light intensity is large. The bright fringes are separated by dark fringes, where there is hardly any light intensity at all.



Plan view - fringe-crossings  
will yield  $U$  in plane of paper.



**d:** fringe spacing.  
**U:** velocity component perpendicular to the fringes.

**Figure 2.** Plan view of fringes formed when two laser beams cross (particle motion across fringes will yield vertical velocity in plane of paper). Note that the region with fringes looks ellipsoidal in shape

As seen from Figures 2 and 3, the region where the fringes exist is an ellipsoid of revolution. Consider a small solid or liquid particle moving perpendicular to the fringes (as shown in the figure). At the same time, imagine that a highly sensitive light detector is looking straight at the light being scattered from the ellipsoid. As that particle enters the first fringe, it starts scattering more light. The detector sees the received light intensity increasing. The intensity reaches a maximum when the particle is centered on the fringe, and decreases thereafter. As the particle reaches the center of the first dark fringe, the intensity sinks to a minimum, and the slowly starts increasing again as the particle approaches the next bright fringe.

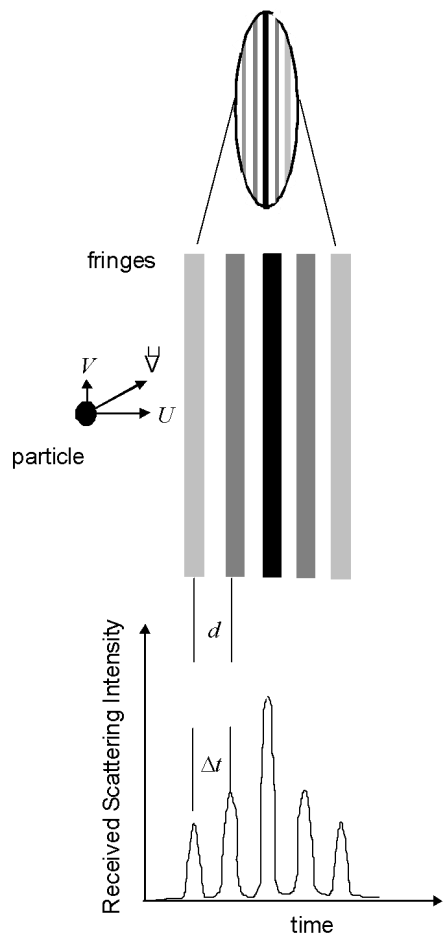


**Figure 3.** Sinusoidal variation in the intensity of scattered light, as a particle crosses the fringes ( $d$ =fringe spacing;  $U$ =velocity component perpendicular to the fringes;  $\Delta t$ =time between scattering peaks or  $1/\Delta t =$  Doppler frequency).

As the particle crosses the ellipsoidal region (the measurement volume of the LDV), the detector sees the light intensity oscillating in a sinusoidal fashion; this is known as a **signal burst** (as seen in Figure 3). If the particle moves faster, the same number of fringes will be crossed in less time, so that the **frequency** of the sinusoidal signal will increase. Thus, the frequency of the signal received at the detector is proportional to the speed of the particle along the direction perpendicular to the fringes. Note that it does not matter, as far as the frequency is concerned, how fast the particle is moving in other directions. Only the speed at which it crosses the fringes is important. Thus, the dual beam LDV is sensitive only to the component of velocity that is perpendicular to the bisector of the two laser beams, and in the plane of the beams.

Let us try to quantify this relationship. The frequency of the detected signal (which can be rigorously shown to be exactly equal to the Doppler shift) must be directly proportional to the velocity component, and inversely proportional to the **fringe spacing** (the distance between the middles of two successive bright fringes). The fringe spacing,  $d$ , for two beams of wavelength  $\lambda$ , intersecting at a half-angle  $\theta$ , is given by:

$$d = \frac{\lambda}{2 \sin \theta}$$

(1)

Thus, the Doppler shift frequency  $f_D$  is simply,

$$f_D = \frac{U}{d} = \frac{2U \sin \theta}{\lambda}$$

(2)

where  $U$  is the velocity component perpendicular to the fringes.

As an example, consider an Argon-ion ( $Ar^+$ ) violet laser with a wavelength of 476.5 nm (not the one in our LDV system). If particles in an air flow are moving at 10.0 m/sec and the half-angle between the laser beams is  $6.0^\circ$ , then the fringe spacing is 2.28  $\mu m$ , and the Doppler shift is 4.39 MHz (a frequency of 1 MHz means that the time between two successive peaks of the signal is  $10^{-6}$  sec).

### Focal Length, Beam Spacing, and Fringe Spacing

Notice that in the above calculation, the only parameter that depended on the flow was the flow velocity; the other parameters (laser wavelength and half-angle) depend on the instrument. Thus, the LDV requires no calibration, unlike many other measurement techniques. The half-angle ( $\theta$ ) between the beams is determined using simple geometry knowing the optical setup, i.e., by the spacing ( $D$ ) between the two beams when they come out of the front focusing lens of the LDV, and the focal length ( $f$ ) of the lens, which is the distance from the middle of the lens to the focal point where the beams cross (see Figure 1).

### Bragg Cell and Moving Fringes

While the simple dual-beam LDV system (such as that shown in Figure 1) is able to isolate and measure a single component of the flow velocity, it can not differentiate between positive and negative velocities. If the flow were to change direction, e.g., from forward to backward, a particle moving through the fringes with the same velocity magnitude would produce the same Doppler shift frequency  $f_D$  for either direction of motion. To overcome this, one of the two laser beams in a dual-beam LDV system can be passed through an acousto-optical modulator\* (called a **Bragg cell**) that can shift the beam's frequency slightly (e.g., by 10s of MHz).



\*In the acousto-optic modulator, the laser beam interacts with sound waves generated (typically by piezo-electric transducers) in an optically transparent material. The laser beam is diffracted off the index-of-refraction pattern caused by the pressure waves in the material.

When the two laser beams intersect, the fringes that are created are no longer stationary in space. The fringe pattern (i.e., the locations of the peaks and valleys) moves at a rate determined by this frequency shift. Now the detector will see a signal with an amplitude that oscillates at a frequency ( $f_{signal}$ ) that is different than  $f_D$ .

Assuming that the fringe pattern moves in the “forward” or “positive” flow direction, the signal frequency is given by

$$f_{signal} = f_{bragg} + (\text{sign}(U) \times f_D)$$

(3)

For example reconsider the particle described above, which was moving at 10.0 m/s through a fringe pattern with a spacing of 2.28  $\mu\text{m}$  ( $f_D = 4.39 \text{ MHz}$ ). If the second laser beam was shifted by a Bragg cell with frequency 10.0 MHz, causing the fringe pattern to move at 10 MHz in the negative direction of the flow, then the light scattered by the particle as it moved through the measurement volume would have an amplitude that oscillated at a frequency of  $10 + (+4.39) = 14.39 \text{ MHz}$  if the particle was moving in the forward direction, or 5.61 MHz if it was going backward.

#### DualBeam, OneComponent, Backward Scatter LDV System

The LDV system for this lab uses a 300 mW  $\text{Ar}^+$  green laser, fiber-coupled to a transceiver unit (see Figure 4). The light coming out of the laser goes to a fiber-coupler unit that first uses a beamsplitter to separate the original beam into two beams. One of these beams is then passed through a Bragg cell that shifts the frequency by 40 MHz. The two beams are then sent to the transceiver unit through fiber optic cables. The laser beams pass through a lens in the transceiver, and are focused down, so that they cross at the focus of the lens and form the measurement volume.

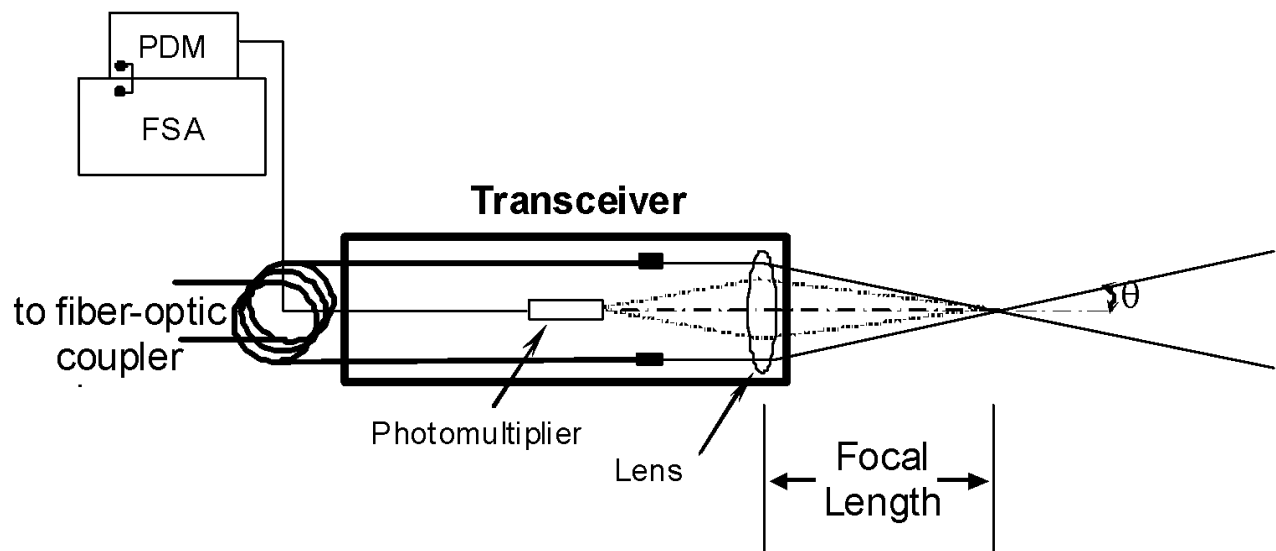


**Figure 4.** Schematic of lab LDV system with combined transmitter and receiver (transceiver) used in back-scattering mode.

#### Light Collection and Signal Processing

The back-scattered light from the focal volume is collected by a lens located in the transceiver, and focused in front of a photomultiplier, a light sensitive detector that can detect even very low light levels. The photomultiplier,

when activated by a high voltage across it, converts incident light (photons) to an electric current (electrons) with a significant gain. Typically, a single input photon striking the photomultiplier can result in a large number (e.g.,  $10^4$ ) output electrons. This electron current, when passed across a high resistance, produces a voltage that we measure (see Fig. 4 in the Unsteady Combustion Lab). The photomultiplier output goes to the Photodetector Module (PDM), which also controls the photomultiplier input voltage (and thus the detector's gain).

Since the receiving optics are located on the same side of the tunnel as the transmitting optics, our LDV uses the **backward scatter** (or **backscatter**) configuration. It turns out that when the diameter of a scattering particle is about the size of the wavelength of the light, most of the light scattered by the particle goes right past the particle, for example a typical value would be 90% of the light in this forward scattering direction. Only about 1% of the light comes straight back along the path of the incident beams, in the backscatter direction. On the other hand, our usual experience of looking in mirrors tells us that, when the size of the scattering object (say, a mirror) is much larger than the wavelength of the light, the light will not go around the object, but gets reflected right back. Thus larger particles will scatter a larger fraction of the incident light in the backward direction.

### The Digital Burst Correlator

The output from the PDM goes to the **FSA** (Frequency and Size Analyzer) digital signal processor. The burst signal is first sent through an 80 MHz low pass filter, then downmixed with a **user-chosen** frequency; essentially the user-chosen frequency is subtracted from the signal. You can use this to subtract part of the shift in the signal frequency that was added by the Bragg cell. For the example given above ( $f_D = 4.39$  MHz, 10 MHz Bragg shift), a downmix frequency of 5 MHz would convert the 14.39 MHz burst frequency to 9.39 MHz.

Selecting a downmix frequency of 40 MHz will eliminate all the 40 MHz Bragg Cell Shift, so only the Doppler frequency is left, which is proportional only to the particle velocity. Selecting 39 means 39 MHz is subtracted from the 40 MHz Bragg cell shift, leaving 1 MHz still added onto the Doppler frequency. This will allow flow reversals up to 1 MHz to be measured. With a 5  $\mu\text{m}$  fringe spacing, this would correspond to flow reversals up to 5 m/s. Entering 36 means 36 MHz is subtracted from the 40 MHz Bragg cell shift, leaving 4 MHz still added onto the Doppler frequency. This would correspond to 20 m/s (assuming 5  $\mu\text{m}$  fringe spacing), in terms of the maximum flow reversal velocity.

After the downmix subtraction, the signal is sent through a bandpass filter to remove content at frequencies that are nowhere near the expected frequencies based on the estimated flow velocities; this is required because there are many possible sources of spurious electrical signals ("noise"). If what remains is the true (Doppler shift) signal caused by the particle crossing the fringes, the remaining signal would ideally just have one frequency. After being filtered, the digital signal processing units digitize the signal and determine the frequency embedded in the burst (similar to what could be achieved with a discrete Fourier transform). This part of the FSA electronics is called the **burst correlator**.

Normally the first parameter to select is the Band Pass Filter setting. If you know the range of frequencies that will be in the flow, you can select the setting directly. Remember that the signal frequency (without frequency shift) is equal to the particle velocity divided by the fringe spacing. To estimate the frequency of the signal input to the signal processor, add the effective frequency shift (equal to 40 MHz minus the downmix frequency).

The system also includes a **threshold** for detection. Unless the burst signal has an amplitude of at least some minimum value, say 30 mV, the electronics can reject it. For example if the signal is too weak and buried in noise,

no useful velocity measurements can be made. This fact puts the burden entirely on the operator of the system to ensure that the signal *going into the correlator is of good quality*, (good **visibility**). *In other words, if you can not see a clear Doppler signal on an oscilloscope, do not expect the burst correlator to see one either.* Of course, if you amplify a noisy signal enough, the unit will faithfully find some frequencies in the noise signal, and may output useless data. The frequency counted may be that of the nearby radio station instead of the Doppler shift, and you may get supersonic flow velocities from your low-speed flow!

### Seeding

Note that a valid signal results only when a solid or liquid particle crosses the measurement volume. *The velocity measured is actually of these particles, not of the air itself!* Thus, care must be used in ensuring that the particles present in the flow are those that are so small that they move at essentially the same speed as the flow. In other words, they must have very small mass, and comparatively low density. If they move at speeds different from the local air flow velocity, the drag force exerted on them must be far greater than the inertia due to their mass, so that they are again very rapidly accelerated or decelerated to the local air velocity. You can easily convince yourself that as the diameter of a particle gets smaller, this becomes a better approximation, since the mass of a sphere is proportional to the cube of the diameter, while the surface area is proportional to the square of the diameter.

Usually, in a laboratory, the air is supposed to be clean and free of dust particles. Hence, the flow must be artificially seeded with particles of the right diameter range. This is done here by means of an atomizer, which works essentially like a paint spray can. A high-pressure air supply is expanded through a small orifice or nozzle to high speed. On the way out, it hits a thin stream of liquid (mineral oil) and shatters it into tiny droplets. This flow is then rapidly decelerated and turned around a sharp corner, and forced to go upwards. All the large droplets hit the walls (low drag, high inertia - they can not turn quickly enough) and drip back down into the oil reservoir. The remaining droplets, with diameters in the range 1-10  $\mu\text{m}$ , go with the air stream and mix with the main flow. If done properly, a uniformly seeded flowfield can be created.

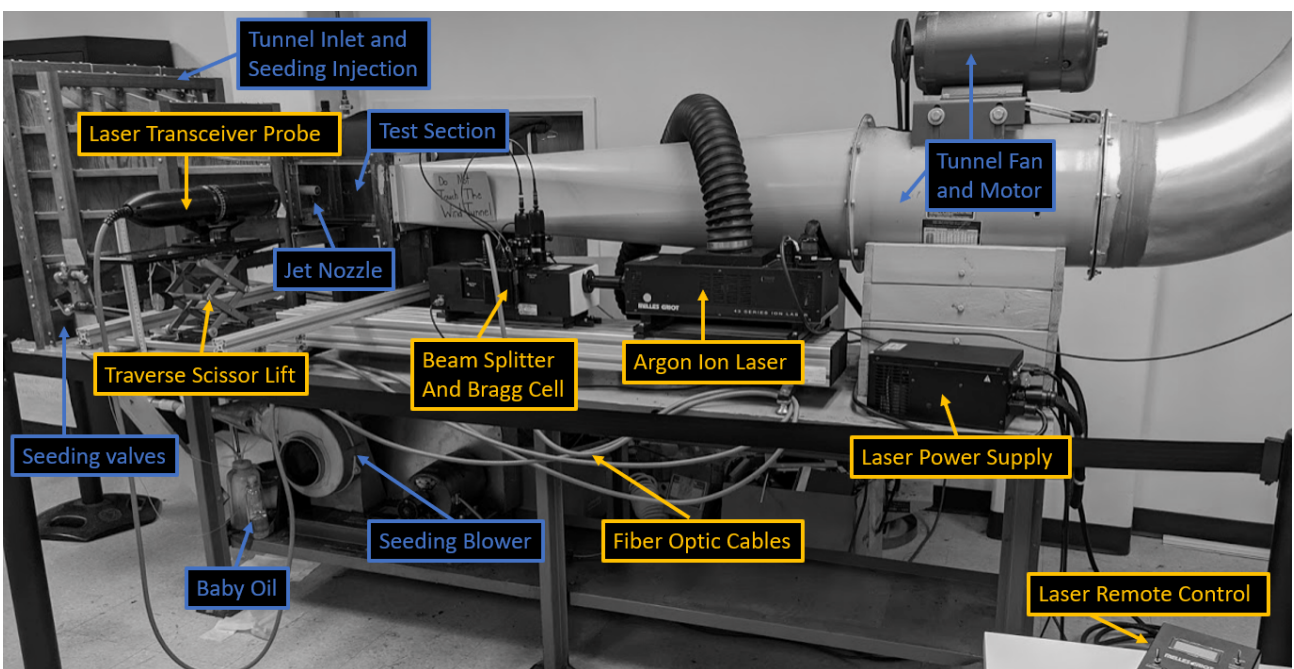
### The AE3610 LDV Experiment

Our LDV system uses an in-house fabricated wind tunnel, seeding system, and manual traverse, with an off-the-shelf LDV system made by TSI Inc. The three figures below show our setup, its primary constituent parts, and a view of the test section when the laser transceiver is energized.



The TSI LDV Manual can be viewed [here](#)

tsi1.pdf - 5MB





## Turbulent (and Fluctuating) Flows and Data Reduction

### Velocity Decomposition

Turbulent flows are not only unsteady, but chaotic in character.\*

i \*For background material on turbulent flows, you may wish to read Anderson's Fundamentals of Aerodynamics, 1984, Chap. 16, or Kuethe and Chow, Foundations of Aerodynamics, 4th Ed., Sections 18.1 - 18.3.

In analysis of many turbulent flows where the fluctuations in velocity are small compared to the mean velocity, we decompose the instantaneous velocity  $u(t)$  as follows

$$u(t) = U + u'(t)$$

where  $\bar{U}$  is the mean velocity and  $u'$  is the fluctuating component (with  $u' \ll U$ ). These may be seen from Figure 5, which illustrates how the velocity at some point would change with time in a turbulent flow.

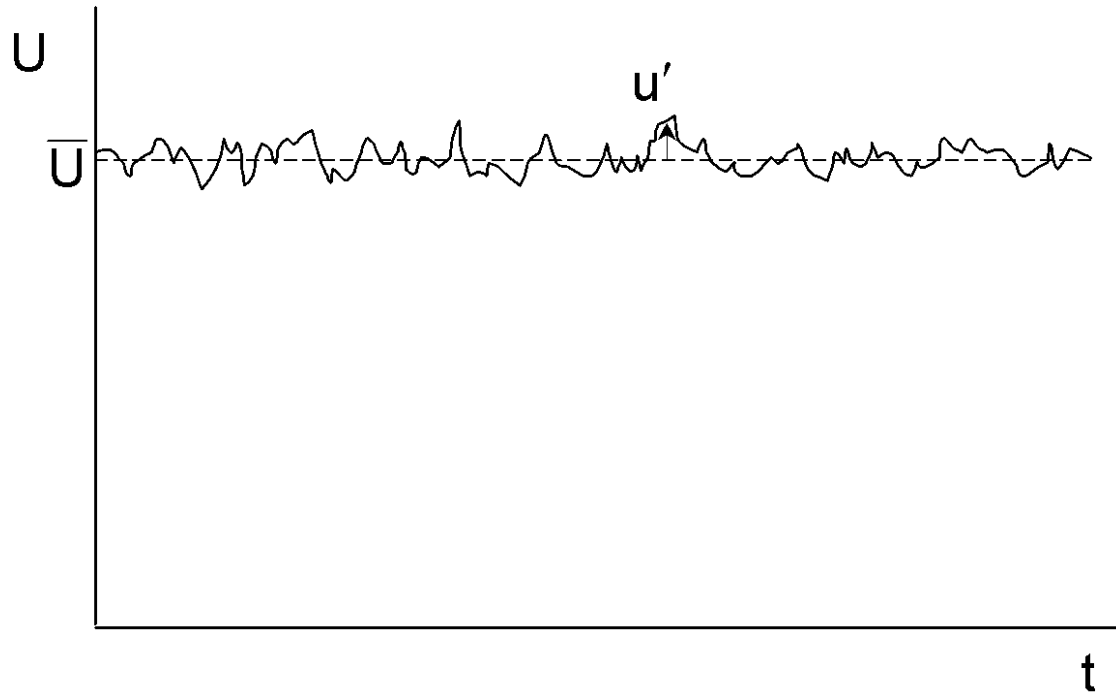


**Figure 5.** Typical velocity history at a single point in a turbulent flow.

Note that the time average of the fluctuating component,  $\bar{u}'$ , should be zero since the fluctuations are random and the  $u'$  at any instant is as likely to be positive as negative. However, the variance  $(\bar{u}')^2$  is not zero, and gives us a measure of the intensity of the fluctuations. The positive square root of the variance is called the root-mean-square, or RMS for short. The variance of the velocity enters directly into the time-averaged Navier-Stokes equation (as described in AE 3030). This quantity will be calculated and used here.

## Data Reduction

### The velocity histogram

The velocity may be expected to vary from one data point (i.e., one particle) to the next. The LDV system collects, say, the first 5,000 points to be measured, converts the time values to velocity, and then sorts these values into "bins" or velocity intervals. Thus, if the highest velocity that you expect is 20 m/s, and the lowest is 10 m/s, and you divide this range into 100, then all the data points which show velocity values between 10.0 and 10.1 m/s will go into the first "bin", all those between 19.90 and 20.0 m/s will go into bin #100, and everything else will go somewhere in between. The mean velocity can be calculated from the binned data with the formula

$$U = \frac{\sum n_i^i U_i}{\sum n_i}$$

(5)

where  $n^i$  is the number of samples in the  $i$ 'th bin, and  $U_i$  is the center velocity of that bin. The root-mean square (or the square-root of the variance) is calculated as:

$$u_{rms} = \sqrt{\frac{\sum n_i(U_i - U)^2}{(\sum n_i) - 1}}$$

(6)

These results are usually displayed on the computer, along with a graphical display of the distribution of data points over the velocity intervals. Such a graph is called a *histogram*. The number of points in each interval has been divided by the total number of points collected. If it were a continuous function, instead of being a series of discrete values for a finite number of intervals, it would be called a *probability density function (PDF)*, whose integral, over the entire range of velocities, should thus be equal to unity.

### Averaging

Usually when this procedure is used, at least  $10^3$  points are needed to yield a good result for the average velocity, and at least  $10^4 - 10^5$  for the RMS. This is if you collect data for a sufficiently long time, so that you have seen all the likely kinds of fluctuations that occur. However, if the flowfield is fluctuating slowly, the average calculated from just one set of data as above may be insufficient. Instead, you may have to average over many data sets, each taken at a different time. For example, suppose there are 6000 data points arriving every second, and you collect the first 3,000. This should take only 0.5 seconds. Suppose now that the flow itself is fluctuating so that the magnitude of velocity goes up and down again once in 2 seconds. Your calculated mean velocity will not be the true mean of the flow. To find the true mean, you will have to average many such data sets. Note from Eq. (6) that you cannot just average the rms values to get a better estimate for the rms; this would have to be done inside the summation sign.

---

## The Jet Flowfield

One feature of the laser velocimeter to bear in mind is that one must have a good idea of the flowfield before attempting to make measurements using it. Very precise measurements can be made by a careful and alert experimentalist, but not without some consideration of the flowfield. Figure 6 shows a schematic of the flow setup in our laboratory. A fan downstream of the tunnel diffuser creates a pressure difference that induces the tunnel freestream, and forces it out of the laboratory. A circular pipe brings air output from a centrifugal blower to the upstream edge of the wind tunnel test section. The flow comes out of the pipe as a jet, with a velocity that can be significantly higher than that of the test section freestream. Both the test section freestream and the flow inside the pipe are seeded with atomized mineral oil.

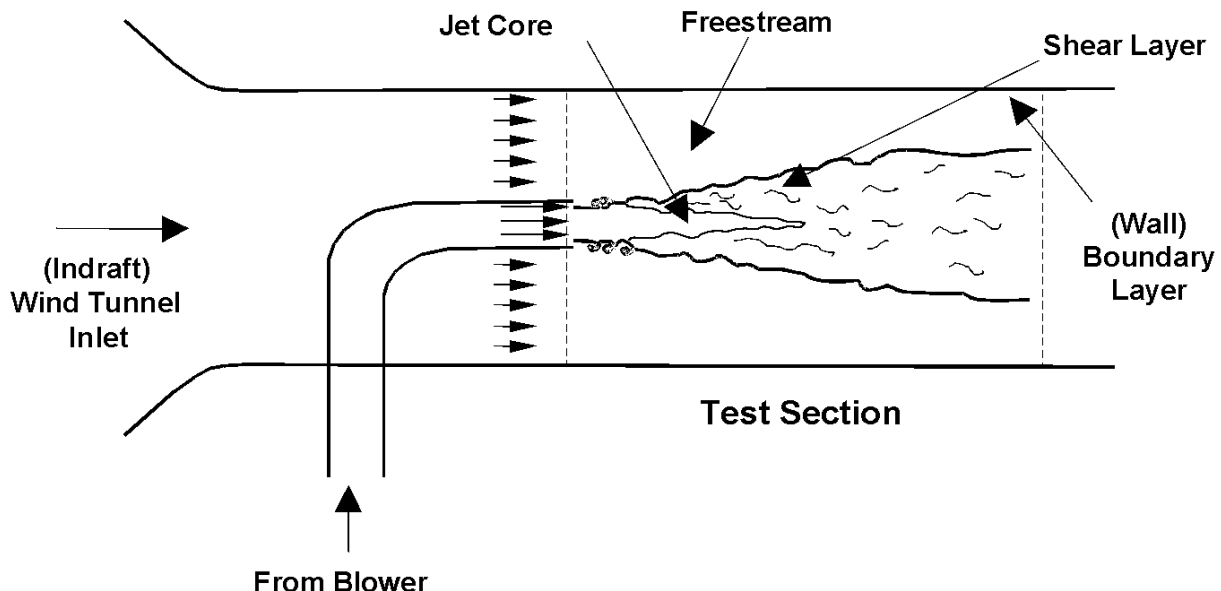


**Figure 6.** Schematic of jet flow in the wind tunnel

If the jet flow leaves the pipe with a high velocity, the effect of viscosity at the edges of the jet causes the surrounding test section flow to accelerate, and the jet flow to decelerate. In fact, the flow at the edges of the jet is forced outward as it is “pulled” by the slower-moving test section air. Thus, some of the jet flow “rolls up” into vortex rings around the jet, so that some air which originated in the test section flow goes into the jet, and vice versa. Thus, there is a *mass transfer* and *momentum transfer* across the jet boundaries. Things rapidly become confused and unsteady at the jet edges, so that the velocity fluctuates. Not too far downstream of where the jet exits the central pipe, the fluctuations are largest inside the **shear layer** at the edges of the jet. Near the center of the jet, there is still a region where the fluctuations have not reached. This is called the **potential core**, and the fluctuation level should be quite low here. The shear layer around the jet grows quickly so that the shear layers from opposite sides merge, and the potential core rapidly disappears as the jet goes downstream. At the same time, the mass and momentum transfer force the time-averaged velocity profile across the jet to become smoother and to gradually disappear, as the jet merges with the test section flow. *You will acquire velocity data along a vertical line extending from somewhere below the top wall to a region below the centerline of the jet.* This line is nominally near the horizontal center of the jet and nearer to the end of the test section.

## Procedure and Data to be Taken

### Preliminary calculations

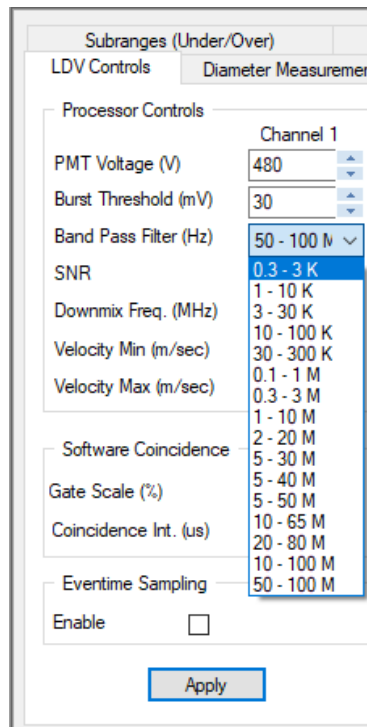
The specifications for our LDV system and software configuration are as follows:

- Laser wavelength,  $\lambda$  : 514.5 nm (Argon-Ion green)
- Beam separation,  $D$  : 50 mm
- Focal length,  $f$  : 362.6 mm
- Approximate range of measured velocities,  $U$  : -2 to 15 m/s

- Bragg cell frequency: 40 MHz
- Burst threshold: 30 mV

Calculate the following parameters:

1. Beam intersection half-angle,  $\theta$
2. Fringe spacing,  $d$
3. Doppler frequency,  $f_d$ , at each end of the velocity range (assuming no Bragg)
4. Assuming no bandpass filter is implemented, what is the absolute minimum downmix frequency needed to enable the required negative velocities to be measured?
5. Given a downmix frequency  $f_{dm}$  and an ideal bandpass filter that operates between  $f_1$  and  $f_2$  Hz, write a closed-form expression for the minimum and maximum observable velocities of the final system
6. Using your answer from Q5, select an integer-number downmix frequency to input into FlowSizer, and select a band pass filter from the available options in "LDV Controls" (see pic below for precise options). Provide the minimum and maximum observable velocities using these settings.



FlowSizer band pass filter options

**i** Hint: everything you need to answer these questions is in this manual, but you may also get some better insight from the LDV manual, and the FlowSizer auto min and max velocity calculation

## Preparing the experiment



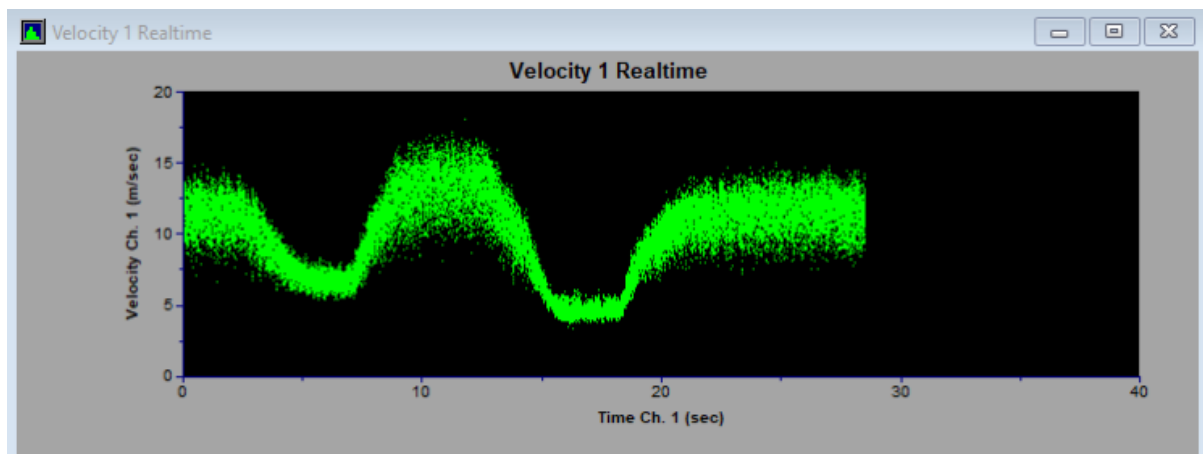
The LDV experiment uses a Class 3B laser and is therefore a significant risk to eye health; Wear laser eye protection at all times once the laser has been powered on

The TAs will now give you an overview of the equipment and lead you through configuration of the experimental hardware and software.

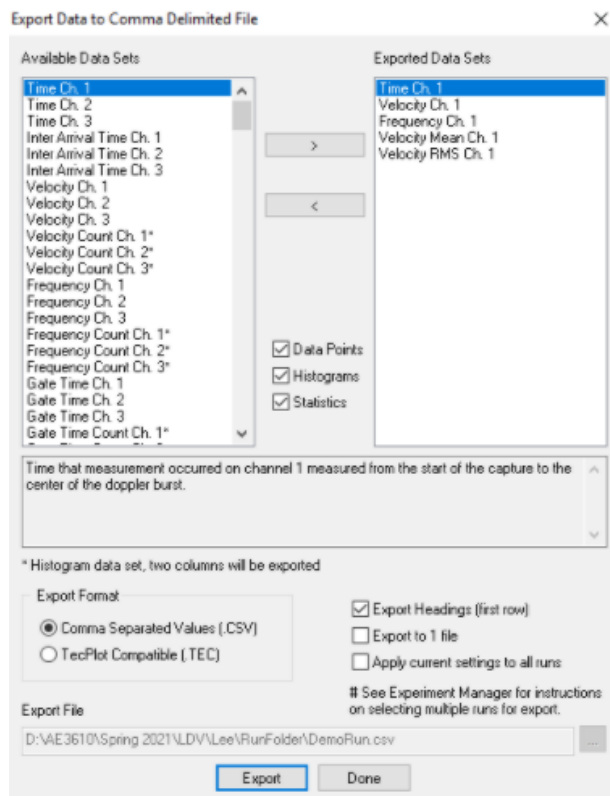
## Testing the equipment and learning the data acquisition workflow

We will now go through a sample experiment to demonstrate operation of the system and how to acquire data:

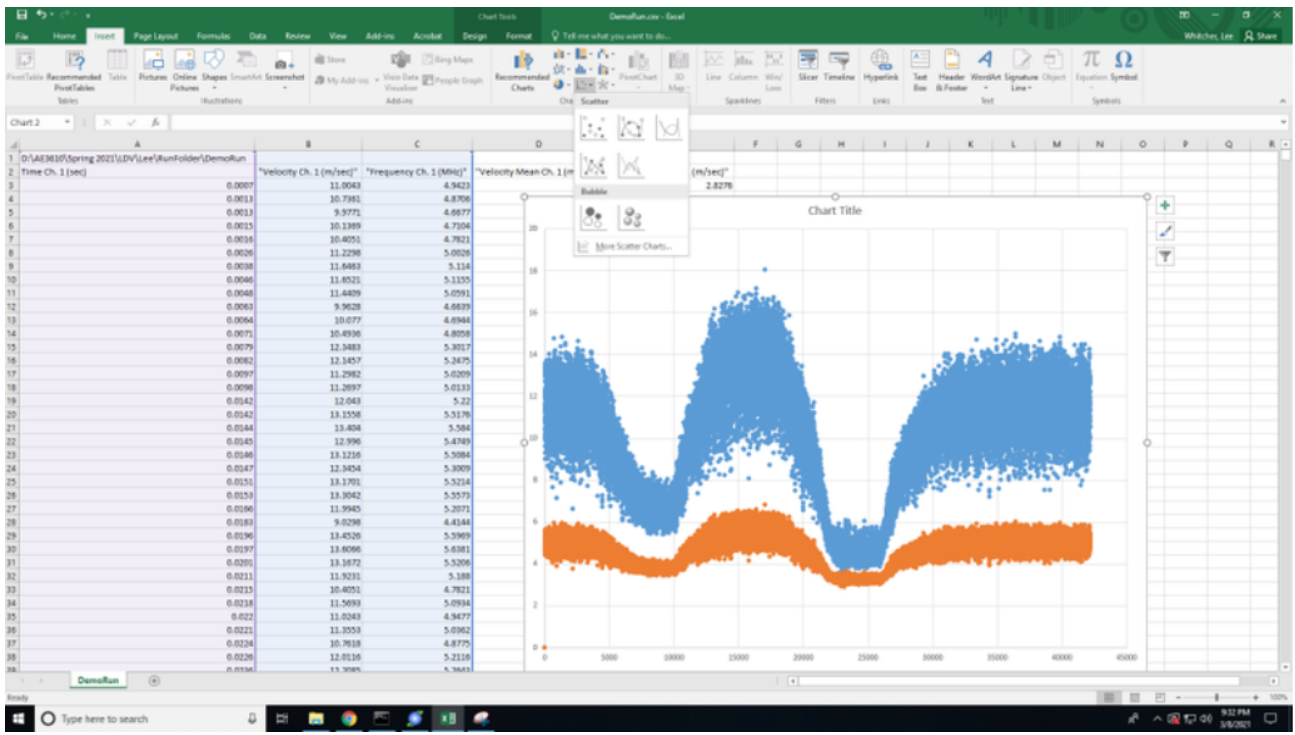
1. Verify the traverse is set such that the transceiver probe is aligned in the center of the jet and the direction of the probe is in the direction of flow (the yellow warning label is on the left when viewing the probe from behind, and angle dial is on 90)
2. Open both seeding valves and verify successful seeding
3. In FlowSizer, click on **Setup** under the **Home** tab and set **Maximum Particle Measurement Attempts** to 100,000 - this is a temporary change that will buy more time for this demonstration (capture time = MPMA / data rate). Also ensure **Screen Update Interval** is set to 0, but it should already be on that setting.
4. Have one TA stand at the seeder blower control (currently at around 1900rpm), then immediately after hitting **Begin Capture** have him/her smoothly but quickly ramp the speed down and up a couple of times, before returning to 1900rpm. The Velocity 1 Realtime graph should show this change in speed with a slight delay, until the run ends, as shown in the figure below.
5. Close the seeding valves and set the laser to **STANDBY**, but otherwise leave everything where it is
6. Click **Save** and call the file something meaningful like DemoRun
7. Click on **Data Sets To CSV File** and select the relevant metrics, shown in the figure below, before clicking **Export**
8. Verify the data exported correctly by navigating in Windows Explorer to the run folder and opening the CSV file. Select the first three columns and click Insert > Scatter to generate a quick preview plot to verify the data makes sense and matches, as shown in the figure below
9. Return the **MPMA** setting to 10,000 in FlowSizer **Setup**



Step 4 - Observing jet velocity change



Step 6: Selecting data sets to export



Step 7: Verifying the data saved correctly in Excel

## Taking Data

Now you are comfortable with the workflow, it's time to capture real data:

1. Move the traverse to the zero position (top of the test section)
  2. Open both seeder valves and verify successful seeding
  3. Set laser to **RUN**
  4. Obtain the jet profile data
    1. Follow the steps in the previous section to obtain a measurement at the zero position
    2. Having decided on a traverse distance (it doesn't have to be constant throughout the test section... bear in mind the expected profile of the flow in the freestream and the jet), move the traverse to your next position and obtain another measurement.
    3. Repeat Step 2 until you have traversed 155mm downwards (just off the bottom of the test section). **You will need to keep a manual list of all traverse positions since this is not logged (or perhaps save your run with a meaningful name).**
  5. Go back and repeat the measurements for at least TWO locations (the first point being in the free stream and second in the shear layer), but with different **Bandpass Filter/Downmix Frequency** settings
  6. Return the filter settings to their proper values, and change the **Burst Threshold** value to 150 mV and repeat the measurements in the shear layer (to see if the original threshold value was a reasonable choice)
  7. Return the **Burst Threshold** to its original value, and repeat the shear layer measurement two more times. The first time, turn off (or nearly off) the free stream seeder. The second time turn the free stream seeder back on and turn off (or nearly off) the jet seeder.
  8. *Rotate the transceiver by 90 degrees counter-clockwise and acquire vertical velocity component data at the same location used above in the jet shear layer (and additional locations if you wish). Note, you will need to adjust the **Bandpass Filter** and **Downmix Frequency** settings to account for the fact that: 1) the vertical velocities are less than the axial velocities and 2) the vertical velocity can be both upward and downward.* When you are done taking data, rotate the transceiver back to its original orientation.
  9. Set the laser to **STANDBY**, close the laser aperture, and close the seed valves, but keep everything else running while you check your data (in case you need to go back and get anything else)
  10. If you didn't do it as you went along, export all your runs to CSV and verify the data looks reasonable. If it doesn't go back and collect any data points.
  11. Sanitize your safety glasses and then assist the TAs in their shutdown procedure if required
- 

## Data to be Taken

1. LDV system settings (burst threshold, band pass filter, downmix frequency, and transceiver orientation), and vertical measurement position for each run.
  2. Velocity measurements for each run.
- 

## Data Reduction

1. Show your calculations for fringe spacing in the laboratory report.
  2. Show your calculations for the filter settings, i.e., what velocities correspond to your chosen filter settings
-

## Results Needed For Report

1. Table containing the LDV settings and vertical positions for each run.
2. A plot of the normalized mean axial velocity profile in the jet,  $U/U_\infty$  versus location, where  $U_\infty$  is the value of  $U$  in the free stream of the wind tunnel.
3. A plot of the normalized turbulence intensity profiles in the jet, *normalized two ways*: first,  $u_{rms}/U_\infty$  and second,  $u_{rms}/U$ .
4. A plot of the instantaneous axial velocities at two locations: in the wind tunnel free stream and in the jet shear layer.
5. Histograms of the velocity values recorded at interesting points in the flow (note, the histograms produced by the TSI software may not be helpful – you will probably have to make your own histograms).
6. A comparison between the points taken with different filter, burst threshold and seeder settings.
7. A comparison of the axial and vertical velocities (mean and rms) acquired at the same jet locations.

# Supersonic Flow

## Objective

This lab covers the use of taps, probes and transducers for measurement of static and stagnation pressures in nominally steady, compressible (subsonic and supersonic) flows. In addition, it includes the use of the schlieren technique to visualize shock and expansion waves in supersonic flows. The various measurements are acquired in a supersonic, blowdown wind tunnel and a supersonic (converging/diverging) nozzle. The experiments also allows the student to experimentally investigate many interesting and important aspects of the behavior of supersonic flows.

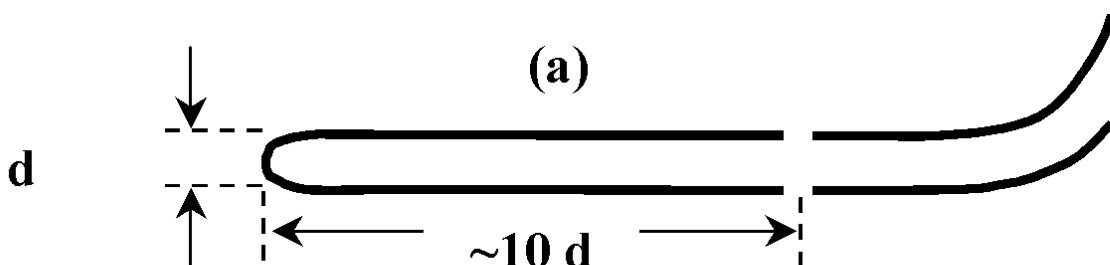
---

## Background

### Measurement Instrumentation

#### Pressure Measurements

Steady pressures are most conveniently and accurately measured using static taps or probes, and stagnation pressure probes. This is the approach used in this laboratory. Static taps and probes, as well as total or stagnation pressure probes (see Figure 1), have been introduced in earlier labs. Typically taps and probes are located quite a distance from the actual pressure transducer, thus they have a relatively slow response. Rapidly fluctuating pressures must be determined using other devices, such as microphones or piezoelectric transducers as covered in previous labs.



#### Stagnation point

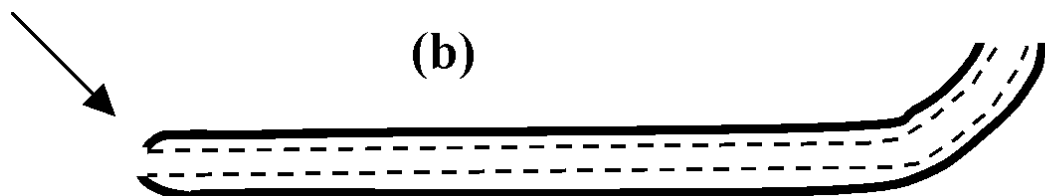


**Figure 1.** Schematic of a) static and b) Pitot pressure probes.

### a) Gravitational Transducers

Transducers that can be used to measure pressure include gravitational transducers, such as mercury or oil manometers. Manometers can be of various shapes, including standard U-shaped tubes and straight long vertical tubes attached to a liquid filled reservoir. Manometers measure relative pressures, specifically the pressure difference between the two ends of the tube. For measurement of stagnation pressures in compressible flows, which can easily exceed 1 atm, long tubes are required (even for a dense liquid such as mercury, measurement of  $\Delta p=1$  atm requires at least a 30 inch long tube).

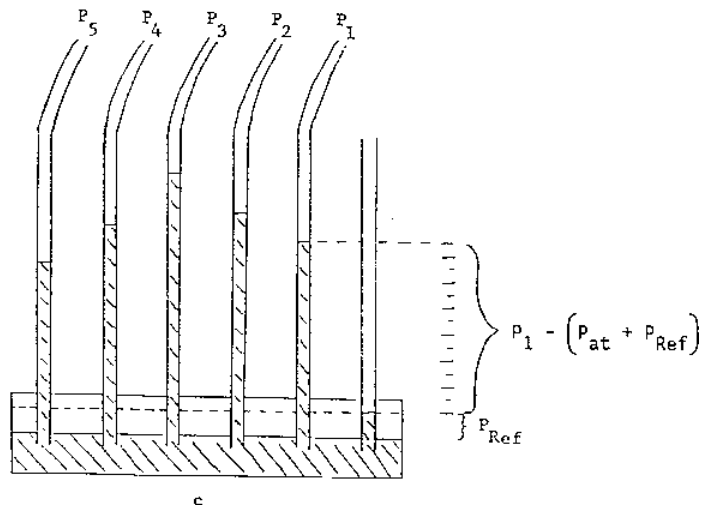
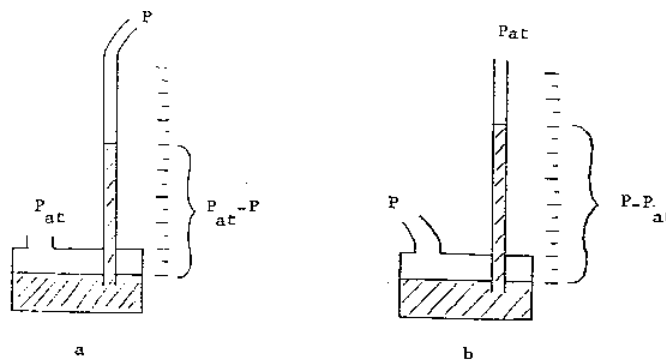


**Figure 2.** Schematic of vertical type manometers: a)  $p < p_{at}$ , b)  $p > p_{at}$ , and c) a manometer bank (with  $p_{at}$ =ambient pressure).

For vertical tubes connected to a reservoir, pressures below atmospheric are measured by connecting the tubing from the probe to the upper, open end of the manometer tube while the reservoir is open to the atmosphere (Figure 2a). Thus, the lower the value of the static pressure, the higher the mercury column in the manometer. On the other hand, if the pressure to be measured exceeds atmospheric (e.g., the total pressure in a blowdown type supersonic tunnel), the tubing from the probe is attached to the reservoir and the upper end of the manometer is left open (Figure 2b). If one is dealing with a manometer bank containing a number of tubes, the level in the reservoir drops as the mercury rises in the tubes. This must be compensated for by measuring the drop in level in a reference tube which is open to atmosphere (Figure 2c).

### b) Elastic Transducers

Another family of pressure measurement devices can be categorized as elastic transducers. In these devices, a deflection or deformation accompanying a balance of pressure and elastic forces is used to measure pressure. A classic example of an elastic pressure transducer is the Bourdon tubes (Figure 3) commonly found in pointer type pressure gages. In these devices an oval section tube is initially coiled into a circular arc. As a pressure is applied to the tube, the oval section tends to become more circular in cross-section. Since the inner and outer lengths of the tubes remain approximately the same as their initial values, the primary result of the applied pressure is an uncoiling of the arc. The uncoiling is coupled to the motion of a pointer, which is used to determine the pressure.

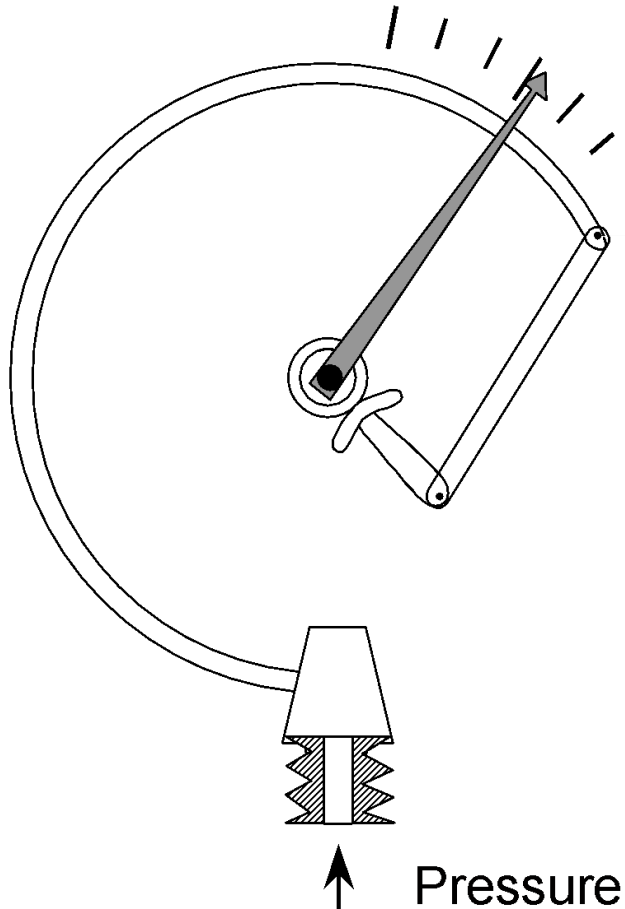


Figure 3. Basic Bourdon-type pressure transducer.

Another type of elastic transducer is the diaphragm type, where the pressure force causes a diaphragm to deflect. Examples of this type include Barocell/Barotron type transducers, in which the pressure deflects a thin diaphragm that forms one plate of a capacitor. Different pressures yield different capacitances that are converted to electrical voltages (and read using a voltmeter in this lab). Barocells and Barotrons typically provide very sensitive measurements of pressure, e.g., Torr/volt, with the calibration (sensitivity) usually supplied by the manufacturer. Other methods can be used to measure the change in the diaphragm, for example resistance strain gages can be applied to the diaphragm surface, and the measured strain can be related to the applied pressure through calibration. Relatively inexpensive transducers can be made by using semiconductor materials. In this case, the semiconductor resistors are “written” as a bridge circuit directly onto a substrate (e.g., silicon) that acts as the diaphragm. The strain on the semiconductor results in a change in semiconductor resistance; this is known as the

*piezoresistive effect*. The change in semiconductor resistance is analogous to the change in metal resistors (recall the strain gauges used in the force balance experiments), except in the latter, the change in resistance is *primarily* due to the change in the metal resistor's cross-sectional area as it is strained. For semiconductor materials, the resistance change is related to other changes in the internal structure of the semiconductor. This type of silicon diaphragm transducer will be used to make differential pressure measurements in the converging-diverging nozzle experiment.

### Flow Visualization

Sudden changes in the density of a gas and the resulting gradient in refractive index can be visualized using the schlieren technique. Such steep refractive index gradients exist, for example, in flames or in shock waves. In this laboratory, shock waves, whose properties will be discussed in the next section, are visualized using schlieren imaging. In this technique (see Figure 4), the light from a source is allowed to expand and is then collimated using a large diameter, long focal length (typically biconvex) lens.

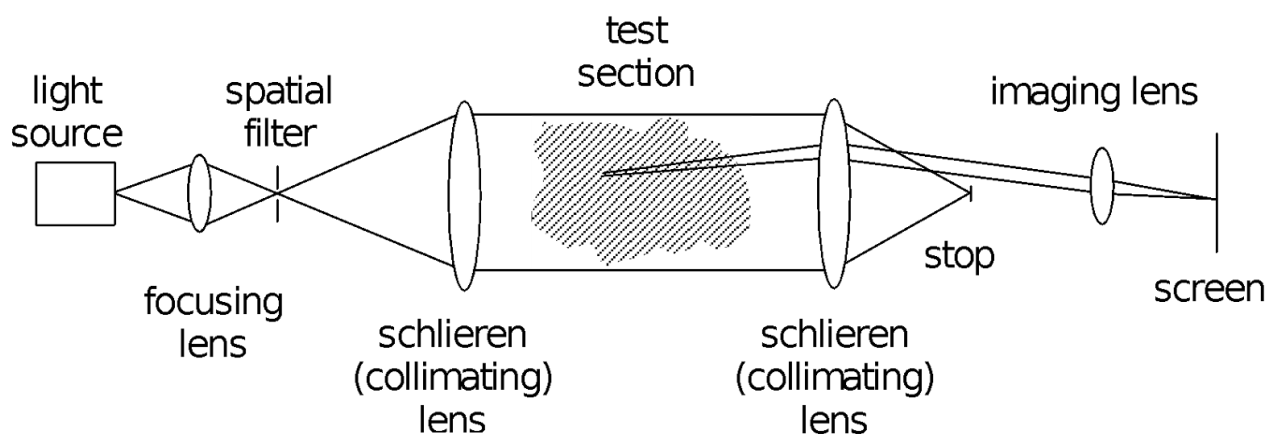


Figure 4. Schematic of a typical schlieren setup.

The resulting parallel beam is then passed through the test section of the wind tunnel before being refocused using a second biconvex lens of similar optical properties to those of the first. A stop placed at the focal point of the second lens blocks all of the undeflected light. However, any light rays that have been refracted in the test section by a refractive index gradient caused by, for example, a shock wave are no longer parallel to the optical axis of the system. These rays will, therefore, be focused at a different location in the focal plane of the second lens and will, thus, bypass the schlieren stop. A focusing lens is then used to create an image of the test region on a screen or photographic plate using only the refracted light. This image displays only those regions of the flow in which a steep refractive index gradient exists, i.e., the shock wave.

### Fluid Mechanics

A brief description of compressible flows (summarizing important details covered in AE 2010) is given below. It is important to note that **inviscid flow** will be assumed throughout this discussion. When a gas, such as room temperature air, flows at velocities greater than approximately 100 m/s (or for Mach number  $M > 0.3$ ), the density changes of the gas *due to changing Mach number* become significant, i.e., the flow becomes *compressible*. This results in some remarkable phenomena, especially at supersonic speeds. For example for *subsonic* flow in a nozzle,  $M$  increases as the cross-sectional area of the nozzle decreases; for *supersonic* flow this trend reverses.

Furthermore, it turns out that an adiabatic flow can only increase from subsonic to supersonic speeds if the transition from  $M < 1$  to  $M > 1$ , (i.e.,  $M=1$ ) occurs at the throat (minimum area) of a nozzle.

Bernoulli's equation, which was derived assuming constant density is no longer valid for compressible flow. Instead, the relationship between the static and stagnation pressures, e.g.,  $p/p_o$ , as a function of Mach number may be obtained for a calorically perfect gas (constant specific heats) from the following (more general) expression.

$$\frac{P_o}{P} = \left[ 1 + \frac{\gamma - 1}{2} M^2 \right]^{\frac{\gamma}{\gamma - 1}}$$

(1)

where  $\gamma$  is the specific heat ratio. As long as the flow remains *isentropic*, the *stagnation pressure is constant* everywhere. The static pressure, on the other hand, decreases as the Mach number increases since more potential energy, which gives rise to the static pressure, is now converted to kinetic energy. This is true for subsonic as well as supersonic flow.

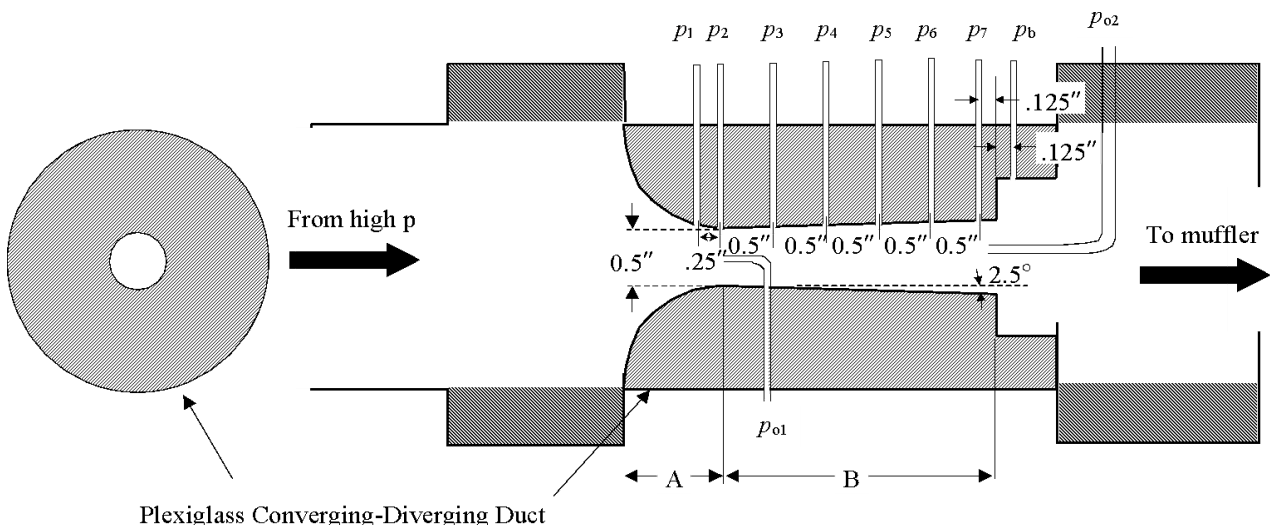


**Figure 5.** Schematic of the converging-diverging nozzle showing location of pressure probes and taps (throat at  $p_2$  ).

Let us now consider the flow in a converging-diverging nozzle (see Figure 5) connected to a high pressure supply at one end and open to the atmosphere at the other. As the pressure in the supply (reservoir pressure) is increased, air begins to flow through the nozzle. As long as the flow in the nozzle is everywhere subsonic, the Mach number increases in the converging part (region A) and decreases in the diverging part (region B) of the nozzle. The static pressure level in the nozzle behaves inversely as the magnitude of the Mach number. Thus for subsonic flow in the nozzle, the static pressure drops in the converging section and rises in the diverging section. At the exit of the nozzle, the flow should reach equilibrium with the back pressure (given by the local atmospheric pressure in this example). As the reservoir pressure is increased further, the mass flow rate through the nozzle increases, causing

a change in Mach number and, thus, in static pressure. The Mach number in the converging part of the nozzle can keep increasing in this manner until the Mach number at the nozzle throat reaches unity. The nozzle is then called "**choked**". The Mach number in region A can no longer be affected by increasing the reservoir pressure (or decreasing the back pressure), and the mass flow rate, *for fixed upstream stagnation conditions*, is a maximum once the flow is choked.

Increasing the reservoir to back pressure ratio ( $p_o/p_b$ ) above the value that corresponds to choking does, however, affect the flow conditions in region B. Beyond the choking condition, the flow downstream of the throat begins to go supersonic and increases in Mach number as the nozzle flow expands. However,  $p_o/p_b$  is not yet high enough to result in completely supersonic (isentropic) flow throughout the entire region B. The flow adjusts to these conditions by suddenly reverting back to subsonic flow in a normal shock somewhere in the expanding part of the nozzle. Across this shock wave the static pressure rises. Behind the shock the flow is subsonic, and, therefore, decreases in Mach number as the nozzle continues to increase in area. The static pressure rises correspondingly until the back pressure is reached at the exit of the nozzle. As  $p_o/p_b$  is raised still further, the position of the shock wave moves towards the nozzle exit, until eventually there is no shock *in* the nozzle.

The presence of the shock wave changes all flow conditions across it except the stagnation temperature (or, more precisely, the stagnation enthalpy) since across the shock the flow is adiabatic. The extent of the influence of the shock upon the flow conditions depends upon the Mach number of the flow going into the shock. For thermally and calorically perfect gases, the ratio of the static pressures across the shock ( $p_2/p_1$ ) as a function of Mach number ahead of the shock ( $M_1$ ) are given by

$$\frac{p_2}{p_1} = \frac{2\gamma M_1^2 - (\gamma - 1)}{(\gamma + 1)}$$

(2)

and the stagnation pressure ratio  $p_{o2}/p_{o1}$  is

$$\frac{p_{o2}}{p_{o1}} = \left\{ \frac{\gamma + 1}{2} \frac{M_1^2}{1 + \frac{\gamma-1}{2} M_1^2} \right\}^{\frac{\gamma}{(\gamma-1)}} \left\{ \frac{2\gamma}{\gamma + 1} M_1^2 - \frac{\gamma - 1}{\gamma + 1} \right\}^{\frac{1}{(1-\gamma)}}$$

(3)

where we have assumed a stationary shock for the stagnation pressure ratio.

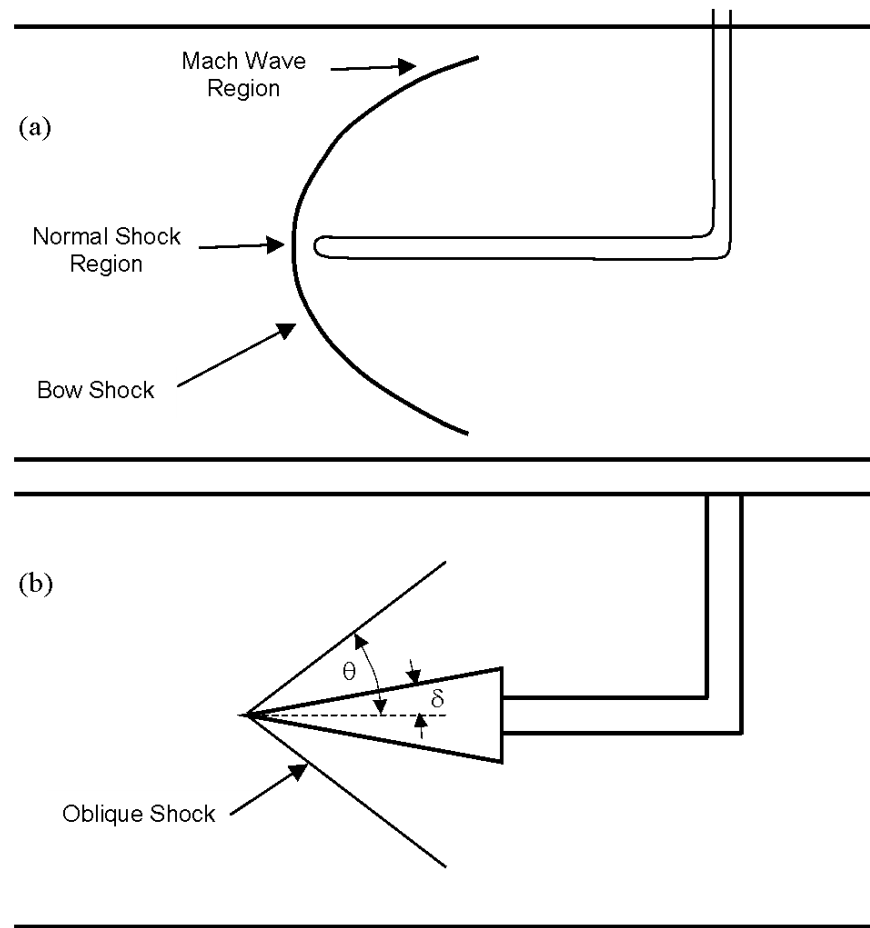


**Figure 6.** Schematic of shock on: a) probe and b) wedge in supersonic flow ( $\theta$  = shock half angle,  $\delta$  = wedge half angle).

If a supersonic flow encounters a solid body, part of the flow must be decelerated to stagnation conditions. Since this necessarily involves a transition from supersonic to subsonic flow, a shock stands ahead of the body. This shock provides the mechanism for the transition. In the case of a thin probe in supersonic flow a small, normal shock stands ahead of the probe tip (Figure 6a). A conically shaped bow shock trails from the normal shock. The bow shock weakens as one moves away from its leading edge and, eventually, turns into a Mach wave across which the flow properties no longer change significantly. Therefore, the stagnation pressure measured using a Pitot probe in supersonic flow is that *behind* a normal shock. In a static probe, on the other hand, the orifice is located far downstream of the probe tip. The effect of the normal shock is then no longer felt and the static pressure measured is essentially equal to that ahead of the shock. If the probe is replaced by a wedge (Figure 6b) a pair of oblique shocks is formed that attach to the tip of the wedge. The relationship between the flow Mach number and the half angles of the shock and of the wedge are plotted in Figure 7.\*



\*Similar plots can be found in most texts on compressible flow.

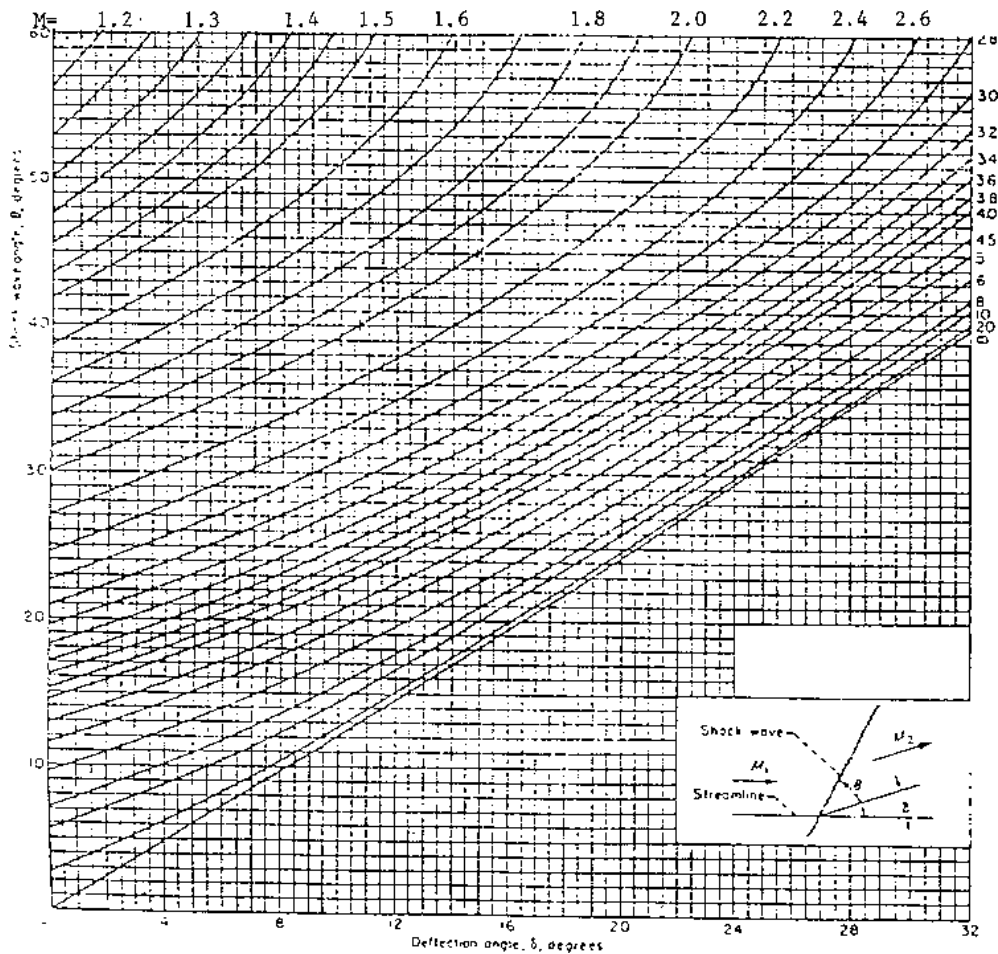


**Figure 7.** Variation of shock-wave angle with flow-deflection angle for various upstream Mach numbers for a thermal and calorically perfect gas with  $\gamma = 1.4$ .

## Flow Facilities

### CD Nozzle

This set of experiments is to be carried out in a converging-diverging (CD) nozzle made of Plexiglas (see Figure 5). The upstream side of the nozzle is attached to a high pressure supply (regulated so as not to exceed  $\sim 50$  psig); the downstream side is connected to a settling chamber and an acoustic muffler before exiting into the room. Between the nozzle and the high pressure supply is a manual valve. The stagnation pressure entering the nozzle is controlled by the setting of this valve (and the pressure downstream of the valve can be monitored using a simple Bourdon tube type gauge). The nozzle is instrumented with two Pitot probes along the axis and eight static pressure taps along the wall. The first Pitot probe is located at the nozzle throat. The second probe is located near the last static pressure port in the nozzle (station 7).

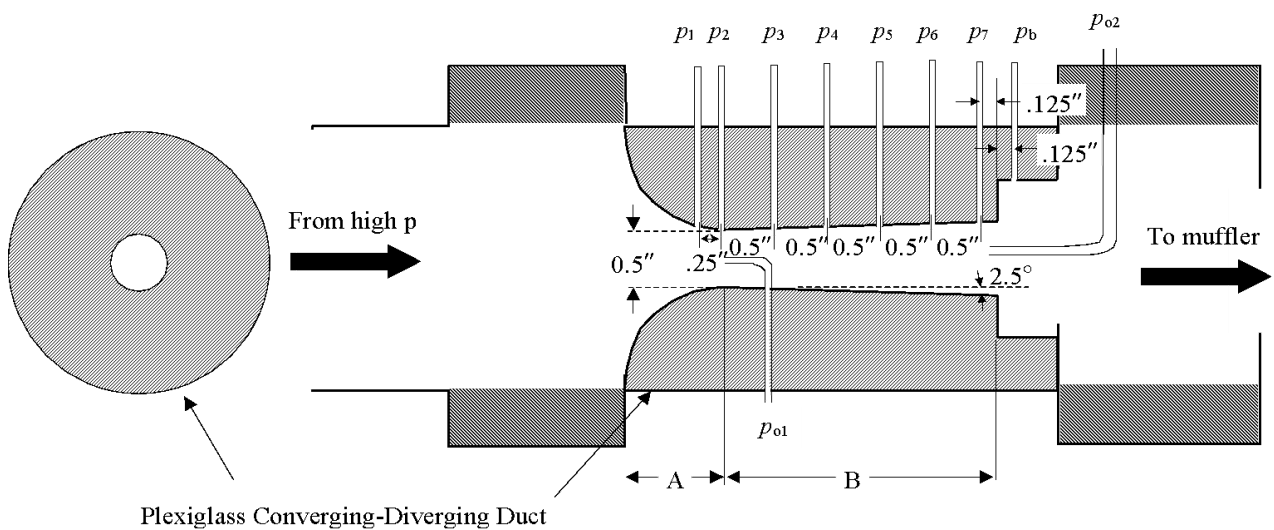


**Figure 5.** Schematic of the converging-diverging nozzle showing location of pressure probes and taps (throat at  $p_2$  ).

As shown in Figure 5, one static pressure tap is located ahead of the nozzle throat, the second at the throat and five tops are located at one half inch intervals along the expanding part of the nozzle. Tap number eight measures the back pressure. The ten pressures will be measured by ten piezoresistive, silicon diaphragm transducers and recorded by a computer data acquisition system. Since some of the pressure gauges can be damaged by operation outside their pressure range, please carefully listed to any guidelines given by the TA's with respect to the maximum pressure you should allow the CD inlet to reach.

#### Blowdown Tunnel

In this facility, air from a large tank at approximately 120 psi is passed through a pressure regulator and a large, manual (butterfly) valve and into a supersonic tunnel of rectangular cross-section. The tunnel (Figure 8) consists, essentially, of a nozzle ( $2'' \times 1.778''$  at its throat) and a test section ( $2'' \times 3''$ ).

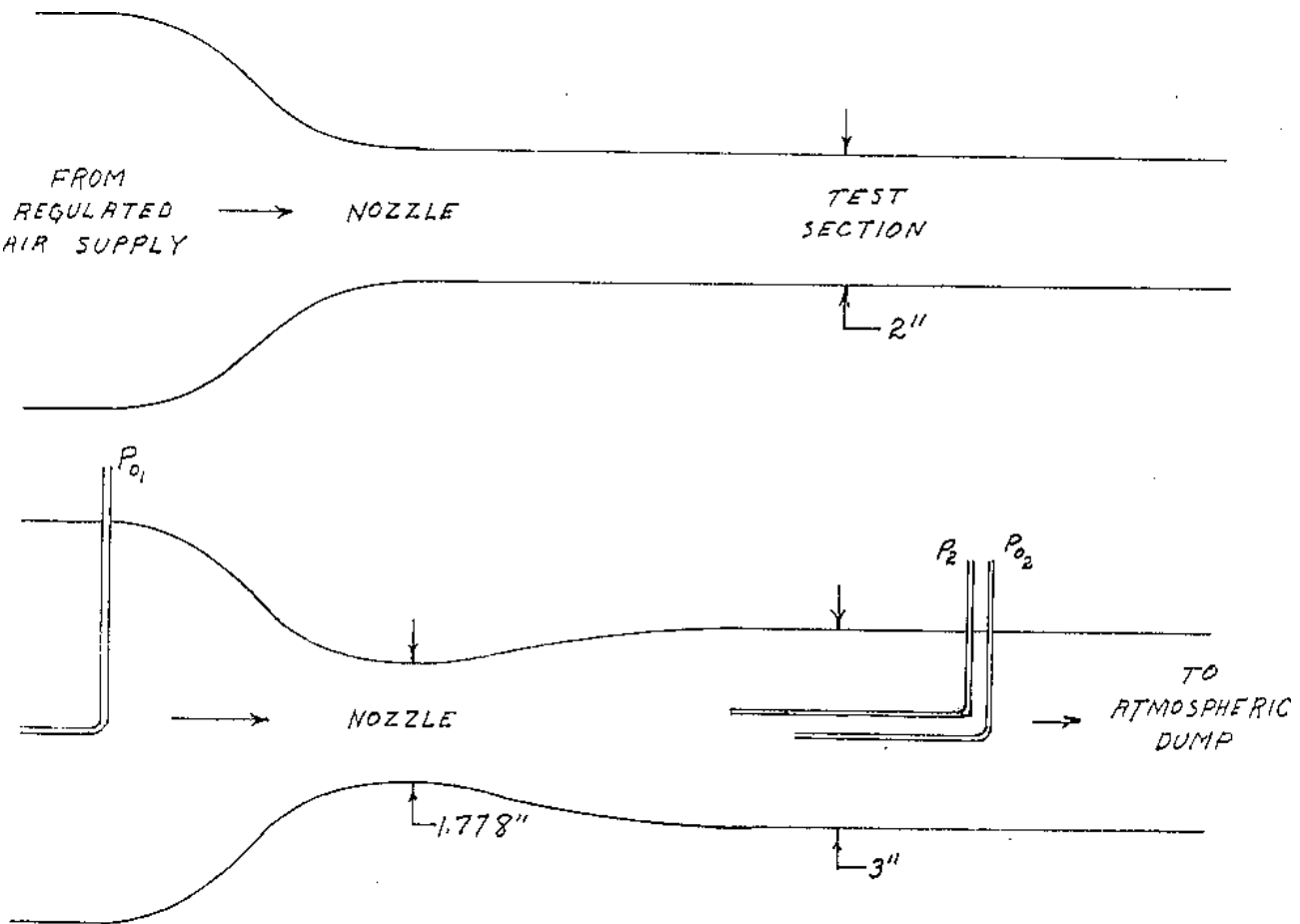


**Figure 8.** Schematic of supersonic blowdown tunnel.

The test section walls are fitted with two parallel windows in order to provide optical access. The tunnel is instrumented with a Pitot probe upstream of the nozzle and a removable Pitot-static probe that mounts in the test section. The orifice of the static pressure probe is aligned with the tip of the Pitot probe in the test section. The Pitot probe upstream of the nozzle is connected to a pressure gauge (which records gage pressure). The downstream Pitot probe can be connected to the Baratron for comparison to the ambient pressure. Similarly, the static pressure probe can be connected to the Baratron while the other side is open to atmosphere. Atmospheric pressure is measured using an electronic barometer. The probes in the test section may be removed and replaced by a wedge or by a solid body of some other configuration.

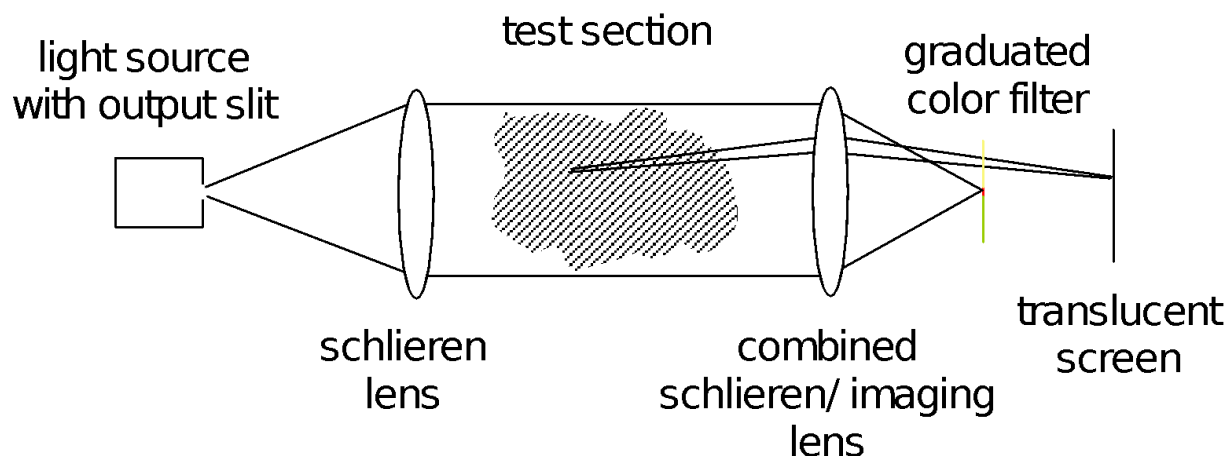


**Figure 9.** Schematic of schlieren setup attached to "2-d" blowdown windtunnel. The graduated color filter has a dark red pattern in the center that acts as the schlieren stop.

A schlieren system (Figure 9) is configured around the test section of the tunnel. A single lens is used to perform both the focusing of the collimated light and to image the test section on the screen. Also, a bicolor filter with an opaque band in the middle is used to produce the schlieren stop. Rays that pass above and below the focal point of the second lens pass through different colored filters. Thus rays that were deflected upwards will show up in one color in the image, while rays that were deflected downward will be a different color. Although the tunnel is fed from a large tank, running times are limited. It is, therefore, important to coordinate the measurements to be made before starting the tunnel. It is a good idea to watch the upstream stagnation pressure to make sure that it is not dropping with time (which would happen if you were overdraining the supply tanks). Since the Mach number in the tunnel depends only upon the area ratio of nozzle to test section (as long as the upstream pressure is sufficient to choke the nozzle), the test section Mach number is not affected by any pressure drop, but your pressure measurements will change.

## CD Nozzle Measurements

### Procedure

**⚠** The compressed air supply for this experiment is not infinite and the flow rate through the tunnels is substantial. As such, keep your runs to a minimum else you run the risk of running the tank down faster than the compressor can keep up with. If this occurs, you will need to wait for the compressor to charge the tank before being able to complete your experiments. To gauge the capacity of the tank open the valve to the blowdown tunnel and check the first pressure gauge in the line; it will read ~120 psi when full, and the compressor will kick in at ~85 psi. Pressures much below this may result in inability to complete the experiment.

The pneumatic fittings used in this experiment are all "push-to-connect" style. To make a connection firmly insert the tube until you feel the inner sleeve give and make the connection. To disconnect, **do not pull on the tube** without first pushing down the black plastic ring around the tube.

#### 1. Preparing the compressed air system

1. Close the small black-handled calibration valve and the large red-handled valve
2. Open the two main compressed air valves on the wall
3. Verify on the first gauge after the yellow hose that the system is energized (around 80-120psi)

#### 2. Preparing the instrumentation

1. Navigate to the experiment folder and open the Supersonic\_Spring2021 VI in Labview
2. Power on the transducer box and both USB DAQ boards
3. Run the VI and verify you have no hardware connection issues (create a folder for your group and set that as your save folder when you run the VI)

#### 3. Calibrating the transducers

1. Connect all transducers to the calibration box. Check the calibration box labels for what goes where. Do not remove the black compression fittings from the calibration box tubes, or remove the tubes from the transducers.
2. Follow the instructions in the VI for performing the calibration
3. Take a screenshot/picture of the final NULL and SCALE values for all 10 transducers, or manually record them for later
4. Take data using the VI at 3 different pressures by **slowly varying the black-handled calibration valve**: ~0 psi, ~14 psi, and another of your choosing somewhere in between. Be sure to also record the corresponding 3 pressures read by the manometer.
5. Make a note of the atmospheric pressure using the weather station on the desk.

#### 4. Performing the experiment

1. Connect the transducers to the correct taps in the experiment (P1 to P7 followed by Pb go in order from left to right when viewed from the side of the test section nearest the gas turbine)
2. **Slowly open the red-handled valve** to allow **subsonic** flow through the CD nozzle. Use the VI to record pressures in the nozzle at a high enough speed to see the subsonic pressure profile clearly, but without going supersonic
3. Open the valve further until the **flow is just choked**, i.e., throat has just reached Mach 1. *You may also hear a distinct change in the noise from the nozzle.* Use the VI to record the pressures
4. Continue opening the valve until a **shock is observed between stations 3 and 4**. You will be able to detect the shock location by a change in sign in the pressure gradient in region B of the nozzle (refer to the figure in the VI for the regions). Once again, record all pressures with the VI
5. Continue opening the valve until **the shock is observed between stations 4 and 5**. Record all pressures using the VI
6. Continue opening the valve until **the shock is observed between stations 5 and 6**. Record all pressures using the VI
7. Repeat steps 2 - 6. This will provide data to assess repeatability

#### 5. Shutting down the experiment

1. Close the most upstream valve on the combustion lab wall and wait for the air to fully purge through the wind tunnel (we don't want to leave any portion of the experiment charged with high pressure air!)
2. Close the red-handled valve on the experiment and the other valve on the wall
3. Click Done on the VI to save all data

## Data Reduction

1. Make a plot of the 3 pressure readings from the manometer ("true") versus the VI readings obtained using the calibration NULL and SCALE readings ("measured"). Discuss the accuracy the calibration and how it could be improved.
2. Convert all of the transducer readings to **absolute** pressure. These will be required for later calculations and plots.
3. Calculate the Mach numbers at stations 1 and 2 from the static and stagnation pressures determined at these locations for the following three conditions:
  1. subsonic flow throughout the nozzle
  2. the "just choked" condition
  3. the condition where the shock stands between stations 4 and 5.

4. Calculate the Mach number at station 6 for supersonic flow in two ways:
  1. using the static pressure at station 6 and a suitable stagnation pressure; and
  2. using the stagnation pressures as measured by the Pitot probes located at the throat (station 2) and at station 7.

Note be sure to use the correct value of the stagnation pressure in these calculations. It will be helpful to sketch for yourself a diagram of the nozzle indicating the position of the pressure taps and probes and the location of the shock wave.

**Show the calculated Mach numbers in steps 3&4 to your TA.**

## Results Needed For Report

1. Make a table of the sensitivity and zero offset values for each pressure transducer.
2. Make a table listing:
  1. atmospheric pressure
  2. the stagnation pressure measured using the two Pitot probes for the cases of:
    1. subsonic flow
    2. a shock between stations 4 and 5
    3. supersonic flow through at least station 6.
3. Make a table listing the Mach numbers at stations 1 and 2 for the three conditions specified under Data Reduction step 3
4. Make a table listing the Mach number at station 6 as calculated by the two methods given under Data Reduction 4
5. Make a graph with axial distance as the abscissa and the ratio of local static pressure to supply stagnation pressure as the ordinate. On this single graph, plot the results for the static pressure measurements for the conditions of:
  1. subsonic flow
  2. a shock between stations 4 and 5
  3. supersonic flow through at least station 6Using different symbols, plot the repeated data on this graph as well. This will show the quality of the repeatability.
6. Make a plot like that described in step 5 above, except plot Mach number as the ordinate.

---

## Blowdown Tunnel Measurements

### Procedure



The compressed air supply for this experiment is not infinite and the flow rate through the tunnels is substantial. As such, keep your runs to a minimum else you run the risk of running the tank down faster than the compressor can keep up with. If this occurs, you will need to wait for the compressor to

charge the tank before being able to complete your experiments. To gauge the capacity of the tank open the valve to the blowdown tunnel and check the first pressure gauge in the line; it will read ~120 psi when full, and the compressor will kick in at ~85 psi. Pressures much below this may result in inability to complete the experiment.

The pneumatic fittings used in this experiment are all "push-to-connect" style. To make a connection firmly insert the tube until you feel the inner sleeve give and make the connection. To disconnect, **do not pull on the tube** without first pushing down the black plastic ring around the tube.

## 1. Preparing the compressed air system

1. Ensure the main blowdown tunnel control valve is fully closed
2. Open the facility valves leading to the blowdown tunnel

## 2. Pitot tube experiments

1. Install the pitot tube plate into the test section
2. Connect the high pressure port of the manometer to the pitot tube stagnation port (the manometer low pressure port should be open to the atmosphere)
3. **!!! Read the following instructions fully before commencing - wasted time is wasted air !!!**
4. Gradually open the main blowdown tunnel control valve until the upstream pressure reads around 14 psi.  
Make a note of the exact pressure obtained.
5. Record the pitot stagnation pressure on the manometer.
6. Working quickly, but not rushing, switch the manometer tube to the static pressure port and record the pressure once it's settled
7. Fully close the main blowdown tunnel control valve
8. Make a note of the atmospheric pressure using the weather station on the desk

## 3. Wedge experiments

1. Remove the pitot tube plate and replace it with the wedge plate
2. Connect the high pressure port of the manometer to either one of the static ports (the manometer low pressure port should be open to the atmosphere)
3. Enable cooling air to the light source by opening the small black-handled valve
4. Turn on the Schlieren light system and wait for the lamp to warm up (*avoid switching the light source on and off unnecessarily since this will shorten its life and may extend your time in the lab if it doesn't re-illuminate quickly*)
5. Using your camera phone take a picture of the wedge's shadow on the screen. Be sure to get orthogonal to the screen and fill the frame as much as possible. Take multiple shots then select the best.
6. **!!! Read the following instructions fully before commencing - wasted time is wasted air !!!**
7. Position yourself around the screen to observe the wedge's shadow
8. Have a TA slowly open the main control valve whilst watching the screen; at some point you will see a new shadow appear around the wedge; the flow is now supersonic and this new shadow is the Mach cone. Tell the TA to stop opening the valve.
9. Record the following things:
  1. Upstream pressure from the gauge near the TA
  2. Static pressure on the manometer
  3. A new picture of the Schlieren screen with the Mach cone visible. Be sure to get orthogonal to the screen and fill the frame as much as possible. Take multiple shots then select the best.
10. Close the main control valve.

#### **4. Variable area diffuser experiments**

1. Unfortunately this experiment is damaged beyond repair this semester so please refer to the remote learning video for this portion. Nothing is required during the lab session.

#### **5. Shutting down the experiment**

1. Turn off the Schlieren lamp (but leave the cooling on)
2. Close the most upstream valve on the combustion lab
3. Open the main control valve on the blowdown tunnel and wait for the air to fully purge through the wind tunnel (we don't want to leave any portion of the experiment charged with high pressure air!)
4. Close the main control valve and the Schlieren cooling valve
5. Disconnect the manometer and pack it up in its case

## **Data Reduction and Report**

1. Calculate the test section Mach number from the ratio of static to stagnation pressure in the test section. Be very careful to use the correct, measured stagnation pressure. A rough sketch of the position of the probes and the location of the shock may help you.
2. Calculate the test section Mach number using the measured stagnation pressures and the shock equations (listed in the Background section) or appropriate shock tables (preferred method).
3. Determine the Mach number in the test section using the values of the half angles of the wedge and the shock that you measured. Use Figure 7 or similar graphs from your compressible flow texts.

**Show the Mach numbers you calculated in steps 1-3 to your TA.**

## **Results Needed For Report**

1. Make a schematic of the various configurations of tubing used in the pressure measurements.
2. Make a table listing the test section Mach number as calculated by using:
  1. the ratio of static to stagnation pressure in the test section
  2. the measured stagnation pressures in the test sections
  3. the shock angle on the wedge
3. Make a table showing the calculated and measured values of the minimum diffuser throat area required for starting this tunnel